Article

Structure-Based Optimization of ML300-Derived, Noncovalent Inhibitors Targeting the Severe Acute Respiratory Syndrome Coronavirus 3CL Protease (SARS-CoV-2 3CLpro)

Sang Hoon Han,[#] Christopher M. Goins,[#] Tarun Arya, Woo-Jin Shin, Joshua Maw, Alice Hooper, Dhiraj P. Sonawane, Matthew R. Porter, Breyanne E. Bannister, Rachel D. Crouch, A. Abigail Lindsey, Gabriella Lakatos, Steven R. Martinez, Joseph Alvarado, Wendell S. Akers, Nancy S. Wang, Jae U. Jung, Jonathan D. Macdonald, and Shaun R. Stauffer*

Cite This: https://doi.org/10.1021/acs.jmedchem.1c00598
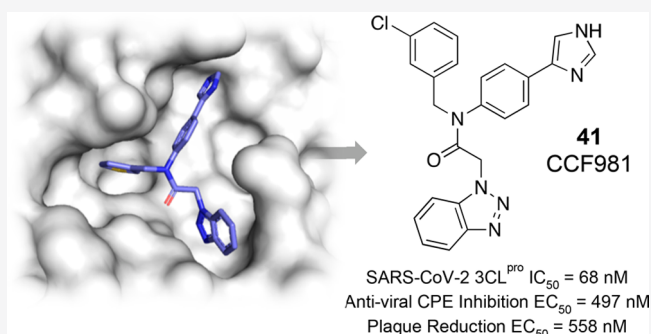
Read Online

ACCESS | Metrics & More | Article Recommendations | SI Supporting Information

ABSTRACT: Starting from the MLPCN probe compound ML300, a structure-based optimization campaign was initiated against the recent severe acute respiratory syndrome coronavirus (SARS-CoV-2) main protease (3CLpro). X-ray structures of SARS-CoV-1 and SARS-CoV-2 3CLpro enzymes in complex with multiple ML300-based inhibitors, including the original probe ML300, were obtained and proved instrumental in guiding chemistry toward probe compound 41 (CCF0058981). The disclosed inhibitors utilize a noncovalent mode of action and complex in a noncanonical binding mode not observed by peptidic 3CLpro inhibitors. *In vitro* DMPK profiling highlights key areas where further optimization in the series is required to obtain useful *in vivo* probes. Antiviral activity was established using a SARS-CoV-2-infected Vero E6 cell viability assay and a plaque formation assay. Compound 41 demonstrates nanomolar activity in these respective assays, comparable in potency to remdesivir. These findings have implications for antiviral development to combat current and future SARS-like zoonotic coronavirus outbreaks.

41
CCF981

SARS-CoV-2 3CLpro IC$_{50}$ = 68 nM
Anti-viral CPE Inhibition EC$_{50}$ = 497 nM
Plaque Reduction EC$_{50}$ = 558 nM

◼ INTRODUCTION

Coronaviruses (CoV's) make up a family of enveloped positive-strand RNA pathogenic viruses that can cause acute and chronic conditions, including central nervous system disorders, the common cold, lower respiratory tract infections, and diarrhea.[1] The 229E and OC43 strains were among the first characterized human CoV strains starting in 1965.[2] The novel severe acute respiratory syndrome CoV reported in 2003,[3,4] now identified as SARS-CoV-1, became the first global human CoV pandemic leading to progressive respiratory failure in more than 8000 individuals and 916 deaths (fatality rate of 10–15%).[5] In the eight years that followed, significantly less lethal human coronaviruses NL64 and HKU1 were identified and characterized.[6,7] Subsequently, in 2012 SARS-like MERS (Middle East respiratory syndrome) was identified and found to have a low transmission rate, but significant lethality with a total of 2567 patients with confirmed infection worldwide, of which 882 (34% fatality) died from 2012 through February 2, 2021. To date, most confirmed MERS cases have been reported from Saudi Arabia.[8] Like the SARS-CoV of 2003 and MERS of 2012, the ongoing novel SARS-CoV pandemic of 2020, known as SARS-CoV-2, the causative agent of COVID-19, presents a worldwide threat due to its

ability to rapidly spread person to person via respiratory droplets and its remarkable capacity to suppress human immune surveillance.[9] Unfortunately, SARS-CoV-2 has been much more extensive than MERS and SARS CoV-1 in its spread, with current worldwide infections, as of March 29, 2021, exceeding 126 million confirmed cases of COVID-19 and 2,778,619 confirmed deaths (fatality rate of ~2%) according to the World Health Organization (WHO).[10]

SARS-CoV-2[11] encodes multiple enzymes that are essential for viral replication.[12,13] As potential therapeutic antiviral targets, the two cysteine proteases, the chymotrypsin-like or main protease (3CLpro or Mpro) and the papain-like protease (PLpro), have garnered significant attention.[14–16] Both SARS-CoV-1 and -CoV-2 genomes encode a large polyprotein that is proteolytically processed by these respective cysteine proteases. In solution, 3CLpro exists primarily as a dimer and has

been confirmed to be the catalytically active species.[17] 3CL[pro] is responsible for processing at 11 different cleavage sites within the coronavirus polyprotein, and PL[pro] is responsible for cleavage at three other unique sites. Without these essential proteases, replication is impaired and shuts down the viral life cycle.[18] CoV 3CL[pro] enzymes contain three structural domains connected by flexible loops. Domains I and II are β-barrel domains and contain the catalytic active site region, whereas domain III is an α-helical domain shown to be critical for dimerization.[19] The active site contains a catalytic dyad consisting of a cysteine residue (Cys145) that acts as a nucleophile and a histidine residue (His41) that acts as the general acid or base.

Many published inhibitors of SARS-CoV-1 3CL[pro] and more recently for SARS-CoV-2 3CL[pro] have been peptide-like and often include a reactive center targeted toward a covalent interaction with the catalytic cysteine, Cys145. In collaboration with Mesecar and co-workers, and other member teams from NIH MLPCN, including the Scripps Research Institute Molecular Screening Center (SRIMSC) and the Vanderbilt Specialized Chemistry Center (VSCC), we participated in efforts to develop inhibitors of a coronavirus 3CL[pro] in the aftermath of the SARS-CoV-1 outbreak, with a particular focus on the development of noncovalent inhibitors, leading to ML300 and ML188 [1 and 2, respectively (Figure 1)].[20,21]
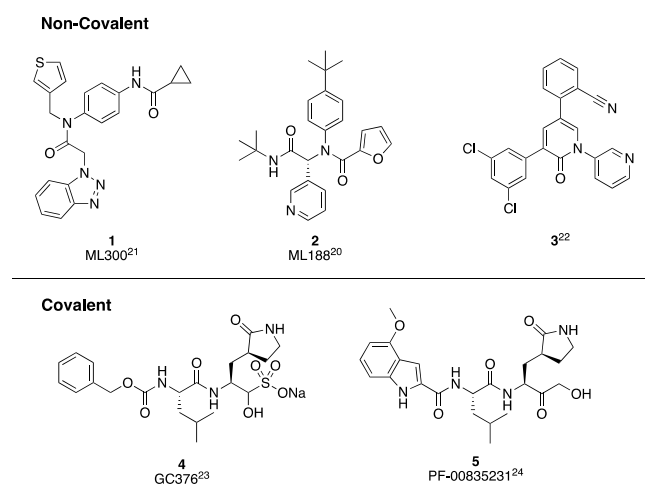

Figure 1. Exemplary structures of reported 3CL[pro] inhibitors for SARS-CoV-1 and SARS-CoV-2 using either a noncovalent (top) or covalent (bottom) mechanism of action.

Examples of *de novo*, noncovalent inhibitors designed toward SARS-CoV-2 3CL[pro] include the recently disclosed pyridone 3.[22] In the course of the COVID-19 pandemic, two covalent inhibitors previously discovered, 4 (GC-376)[23] and 5 (PF-00835231),[24] have advanced into clinical trials in 2020. The phosphate prodrug of 5, PF-07304814, is also under clinical evaluation.[25]

Among human novel CoV's, the highest degree of sequence homology for the 3CL[pro] protease exists between SARS-CoV-1 and SARS-CoV-2, with an overall 96% sequence identity and 100% identity in the active site, giving rise to similar substrate specificity,[26] thus providing the field with an advanced starting point for the development of SARS-CoV-2 3CL[pro] inhibitors. Structural biology has played a critical role in 3CL[pro] protease inhibitor development, beginning with the first X-ray structure in 2003 with a hexapeptidyl chloromethyl ketone inhibitor

bound to TGEV 3CL[pro] [Protein Data Bank (PDB) entry 1P9U][27] and SARS-CoV-1 3CL[pro] (PDB entry 1UK4).[28] Today, a multitude of X-ray crystal structures have emerged comparing CoV 3CL[pro]'s, including SARS-CoV-2, to aid and galvanize inhibitor design efforts. High-impact early contributions in the context of the ongoing pandemic include those from the Diamond Light Source XChem X-ray fragment screening program,[29] Shanghai Tech University N3-peptide,[30] University of Lübeck dicarbonyl compound 13b,[26] peptide-based aldehydes similar to 5 reported by Dai and co-workers at the Chinese Academy of Sciences,[31] and baicalein and related natural products from University of Chinese Academy of Sciences.[32] More recent developments include evidence from a March 2020 report from Qiao and co-workers[33] at Sichuan University demonstrating preclinical *in vivo* efficacy in a human angiotensin converting enzyme 2 (hACE2) transgenic SARS-CoV-2 murine model. Using a moderate infection threshold, the Sichuan team developed a peptidyl aldehyde based upon a Boceprevir design. One of the lead orally bioavailable inhibitors, MI-09, was administered at 100 mg/kg BID 1 h prior to virus inoculation and then continuing for 5 days after infection. In this study, compound MI-09 demonstrated significant viral RNA load reduction within 3 days, with almost no virus detected by day 5, thus setting the stage for emerging tool compounds to be evaluated and assessed against for their efficacy and overall PK−PD.

Our focus was directed to the synthesis and further optimization of nonpeptidic, noncovalent inhibitors of SARS-CoV-2 3CL[pro] that are derived from ML300.[21] We were intrigued to investigate the ML300 series against SARS-CoV-2 for several reasons. Notably, in contrast to ML188 and prior peptidomimetics bound to 3CL[pro] in a canonical binding mode wherein the inhibitor accommodates substrate subpockets in the enzyme active site, the SARS-CoV-1 3CL[pro] X-ray structure of the ML300 series HTS hit, compound 6 (Figure 2A), favors an induced-fit complex in which key flexible amino acid side chains, specifically Gln189 and Met49, take on distinct
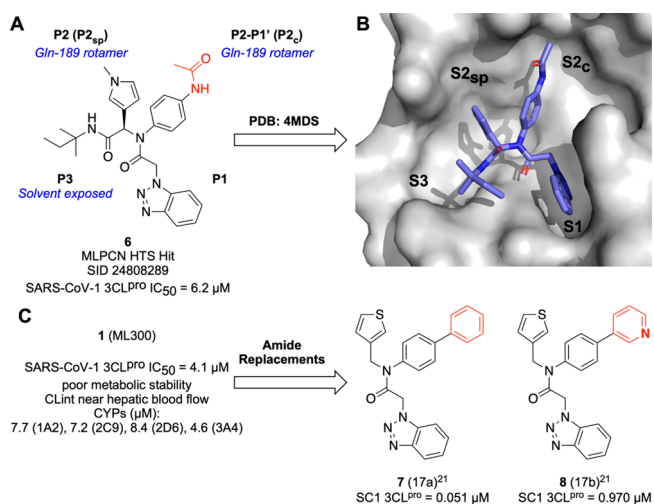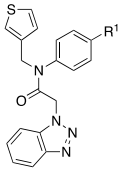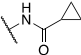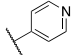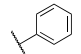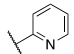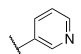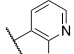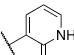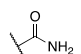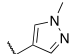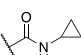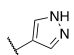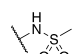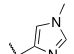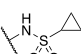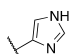

Figure 2. Noncanonical mode of binding of MLPCN HTS compound 6 (SID 24808289) and evolution to ML300 and related biphenyl analogues 7 and 8 originally developed for SARS-CoV-1 3CL[pro]. (A) Schematic of the binding mode of 6 orienting the binding site. (B) Solvent accessible surface of the 6 3CL[pro] complex, illustrating the flexibility and reorganization of the binding pocket (PDB entry 4MDS). (C) Profile of 1 (ML300) and biaryl analogues 7 and 8.

Table 1. SARS-CoV-1 and SARS-CoV-2 3CL[pro] Inhibition Data, Exploring the SAR of P2[c][c]

Compound	R[1]	[a]SC1 3CL[pro] IC$_{50}$ (μM)	[b]SC2 3CL[pro] IC$_{50}$ (μM)	Compound	R[1]	[a]SC1 3CL[pro] IC$_{50}$ (μM)	[b]SC2 3CL[pro] IC$_{50}$ (μM)
1 (ML300)[21]		4.45 ± 0.26	4.99 ± 0.62	**14**		1.57 ± 0.60	2.09 ± 0.27
7 (17a)[21]		16.82 ± 4.72	31.18 ± 4.65	**15**		0.90 ± 0.12	1.40 ± 0.21
8 (17b)[21]		0.93 ± 0.05	0.95 ± 0.06	**16**		3.09 ± 0.52	5.07 ± 0.60
9		19.73 ± 3.01	18.87 ± 1.34	**17**		0.78 ± 0.15	0.92 ± 0.21
10		0.38 ± 0.04	0.44 ± 0.06	**18**		22.78 ± 1.87	20.39 ± 0.42
11		16.55 ± 0.44	15.94 ± 1.01	**19**		0.109 ± 0.020	0.106 ± 0.025
12		1.40 ± 0.41	1.61 ± 0.44	**20**		11.31 ± 1.52	9.55 ± 0.99
13		7.98 ± 0.42	8.77 ± 0.20	**21**		0.148 ± 0.038	0.063 ± 0.014

[a]SARS-CoV-1 3CL[pro]. [b]SARS-CoV-2 3CL[pro]. [c]IC$_{50}$ values are averages of at least three independent assays, each run as technical duplicates.

conformations and in tandem reorganize the S4 and S2 binding surface. The observed induced fit allows the bis-aniline to occupy a newly formed channel proximal between what is traditionally the canonical S1′ and S2 pockets (hereafter referred to as S2$_c$ or S2 channel). Conversely, the pyrrole ring of **6** exists in a deeper subpocket of S2 (S2$_{sp}$) that is more proximal to the traditional S4 pocket.[34] Second, while the original ML300 series achieved nanomolar inhibition against SARS-CoV-1, leading to compounds such as **7** and **8** (Figure 2C), the series was far from optimized. For example, only a handful of amide replacements presumed to occupy the upper rim of the S2$_c$ were explored. In the S2$_{sp}$ region, in which the ML300 3-thienyl ring was presumed to act as a P2$_{sp}$ group (Figure 2B), only these two π-excessive heterocycles were examined during hit expansion. Moreover, cellular antiviral structure–activity relationships (SARs) of the ML300 series against SARS CoV's remained largely unknown, although the potential for broad spectrum utility was precedent on the basis of studies examining ML300 analogues targeting HKU4, a suspected reservoir host for MERS.[35] Lastly, *in vitro* ADME properties of ML300 revealed significant hurdles, including metabolic instability with no knowledge of the mechanism or site of metabolism. On the basis of these fundamental gaps and our interest in contributing to understanding if the benzotriazole-based ML300 series may have potential as a lead for COVID-19 or future broad spectrum 3CL[pro]-based

CoV antiviral therapies, we assembled a team highly focused on the goals and inquiries outlined above.

The compounds disclosed herein provide significantly improved characteristics in several areas compared to those in the original ML300 report, achieving robust nanomolar biochemical inhibition against SARS-CoV-2 3CL[pro], submicromolar antiviral and plaque formation inhibition against the SARS-CoV-2 live virus, and a systematic DMPK and metabolite profile to support directions for future optimization. In addition, we compare and contrast several new X-ray structures of inhibitors bound to SARS-CoV-1 and CoV-2 3CL[pro], including ML300 and a number of analogues generated using structure-based design.

■ RESULTS AND DISCUSSION

Our efforts began by initially synthesizing **1** (ML300), **7**, and **8** and rescreening against SARS-CoV-1 3CL[pro] (SC1), obtaining for **1** an IC$_{50}$ of 4.45 μM (Table 1), which was in agreement with reported data; a similar IC$_{50}$ value against SARS-CoV-2 3CL[pro] (SC2) was also obtained. However, to our surprise, the previously published biphenyl derivative, **7**[21] did not confirm its prior published value of 51 nM and was drastically less potent. On the basis of the concentration–response curves (CRCs) of compound **7**, an SC1 IC$_{50}$ of 16.8 μM and an SC2 IC$_{50}$ of 31.2 μM were calculated, which represents potency more similar to that of unsubstituted compound **9** (Table 1).

C

In contrast, 3-pyridyl congener **8** maintained an IC_{50} between 930 and 950 nM for both SC1 and SC2 enzymes that mirrored the initial report from 2013. Relative to **1**, pyridyl biaryl **8** results in an increase in ligand efficiency (LE) from 0.23 to 0.27 based upon SC2 mean IC_{50} values. Because our findings regarding biphenyl **7** stand in contrast to the original work, we carefully examined our assay reagents, protocols, and compound fidelity. For each 3CL[pro] construct, we utilized the native sequence of the enzyme that represents the *in vivo*, postproteolytic form using the protocol and conditions reported by Mesecar and co-workers.[36] We also utilized the same FRET-based 3CL[pro] peptide substrate as reported and achieved excellent plate uniformity using a 384-well plate format (Z-prime > 0.8). Compound CRC's were generated and tested from at least three experiments using a 384-well plate format with technical replicates on each plate. SC1 and SC2 reported IC_{50} values listed in Tables 1−3 reflect *n* = 3, with further repeats as required until a CV of ≤0.3 was achieved. The standard deviation is reported and shown for reference. As per published protocols, 0.01% Triton X-100 was included in the assay buffer to remove potential promiscuous inhibition caused by aggregation. At this time, the >300-fold SC1 IC_{50} discrepancy for biphenyl **7** cannot be fully explained; however, it is clear that the inherent high lipophilicity of this molecule may have been a contributing factor on the basis of its calculated physicochemical properties (for **7**, cLogP = 5.61 and LogS = −6.85; ChemDraw 19.0) and behavior in FRET CRC measurements. For example, Figure 3 shows a
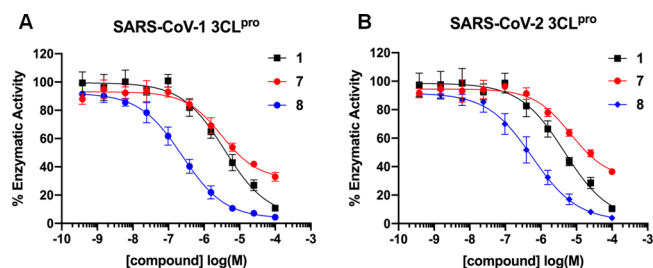

Figure 4. X-ray co-crystal structures of (A) **1** in complex with SC2 3CL[pro] (PDB entry 7LME) and (B) **8** in complex with SC1 3CL[pro] (PDB entry 7LMH). In the left panel, key residues are highlighted as sticks and interatomic distances depicted as dashes; the right panel shows the solvent accessible surface with occupied and neighboring pockets labeled. The binding orientation of each inhibitor is the same in the active site of each monomer of the dimer in the asymmetric unit; only one active site is shown for the sake of clarity.

Figure 3. 3CL[pro] concentration−response curves for compounds **1**, **7**, and **8**, against (A) SC1 and (B) SC2 enzymes.

comparison of the SC1 and SC2 3CL[pro] FRET inhibition curves for **1**, **7**, and **8**. Incomplete inhibition is clearly observed for compound **7** on the basis of the curve profile when tested up to 100 μM (Figure 3, 4-fold serial dilution). In addition, there is a plateau of inhibition that appears to begin at concentrations of 25 μM and higher, suggesting a likely solubility limit. In contrast, compound **8** behaves well up to a top assay concentration of 100 μM, achieving complete inhibition.

Encouraged by the submicromolar SC1 and SC2 inhibitory activity of pyridyl **8**, we pursued a series of X-ray crystal studies and obtained high-resolution structures of **8** bound to SC1 3CL[pro] at 1.85 Å via soaking method, in addition to a co-crystal of **1** (ML300) bound to SC2 3CL[pro] at 2.1 Å resolution via co-crystallization. Shown in Figure 4 is a depiction of key residues and the binding poses of the **1**−SC2 3CL[pro] (panel A) and **8**−SC1 3CL[pro] (panel B) complexes.

Comparison of the X-ray Structures of the 6−SC1 3CL[pro], 1−SC2 3CL[pro], and 5−SC2 3CL[pro] Complexes. Overall, the binding orientation of **1** in the SC2 3CL[pro] binding pocket (Figure 4A) retains many of the key interactions found
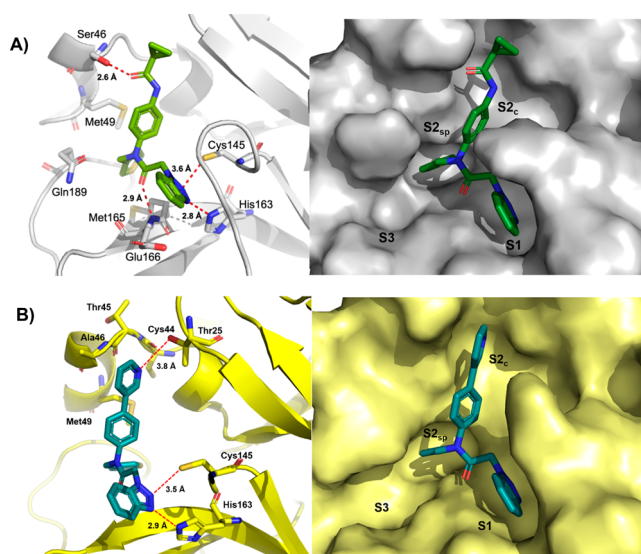
in the **6**−SC1 3CL[pro] complex (Figure 2B); however, key distinctions within the binding site that illuminate prior SAR trends are observed.[21] In general, removal of the P3 amide of **6** as the major difference versus inhibitor **1** does not grossly effect the ligand bioactive conformation, leaving the solvent-exposed S3 pocket unoccupied. In the S1 pocket, identical to the **6**−SC1 3CL[pro] complex, the benzotriazole of **1** forms neighboring putative H-bonding interactions with His163 and Cys145, at 2.8 and 3.6 Å, respectively. Similarly, the amide carbonyl oxygen retains a key anchoring hydrogen bond with the backbone NH of Glu166. Within the S2 pocket, as seen previously within the compound **6**−SC1 3CL[pro] complex, the dynamic nature of the Gln189 loop allows a new $S2_{sp}$ to form to accommodate the thiophene ring, resulting in the thiophene sulfur being sandwiched between Met165 and Met49. Interestingly, the *N*-methyl pyrrole and thiophene conformationally present distinctly within the $S2_{sp}$. Specifically, the bulkier *N*-methyl pyrrole adopts an 18° torsion to reach into the $S2_{sp}$ pocket, while the 3-thienyl of **6** adopts a 98° torsion with respect to the aniline ring to fill this pocket. In addition, there is a slight frame shift of the *N*-benzyl amide backbone resulting in rotational shift of the aniline vector toward the $S2_c$ upper rim that appears to favorably accommodate the larger cyclopropyl amide. Relative to the **5**−SC2 3CL[pro] peptide complex (see Figure S1, PDB entry 6XHM), **5** and **1** share common H-bond interactions with Glu166 and His163 in the S1 region; however, **5** forms a covalent interaction with the catalytic Cys145 and occupies the solvent-exposed S3 pocket. In contrast to the **6**−SC1 3CL[pro] complex, for ligand **1** in chain A of the asymmetric unit the cyclopropyl anilido amide moiety maintains a rotamer in the $S2_c$ channel that positions the carbonyl at a 50° torsion from co-planarity relative to the central aniline ring, giving rise to a unique hydrogen bond with the side chain of Ser46 (Figure 4, left). In chain B in the asymmetric unit, the cyclopropyl moiety points further from

the pocket toward solvent; however, for chain B, the B-factor values indicate significant motion versus the chain A inhibitor. Interestingly, this observed hydrogen bonding interaction represents an amino acid difference between the SC1 and SC2 3CL^{pro} enzymes, namely an Ala46 in SC1 for Ser46 in SC2. Residue 46 defines part of a short helix−loop−helix motif spanning Arg40−Lue50. Peptidomimetics efforts to date with a canonical mode of inhibition acknowledge that amino acids within the active site between SC1 and SC2 3CL^{pro} are 100% identical in sequence. With regard to a tailored CoV 3CL^{pro} inhibitor design versus a broad spectrum inhibitor strategy, the observed interactions and residue differences noted within and near S2$_c$ for this ML300-based series may present unique challenges as well as opportunities not available to traditional inhibitor scaffolds depending on the approach.

Comparison of the X-ray Structures of 1−SC2 3CL^{pro} and 8−SC1 3CL^{pro} Complexes. Relative to the 1−SC2 3CL^{pro} complex, the 8−SC1 3CL^{pro} binding pose and interactions are otherwise identical with the exception of interactions found within the S2$_c$ upper rim region (Figure 4, right vs left). With regard to nearby polar residues that might engage the pyridyl nitrogen, Thr25 side chain is the most spatially close residue; however, the distance measured at 3.8 Å would indicate this is less than favorable. Furthermore, no apparent water-mediated interactions were observed with the ligand. In terms of π-interactions with the pyridyl ring of 8, a Ala46 backbone amide−π interaction is apparent on the basis of the proximity and distances from the backbone carbonyl carbon and the pyridyl centroid (3.5−3.8 Å). This stacking interaction may contribute to the beneficial increase in potency of 8 versus biphenyl 7.

With the new structural information presented above and encouraging potency for compound 8 in hand, we investigated more extensive amide variants and heterocyclic modifications (Table 1). The reverse amide of ML300, 11, exhibited a 3-fold decrease in activity versus that of the parent, while the primary amide, 10, displayed nanomolar inhibition against both proteases. Sulfonamides 12 and 13 both measured low micromolar inhibition. Reviewing the SC1 3CL^{pro} X-ray structure of 8, while we did not observe any obvious direct hydrogen bonding interactions between the pyridyl group and the protein, we did find it was clear that the orientation of this compound series was directed toward multiple residues for potential interaction. The activities of additional isomeric analogues such as 4-pyridyl 14 and 2-pyridyl 15 were within 2-fold of the activity of 8 for both SC1 and SC2 3CL^{pro}. 2-Methoxy-pyridyl 16 lost 3−5-fold of its activity for both enzymes, while pyridone 17 was essentially equipotent to compound 8. Encouraged by 17 and the observed interactions of 1 within the S2$_c$ upper rim, we continued to design and pursue modifications in the S2$_c$ exploring various H-bond donors both neutral and potentially charged in nature. To our delight, a significant enhancement was found with the NH-pyrazole and imidazole derivatives, 19 and 21, respectively, reaching an IC$_{50}$ of 60 nM versus SC2 3CL^{pro} in the case of imidazole 21. The potency of N-methyl analogues 18 and 20 was drastically diminished, between 160- and 185-fold versus those of their nonmethylated analogues, underscoring the importance of the presence and nature of a H-bond donor in the P2$_c$ group.

The obtained X-ray co-crystal structures of 19 and 21 in SC2 3CL^{pro} indeed demonstrate the potential for multiple H-bonding interactions from these heterocyclic azole nitrogens

(Figure 5A,B). There are prospective H-bonds with both the hydroxyl side chain of Thr25 and the backbone carbonyl of
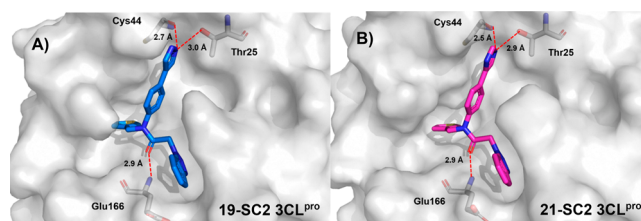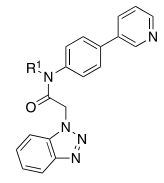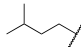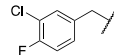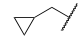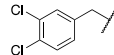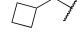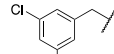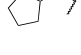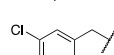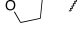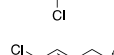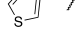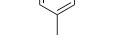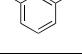

Figure 5. X-ray co-crystal structures of compounds 19 and 21, in which select residues are shown as sticks with key hydrogen bonds shown as dashes. (A) 19 in complex with SC2 3CL^{pro} (PDB entry 7LMD). (B) 21 in complex with SC2 3CL^{pro} (PDB entry 7LMF).

Cys44. The bound pose of the azole heterocycle is co-planar with the central phenyl in both cases and juxtaposed between the residues with distances from the closest nitrogen within acceptable interheteroatom H-bonding distances of 2.8−3.0 Å. The hydrogen bonding array revealed in both structures would suggest the azole is acting as a hydrogen bond donor to the carbonyl of Cys44 and then an acceptor from Thr25. We also obtained X-ray structures of these same two compounds in SC1 3CL^{pro}, and in both cases, we observed an almost identical binding pose, and binding site orientation, with the exception of a subtle difference in the S2$_{sp}$ region (Figure S1A). Here, there is movement of the unstructured loop, and rotation of Gln189, which leads to a small difference in the thiophene ring torsion (86° vs 64°). This observation is presumed to be driven by different crystallization conditions used for the two proteins; SC2 was co-crystallized, while compounds for SC1 were soaked in apo-3CL^{pro} with increasing amounts of glycerol in the buffer solution. Indeed, the density for a glycerol unit is found in the nearby S4 region for all of our SC1 determined 3CL^{pro} structures.

Simultaneously with the synthesis of our first series expanding the scope of the biaryl 8 SAR, we explored thiophene replacements at P2$_{sp}$ (Table 2) holding the P2$_c$ group constant as 3-pyridyl. A range of acyclic and cyclic aliphatic groups were targeted, including 22−26, with cyclobutyl derivative 24 affording a slight improvement relative to parent 8. Introduction of an ether oxygen via tetrahydrofuran 26 was highly deleterious. Thiazole analogue 27 offered similar inhibition within 2-fold of those of 8 and 24 with early evidence of an improvement in microsomal stability compared to that of 8 (vide infra). It was quickly established that a 3-chlorophenyl group led to a significant increase in potency against both SC1 and SC2, namely compound 28, and subsequent analogues explored the SAR of this ring in more depth, 29−34. A 3,4-substitution pattern was clearly not tolerated (29 and 30), an observation that was consistent with our emerging X-ray structures and docking studies suggesting a limited steric bulk near loop residue Arg188. This observation is in contrast to the mobility in the loop region near Asn189. A 3,5-substitution afforded examples with inhibition below 200 nM, including analogues 31 and 32, with 5-fluoro derivative 31 among the most potent in this subseries with IC$_{50}$ values ranging from 74 to 119 nM. The addition of a pyridine nitrogen to improve the physicochemical properties of this subseries was tolerated, but with a reduction in SC2 inhibition to 540 nM.

E

Table 2. 3CL^{pro} Inhibition Data, Exploring the SAR of P2$_{sp}$[c]

Compound	R^1	[a]SC1 3CL^{pro} IC$_{50}$ (μM)	[b]SC2 3CL^{pro} IC$_{50}$ (μM)	Compound	R^1	[a]SC1 3CL^{pro} IC$_{50}$ (μM)	[b]SC2 3CL^{pro} IC$_{50}$ (μM)
22		4.21 ± 0.19	4.62 ± 0.13	29		4.87 ± 1.87	8.53 ± 1.82
23		2.44 ± 0.39	2.51 ± 0.44	30		> 200	> 200
24		0.78 ± 0.06	0.83 ± 0.03	31		0.074 ± 0.01	0.119 ± 0.005
25		1.00 ± 0.21	1.16 ± 0.19	32		0.111 ± 0.018	0.176 ± 0.025
26		20.5 ± 1.59	23.0 ± 1.38	33		0.418 ± 0.065	0.312 ± 0.073
27		1.13 ± 0.26	1.59 ± 0.44	34		0.370 ± 0.105	0.540 ± 0.070
28		0.25 ± 0.07	0.39 ± 0.11				

[a]SARS-CoV-1 3CL^{pro}. [b]SARS-CoV-2 3CL^{pro}. [c]IC$_{50}$ values are averages of at least three independent assays, each run as technical duplicates.
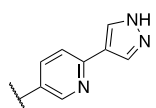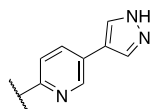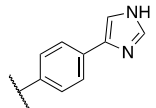
On the basis of the data presented above, we elected to hold the P2$_{sp}$ 3-chlorophenyl and P1 benzotriazole constant while exploring combinations of P2$_c$ pendant biaryls with a handful of aniline modifications (Table 3). Interestingly, a number of the prior P2$_c$ favorable modifications, such as pyridone 17 and pyrazole 19, led to active compounds 35 and 36; however, a differential SAR was noted. For example, within the pyridone subseries 3-chlorophenyl (35) versus 3-thienyl (17), 3CL^{pro} inhibition is nearly identical. Within the more active pyrazole comparators (e.g., 36 versus 19), there is a 3-fold preference for the 3-thienyl subseries, which is in the opposing direction from that described in Table 1. This differential SAR is observed in both SC1 and SC2 3CL^{pro} data, suggesting a parallel phenomenon and a dynamic SAR presumably resulting from the P2$_c$ upper rim inhibitor-enzyme interactions identified. Relative to 36, modifications within the aniline core such as methoxy analogues 37 and 38 are tolerated with 2-methoxy being slightly preferred relative to 36 with an IC$_{50}$ of 197 nM for SC2 3CL^{pro}. A similar trend was noted for the central pyridyl congeners 39 and 40 with 2-pyridyl displaying identical 1.6-fold increases in potency for both SC1 and SC2 enzymes. Investigation of the 3-chlorophenyl P2$_{sp}$ analogue imidazole 21 afforded compound 41. Once again similar to the pyrazole-matched pairs described above, more potent P2$_c$ modifications appear to engender a differential SAR in the context of the P2$_{sp}$ group. In the case of SC1 3CL^{pro}, an 8-fold increase in IC$_{50}$ is noted substituting 3-thienyl for 3-chlorophenyl (for 21, IC$_{50}$ = 148 nM; for 41, IC$_{50}$ = 19 nM). However, in the case of SC2 3CL^{pro}, flat SAR was noted with no real improvement in inhibition when the P2$_c$ substituent was C4-imidazole.

As part of the ongoing optimization efforts, we spot-checked compounds for DMPK properties throughout, including human and rat intrinsic clearance, plasma protein binding, MDCK passive permeability, and P450 isozyme reversible inhibition at 10 μM. A complete summary is presented in Table S1. Beginning with 1 (ML300) and throughout most of the SAR presented, we observed exceptionally high microsomal clearance, with hepatic clearance equivalent to hepatic blood flow in both humans and rats. We hypothesized that the P1-benzotriazole group may be a source of significant metabolism, and indeed, the carbon-linked 3-pyridyl and 5-pyrimidyl analogues 42 and 43, respectively (Figure 6), do show a noteworthy improvement in CL$_{int}$, with 2- and 4-fold decreases, respectively, compared to that of 36 in microsomes (human and rat) and in the human S9 fraction. Unfortunately, these groups afforded a drop in primary biochemical potency back to micromolar levels, demonstrating further P1 optimization is required. The monodirectional cellular permeability is high, as measured in MDCK-MDR1 cells, across the series, and multiple examples have modest free fractions at or above 1% unbound in humans [e.g., 21 and 41 (Table S1)]. We have also assessed an initial CYP inhibition profile for this series of compounds, and relatively strong inhibition at 10 μM was noted in general with few exceptions (3A4, 2D6 $\gg$ 50%). Given the structural features of these molecules, this finding was not unexpected, and further optimization is ongoing to mitigate P450 inhibition.

Subsequently, we initiated soft-spot metabolite ID analysis of a representative benzotriazole, namely 3-chlorobenzyl derivative 36, to further understand the generally high hepatic oxidative metabolism observed and guide future target design.

Table 3. 3CL^{pro} Inhibition Data and Analogues Exploring Aniline−Biaryl P2$_c$ Combinations^c

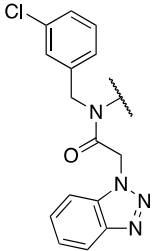| Compound	R^1	^{a}SC1 3CL^{pro} IC$_{50}$ (μM)	^{b}SC2 3CL^{pro} IC$_{50}$ (μM)
35		0.657 ± 0.405	0.746 ± 0.098
36		0.334 ± 0.126	0.270 ± 0.067
37		0.206 ± 0.052	0.328 ± 0.027
38		0.208 ± 0.077	0.197 ± 0.050
39		0.336 ± 0.065	0.333 ± 0.093
40		0.214 ± 0.063	0.171 ± 0.029
41		0.019 ± 0.005	0.068 ± 0.023

^{a}SARS-CoV-1 3CL^{pro}. ^{b}SARS-CoV-2 3CL^{pro}. ^{c}IC$_{50}$ values are averages of at least three independent assays, each run as technical duplicates.
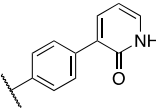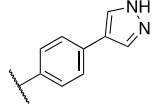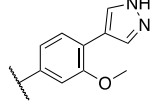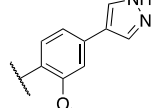
This analysis demonstrated that while there is NADPH-dependent oxidative metabolism of the benzotriazole moiety, this is a secondary metabolite in comparison to oxidation of the benzylic 3-chlorophenyl ring (Figure 7). The M1 metabolite is estimated at 60% on the basis of the UV total peak AUC, while M2 is 33%. We note that sample depletion was not observed in the absence of NADPH (data not shown), indicative of oxidative metabolism mediated by P450. A third, minor metabolite (M3, 7%) resulting from cleavage of the 3-chlorobenzyl group is also observed. Additional profiling of related compounds is ongoing to support this observation that benzylic P2$_{sp}$ is the major soft spot in human hepatic S9 fractions. Strategies for reducing oxidative metabolism and increasing the in vitro half-life are being developed.

We next turned to the evaluation of promising compounds for their antiviral activity. The antiviral efficacy of compounds

against infectious SARS-CoV-2 virus in Vero E6 cells was evaluated by cytopathic effect (CPE) inhibition and in a plaque reduction assay. The results are summarized in Table 4. The CPE inhibition assay was performed with a six-point dilution with three independent experiments for each compound; these results were then validated via a plaque reduction assay performed with four to six concentrations of compound, depending on the measured CPE inhibition.

The original declared MLPCN probe ML300 displayed weak activity in the high micromolar range (Table 4, CPE EC$_{50}$ = 19.9 μM, plaque reduction EC$_{50}$ = 28 μM). The pyrazole and imidazole P2$_c$-containing derivatives, 19 and 21, respectively, which are among the more biochemically potent analogues of ML300, showed improved EC$_{50}$ values between 1.7 and 8 μM in both assays.

Interestingly, the potencies of the matched pair analogues 36 and 41 that substitute the P2$_{sp}$ 3-thienyl for 3-chlorophenyl are greatly improved with the EC$_{50}$ of 41 achieving submicromolar activity in both assays. In addition, the 50% cytotoxic concentration of 41 (CC$_{50}$) in the CPE antiviral assay was found to be >50 μM, indicating an excellent selectivity index [SI > 100 (see Figure S4 and Table S5)]. Comparison of EC$_{50}$/IC$_{50}$ ratios of the noncovalent compounds can help guide compound design in terms of estimating the required target IC$_{50}$ to achieve a desired pharmacological effect. For example, for 19 and 21, the respective EC$_{50}$/IC$_{50}$ ratios are 52 and 29, respectively. These are far from a desired profile. In contrast, 3-chlorophenyl analogues 36 and 41 have EC$_{50}$/IC$_{50}$ ratios of 7.3 and 7.4, respectively. To the best of our knowledge, these values are equivalent to those of the best noncovalent inhibitors of SC2 3CL^{pro} reported to date. In addition, the efficacy of 41 was shown in our assays to be comparable to that of the clinically utilized polymerase inhibitor, remdesivir (Figure 8).[37,38]

Chemistry. The nature of our starting point, 1 (ML300), led to the possibility of modular and systematic exploration of the SAR in different vectors of the 3CL^{pro} binding pocket. Our initial focus was on optimization of the groups at P2$_c$, which was previously found to be a source of varied SAR.[21] Here, the P2$_{sp}$ group was fixed and thiophene-3-carbaldehyde, 44, was reacted with various anilines via reductive amination (Scheme 1). Amides 10 and 11, the reverse amide relative to 1, were synthesized via benzoic acid intermediate 45, while sulfonamides 12 and 13 were synthesized via 1,4-dianiline intermediate 46. Aryl bromide 47 afforded a versatile intermediate that afforded bi(hetero)aryl analogues 8 and 14−21 using Suzuki−Miyaura cross-coupling conditions. The pyridone example, 17, was synthesized by hydrolysis of fluoropyridine intermediate 48. The NH-pyrazole could be introduced directly, without protection, to afford 19; however, reaction with the analogous NH-imidazole was unsuccessful. In this instance, we utilized 4-bromo-1-trityl-imidazole and the corresponding pinacol ester of 47 to furnish the desired product 21 after deprotection.

We simultaneously explored the nature of the P2$_{sp}$ substituent, with a desire to replace the thiophene moiety of ML300 (Scheme 2). Here, various aldehydes were reacted with biaryl aniline 51 via reductive amination, and then amide bond formation with benzotriazole-1-acetic acid (50) in the presence of propylphosphonic anhydride (T3P) afforded compounds 22−34.

Similar to our initial library, for compounds 35−43 the P2$_{sp}$ 3-chlorophenyl moiety was held constant as a thiophene

36
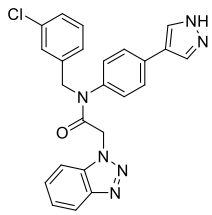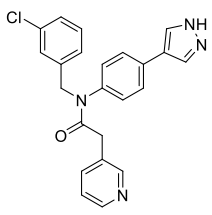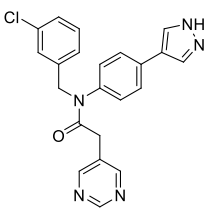
SC2 3CL^pro IC_50 = 0.270 μM

hS9 CL_int = 436 mL/min/kg

CL_int (h, r) = 2621, 5668 mL/min/kg

f_u (h, r) = 0.1, - %

MDCK-MDR1 P_app = 39.4 x10^-6 cm/s

CYP's % inh @ 10 μM:

96% (3A4), 63% (2D6), 99% (2C9)

42

SC2 3CL^pro IC_50 = 1.27 μM

hS9 CL_int = 256 mL/min/kg

CL_int (h, r) = 981, 3555 mL/min/kg

f_u (h, r) = 0.4, 3.5 %

MDCK-MDR1 P_app = 61.8 x10^-6 cm/s

CYP's % inh @ 10 μM:

99% (3A4), 55% (2D6), 99% (2C9)

43

SC2 3CL^pro IC_50 = 3.44 μM

hS9 CL_int = 145 mL/min/kg

CL_int (h, r) = 620, 3302 mL/min/kg

f_u (h, r) = 1.8, 11 %

MDCK-MDR1 P_app = 66.7 x10^-6 cm/s

CYP's % inh @ 10 μM:

88% (3A4), 26% (2D6), 92% (2C9)

Figure 6. SC2 3CL^pro potency and DMPK profiles for lead benzotriazoles **36**, **42**, and **43**.
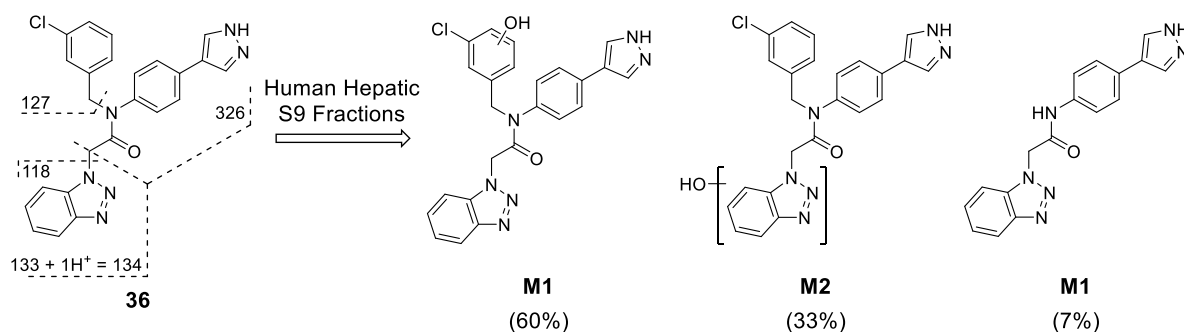
Figure 7. Soft-spot metabolite identification studies of **36** using human hepatic S9 fractions. Metabolite formation (%) is based on the total peak area of the three principle metabolites, M1–M3 (see also Table S2).

Table 4. Assessing the Antiviral Efficacy of Compounds, Measuring *In Vitro* Viral Replication

compound	CPE inhibition assay EC_50 (μM)	plaque reduction assay EC_50 (μM)
remdesivir	0.34 ± 0.01	0.43 ± 0.06
1 (ML300)	19.90 ± 6.32	28.15 ± 1.30
8	12.07 ± 0.31	14.55 ± 1.22
19	5.76 ± 1.96	7.63 ± 1.65
21	1.74 ± 0.19	1.75 ± 0.25
28	7.61 ± 1.43	11.14 ± 0.37
35	8.77 ± 1.14	16.69 ± 2.44
36	1.98 ± 0.24	3.31 ± 0.10
37	2.93 ± 0.28	3.24 ± 0.27
38	2.30 ± 0.33	2.01 ± 0.49
39	3.81 ± 0.18	4.65 ± 0.11
40	1.91 ± 0.30	3.39 ± 0.21
41	0.497 ± 0.009	0.558 ± 0.041

replacement (Scheme 3). Reductive amination of 3-chlorophenyl-benzaldehyde, **53**, with anilines afforded intermediates that follow a synthetic sequence similar to that described above. Bromo intermediate **58** provided synthetic flexibility, as subsequent Suzuki–Miyaura reaction, followed by T3P amide coupling, led to products **35**, **36**, **42**, and **43**. Alternatively, the 1,2,3-benzotriazole moiety could be introduced first to give bromide **61**, which was then subjected to Miyaura–Ishiyama–Hartwig borylation and subsequent Suzuki–Miyaura cross-coupling conditions to afford **41** in acceptable yield.

■ CONCLUSIONS

As for many scientists around the globe, the huge effect on our lives caused by the COVID-19 pandemic inspired us to assess how we could have an impact, however large or small, in the study of this disease. Having prior experience targeting the 3CL protease of SARS-CoV-1 working with leaders in the field, we were compelled to further investigate ML300 as a starting point employing all disciplines within our newly formed center and partnering with our CCF Institute virologist colleagues and experts in the field. After initial disappointment and intrigue, we found that the addition of H-bond-donating azole heterocycles, in particular pyrazole- and imidazole-containing analogues, including **19** and **21**, directed to S2_c afforded an appreciable increase in potency. This discovery combined with the 3-chlorobenzyl modification in S2_sp advanced our optimization efforts to a series of compounds routinely reaching primary IC_50 SC2 3CL^pro inhibition values of <500 nM. As such, the ML300 amide series continues to display an interesting mode of action with a differential SAR worthy of further exploration and investigation.

Historically the ML300 series has demonstrated basic *in vitro* DMPK properties that were not conducive to warrant probe utility beyond *in vitro* settings. While we have observed improvements, the compounds disclosed still lack the properties needed for a full *in vivo* evaluation in animal models of SARS-CoV-2 infection. The addition of metabolite ID has highlighted key areas of the molecule for further optimization to reduce the high clearance and metabolic turnover in the series. Similarly, while the unbound fraction and cellular
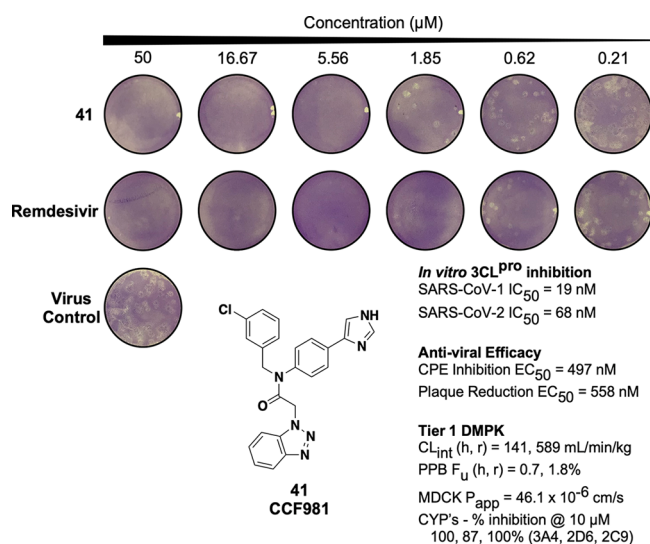
Figure 8. Summary of the data for compound **41** (CCF0058981). Images show antiviral activity of **41** and remdesivir against SARS-CoV-2 determined by a plaque reduction assay. Vero E6 ACE2 cells were infected with approximately 50 plaque forming units per well of SARS-CoV-2. After incubation for 1 h, the viral inoculum was removed, and the cells were overlaid with DMEM containing 1% low-melting agarose and the indicated concentration of the test compounds. Three days after infection, the cells were fixed with 4% formaldehyde for at least 1 h. The overlay was then removed, and cells were stained with 0.2% crystal violet containing 20% ethanol. The images are representative of two repeats. Tier 1 DMPK data were obtained at Q^2 Solutions.

permeability of these compounds are promising, a further hurdle these compounds must overcome is their strong inhibition of CYP enzymes that is currently an active area of ongoing research.

Noncovalent small molecule SARS-CoV-2 inhibitor **41** (CCF0058981) provides a significant advance from the original SARS-CoV-1 ML300-derived inhibitor, with low nanomolar biochemical inhibition and efficacy in cellular models comparable to that of the FDA-approved RNA polymerase inhibitor remdesivir. Optimization of the series of compounds is ongoing, with a particular focus on improving the DMPK profile, as well as further improving the biochemical and cellular efficacy. In addition, we look forward to future opportunities to profile the series and compounds herein against a wider panel of coronaviruses, including MERS. We anticipate that investigators targeting SC1 and SC2 3CL[pro] will benefit from the disclosed SAR and X-ray crystal structures. Furthermore, these findings have implications for antiviral development to combat future SARS-like zoonotic coronavirus outbreaks.

■ EXPERIMENTAL SECTION

SARS-CoV-1 and -2 3CL[pro] Protein Expression and Purification. SARS-CoV-1 and -2 3CL[pro] enzymes were cloned using previously published methods.[30,39] Briefly, genes encoding each protein were codon optimized for *Escherichia coli*, synthesized, and inserted into a pGEX-6P-1 plasmid between the BamHI and XhoI cut sites (note that additional residues "AVLQ" and "GPHHHHHH-stop" were added to the N- and C-termini, respectively, of the proteins as previously described).[30,39] The resulting expression

Scheme 1. Synthesis of Compounds 8−21 from Thiophene-3-carbaldehyde 44[a]
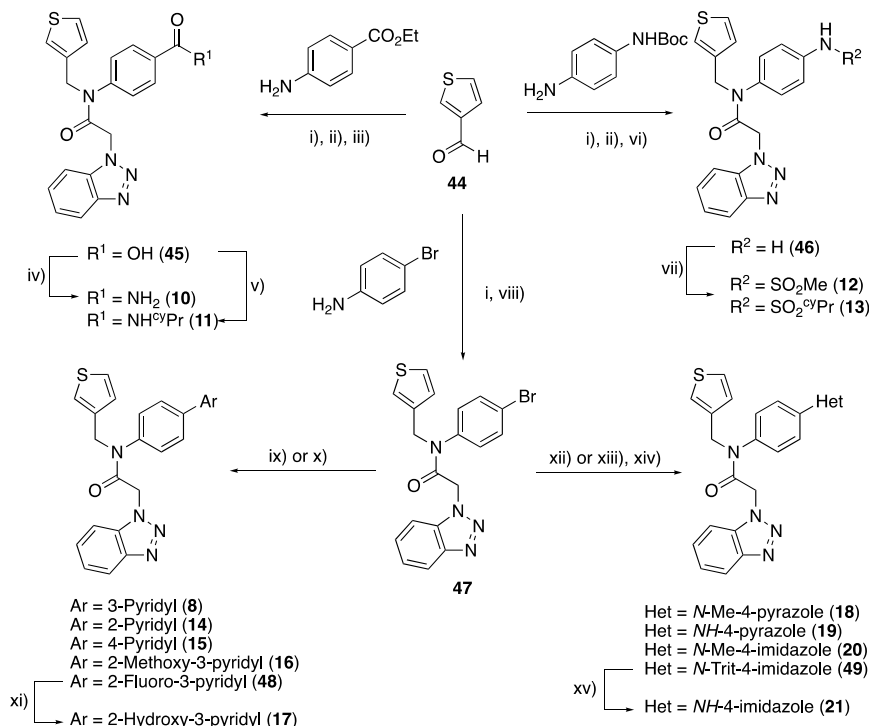
[a]Reagents and conditions: (i) NaBH(OAc)$_3$, AcOH, DCE, rt; (ii) benzotriazole-1-acetic acid (**50**), T3P, EtOAc, rt; (iii) LiOH, THF, rt; (iv) NH$_4$Cl, EDC, HOBt, Et$_3$N, THF, rt; (v) cyclopropylamine, COMU, DIPEA, DCM, rt; (vi) TFA, DCM, rt; (vii) R-SO$_2$Cl, Et$_3$N, DCM, rt; (viii) **50**, HATU, Et$_3$N, DCM, rt; (ix) Ar-B(OH)$_2$, Pd(OAc)$_2$, dppf, CuCl, Cs$_2$CO$_3$, DMF, 100 °C; (x) Ar-B(OH)$_2$, Pd(PPh$_3$)$_4$, THF/H$_2$O, 100 °C; (xi) aqueous HCl, dioxane, 80 °C; (xii) Ar-Bpin, Pd(dppf)Cl$_2$·DCM, K$_2$CO$_3$, dioxane, 100 °C; (xiii) B$_2$pin$_2$, Pd(dppf)Cl$_2$·DCM, KOAc, dioxane, 80 °C; (xiv) 4-bromo-1-trityl-imidazole, Pd(dppf)Cl$_2$·DCM, K$_2$CO$_3$, dioxane, 100 °C; (xv) AcOH, MeOH, 65 °C.

Scheme 2. Synthesis of Compounds 22−34 with Various P2$_{sp}$ Substituents[a]
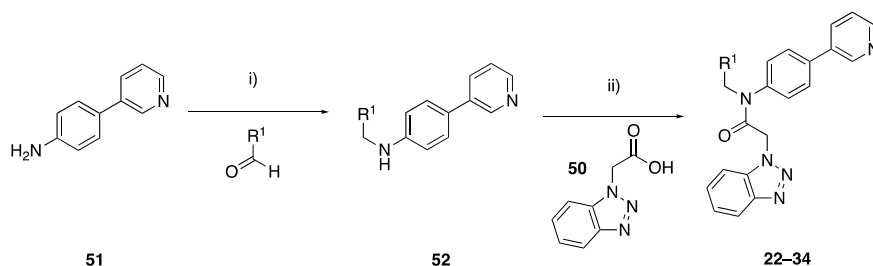
[a]Reagents and conditions: (i) NaBH(OAc)$_3$, AcOH, DCE, rt; (ii) T3P, pyridine, DMF, rt.

constructs yield unscarred, native enzymes following protein purification.

Both enzymes were recombinantly expressed using New England Biolabs T7 Express lysY/Iq cells transformed with 3CL^{pro} expression plasmids. The enzymes were expressed and purified using identical methods derived from previously published work.[30] Inoculated cultures of Lauri Broth media supplemented with ampicillin were grown at 37 °C with shaking to an OD$_{600}$ of 0.6−0.8. The incubator/shaker temperature was then reduced to 16 °C, and the cultures were induced with 0.5 mM IPTG. Following overnight induction, cells were harvested via centrifugation at 3900 rpm (Eppendorf 5810R, S-4-104 rotor) for 25 min and resuspended in 20 mM TRIS, 300 mM NaCl, pH 8.0 buffer (buffer A). Resuspended cells were lysed via sonication and centrifuged at 10500 rpm (Eppendorf 5810R, FA45-6-30 rotor) for 30 min, and the clarified lysate was loaded onto a 5 mL Ni-charged Nuvia IMAC column equilibrated with buffer A. The column was washed with 10 column volumes (CV) of buffer A and eluted with a 7 CV gradient of 0−100% buffer B (buffer A with 500 mM imidazole). Fractions containing pure 3CL^{pro} were pooled, diluted in half with buffer A, and dialyzed overnight at 4 °C with PreScission Protease against a 50 mM TRIS, 150 mM NaCl, 1 mM DTT, pH 7.5 buffer. Cleaved protein was passed through a 5 mL Ni-charged Nuvia IMAC column equilibrated with a 50 mM TRIS, 150 mM NaCl, pH 7.5 buffer. The collected flow-through was concentrated to 5 mL using an Amicon Ultra 10K centrifugal filter and diluted to 25 mL with 50 mM TRIS (pH 7.5). Diluted protein was passed through a 5 mL HiTrap Q FF anion exchange column equilibrated with 50 mM TRIS, 25 mM NaCl, pH 7.5 buffer (buffer C). The Q FF column was washed with 10 CV of buffer C, and bound proteins eluted with a 5 CV 0% to 100% gradient of buffer D (buffer C with 1 M NaCl). Pure 3CL^{pro} was found to be in the nonbound and wash fractions from this chromatographic step. The final purity was assessed via Coomassie-stained sodium dodecyl sulfate−polyacrylamide gel electrophoresis. The purified protein in a 50 mM TRIS, 25 mM NaCl, pH 7.5 buffer was pooled, concentrated, aliquoted, and frozen at −80 °C for biochemical assays or used fresh for protein crystallography studies.

SARS-CoV-1 and -2 3CL^{pro} Biochemical Assay. The protease activity and subsequent 10-point IC$_{50}$ curves were spectroscopically determined using a scaled down, end point assay adapted from a previously described peptide-based Forster resonance energy transfer (FRET) assay.[20,40] Compounds (as 10 mM DMSO stocks) were serially diluted 4-fold using 100% DMSO in a LabCyte 384-well LDV plate and acoustically transferred using a LabCyte ECHO 550 instrument into Corning 384-well black NBS plates. The standard 10-point IC$_{50}$ 384-well plate layout is as follows. First, 100 μM 8 was stamped into columns 1 and 24 (low control), DMSO was stamped into columns 2 and 23 (high control), and serially diluted compounds were stamped from high (100 μM) to low (0.38 nM) concentrations in columns 3−12 (replicate 1) and 13−22 (replicate 2). To run the assay, assay wells stamped with 0.25 μL of compound or DMSO were filled via a ThermoFisher Multidrop Combi liquid dispenser with 14.5 μL of 150 or 200 nM (concentration for a 25 μL final reaction volume) SARS-CoV-1 or SARS-CoV-2 3CL^{pro}, respectively, in assay buffer [50 mM HEPES, 0.1 mg/mL BSA, 0.01% (v/v) TRITON

X100, and 2 mM DTT (pH 7.5)]. Assay plates were then centrifuged at 1000 rpm (Eppendorf 5810R, S-4-104 rotor) for 1 min, covered, and incubated at room temperature for 15 min. Reactions were initiated using the Multidrop Combi liquid dispenser to titrate 10 μL of 2 μM (concentration for a 25 μL final reaction volume) fluorophore-quencher peptide substrate [HiyteFluor-488ESATL-QSGLRKAK-(QXL)-NH$_2$ from AnaSpec, Inc. catalog no. AS-65599] solubilized in assay buffer into each well. Assay plates were again centrifuged at 1000 rpm for 1 min, covered, and incubated at room temperature for 30 min. Biochemical assays were quenched through the addition of 5 μL of 500 mM acetic acid via a Multidrop Combi liquid dispenser. Assay plates were then centrifuged at 1000 rpm for 1 min, and the resulting fluorescence intensity was measured on a BioTek Cytation 5 multimode plate reader (λ_{ex} = 485 nm; λ_{em} = 528 nm).

Data Analyses. Raw fluorescence values were normalized (RF$_{norm}$) by dividing each value by the average of DMSO control wells, which represents the maximal fluorescence signal (RF$_{norm}$ = RF$_{sample}$/Ave RF$_{DMSO\ control}$). Dose−response curve fitting was performed using Dotmatics Studies (version 5.4.2), which computes IC$_{50}$ values utilizing a four-parameter logistical fit. Reported values are average IC$_{50}$ values from at least three independent experiments.

Protein Crystallization, Data Collection, and Structure Refinement. SARS-CoV-2 3CL^{pro} was concentrated to 6.5 mg/mL and titrated with the inhibitor to give a final concentration of 3% (v/v) inhibitor (10 mM DMSO stocks of 19 and 21 and 20 mM DMSO stock of 1). Protein−inhibitor complexes were left at room temperature for 1 h prior to setting up crystallization drops. Diffraction quality crystals were obtained by hanging drop vapor diffusion experiments comprised of 1 μL of a protein/inhibitor mix and 1 μL of crystallization solution drops incubated at 16 °C. The Hampton Research Index Screen (HR2-144) yielded a high rate of crystal formation, with optimal crystals forming in 0.2 M lithium or ammonium sulfate, 0.1 M Bis-TRIS or HEPES (pH 6.5−7.5), and 25% polyethylene glycol 3350. Protein crystals were directly looped, flash-frozen in liquid nitrogen, and shipped for remote collection of X-ray diffraction data at Advanced Photon Source LS-CAT beamline 21-ID-F. Diffraction data were indexed and scaled using HKL2000 and phased (Phaser-MR) using molecular replacement with the search molecule PDB entry 6WQF.[41−43] Inhibitor coordinates were generated using ELBOW, and the resulting protein−inhibitor structures were refined and built using iterative rounds of refinement and manual manipulation with PHENIX Refine and COOT.[44−46] X-ray diffraction and model refinement statistics are listed in Table S1. The final coordinates and electron density maps were deposited in the Protein Data Bank.

SARS-CoV-1 3CL^{pro} was concentrated to 6.0 mg/mL and titrated with inhibitor to give a final concentration of 4% (v/v) inhibitor (10 mM DMSO stocks of 35 and 25 mM DMSO stock of 1). Protein−inhibitor complexes were left at room temperature for 30 min prior to setting up crystallization drops. Diffraction quality crystals were obtained by hanging drop vapor diffusion experiments comprised of 1 μL of the protein/inhibitor mix and 1 μL of crystallization solution drops incubated at 16 °C. The Hampton Research Index Screen (HR2-144) yielded a high rate of crystal formation, with optimal

Scheme 3. Synthesis of Compounds 35−43[a]
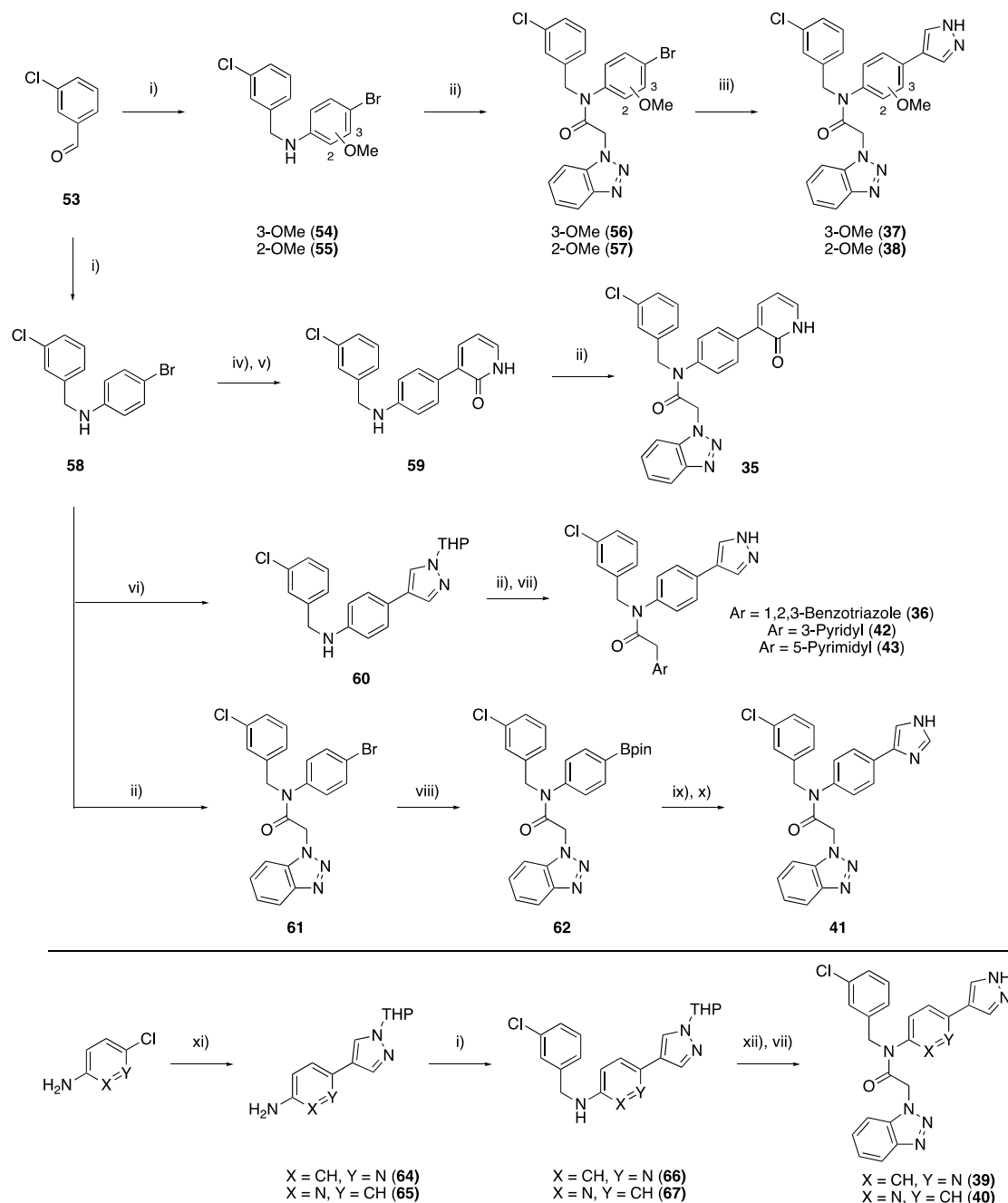
[a]Reagents and conditions: (i) aryl-amine, NaBH(OAc)$_3$, AcOH, DCE, rt; (ii) aryl acetic acid, T3P, pyridine, DMF, rt or 60 °C; (iii) 4-Bpin-[1]H-pyrazole, Pd(dppf)Cl$_2$·DCM, K$_2$CO$_3$, dioxane, 110 °C; (iv) 2-fluoropyridine-3-boronic acid, Pd(dppf)Cl$_2$·DCM, K$_2$CO$_3$, dioxane/H$_2$O, 100 °C; (v) aqueous HCl, dioxane, 80 °C; (vi) 1-THP-4-Bpin pyrazole, Pd(dppf)Cl$_2$·DCM, K$_2$CO$_3$, dioxane/H$_2$O, 100 °C; (vii) 4 M HCl, dioxane, 60 °C; (viii) B$_2$pin$_2$, Pd(dppf)Cl$_2$·DCM, KOAc, dioxane, 100 °C; (ix) 4-bromo-1-trityl-imidazole, Pd(dppf)Cl$_2$·DCM, K$_2$CO$_3$, dioxane/H$_2$O, 100 °C; (x) AcOH, MeOH, rt; (xi) 1-THP-4-Bpin pyrazole, S/XPhos Pd G2, K$_2$CO$_3$, 1-BuOH, 100 °C; (xii) 50, cyanuric fluoride, pyridine, DCM, rt, then 66 or 67, Et$_3$N, THF, 60 °C.

crystals forming in ammonium sulfate, HEPES (pH 7.5), and 25% polyethylene glycol 3350. For collecting X-ray diffraction data, the crystals were flash-cooled in liquid nitrogen followed by dragging the crystals through the crystallization solution. In another method, SARS-CoV-1 3CL^{pro} was crystallized at 20 °C using the hanging drop vapor diffusion method by mixing 6 mg/mL 3CL^{pro} in a 1:1 ratio with 100 mM MES buffer (pH 5.5), 12−18% (w/v) polyethylene glycol 6000, 10% (v/v) glycerol, and 2% (v/v) DMSO. Single crystals were transferred to 5 μL of the mother liquor with 400 μM inhibitor (10 mM DMSO stocks of 8, 19, and 21). After incubation at 16 °C for 5

min, the crystals were looped and dragged out through the crystallization solution cryoprotected by 20% (v/v) glycerol. The crystals were then shipped for the remote collection of X-ray diffraction data at Advanced Photon Source LS-CAT beamline 21-ID-F. Diffraction data were indexed and scaled using HKL2000 and phased with the CCP4i molecular replacement program with the search molecule PDB entry 3VB3.[47] Inhibitor coordinates were generated using ELBOW, and the resulting protein−inhibitor structures were refined and built using iterative rounds of refinement and manual manipulations with Refmac (ccp4i)[48] and COOT. X-ray

diffraction and model refinement statistics are listed in Table S2. The final coordinates and electron density maps were deposited in the Protein Data Bank.

Virus Propagation and Titration. The following reagent was deposited by the Centers for Disease Control and Prevention and obtained through BEI Resources, NIAID, NIH (SARS-related coronavirus 2, isolate USA-WA1/2020, NR-52281). The virus was propagated in Vero E6 cells expressing the ACE2 receptor (a gift from Y. Choi, Cleveland Clinic Lerner Research Institute) in DMEM supplemented with 1× penicillin-streptomycin (Gibco) and 0.5 μg/mL TPCK-treated trypsin (Worthington Biochemical) at 37 °C in a humidified incubator with 5% CO_2. Propagated virus was aliquoted and stored at −80 °C until further use.

The virus titer was determined by a plaque assay as previously described with a slight modification.[49] Briefly, confluent monolayer Vero E6 ACE2 cells cultured in a six-well plate were infected with 10-fold serially diluted virus inoculum incubated on a rocker for 45 min in 37 °C for virus adsorption. After the removal of the virus solution, cells were overlaid with DMEM containing 1% low-melting point agarose and incubated in a humidified incubator at 37 °C and 5% CO_2 for 4 days. To visualize the plaques, the cells were fixed with 4% formaldehyde and stained with a 0.2% crystal violet solution containing 20% ethanol.

Virus Inhibition Assays. Initial antiviral screening was done by using a CPE inhibition assay.[50] Briefly, Vero E6 ACE2 cells were cultured in 96-well flat-bottom plates at a density of 2 × 10⁴ cells per well. Following infection of the cells with a 100 $TCID_{50}$ of SARS-CoV-2, the plates were incubated on a rocker in 37 °C for 45 min for virus adsorption. The cells were then washed with DMEM, and the medium containing the test compounds at the desired concentration was added. Both the uninfected cells and the infected cells treated with 10 μM remdesivir were used as controls. The antiviral efficacy of test compounds was determined by the uptake and subsequent extraction of neutral red dye. After infection (68 h), cells were incubated with 0.034% neutral red dye for 3 h at 37 °C. Free dye was washed from the wells, and dye uptake was quantified using a microplate reader with absorbance at 540 nm. Absorbance values were expressed as percentages of uninfected control cells, and EC_{50} values of the test compounds were determined using Prism (GraphPad).

The initial CPE inhibition results were validated by testing the compounds by a plaque reduction assay.[51] Confluent monolayers of Vero E6 ACE2 cells in 12-well plates were washed once with DMEM and infected with approximately 50 plaque forming units (PFUs) of SARS-CoV-2 in each well. The plates were incubated on a rocker at 37 °C for 45 min for virus adsorption. The virus inoculum was removed and replaced by overlay medium (DMEM containing 1% low-melting point agarose without serum) containing 3-fold serial dilutions of the test compounds and placed in a 37 °C CO_2 incubator until plaques could be visualized under light. The cells were then fixed with a 4% formaldehyde solution for at least 30 min, and the overlaid agarose was removed and stained with a 0.2% (w/v) crystal violet solution. The plaques were counted by visual examination, and the required concentration to reduce the 50% plaque number (EC_{50}) was calculated relative to the control without test compounds.

Hepatic S9 Metabolic Stability Assessment of Compounds. The metabolic stability compounds were investigated in human hepatic S9 fractions pooled from 20 mixed gender donors [Xenotech, catalog no. H0606.S9(AX), lot 1710129] using a substrate depletion methodology (percentage of parent compound remaining). Potassium phosphate-buffered (0.1 M, pH 7.4) solutions of the test article (1 μM) and S9 (2.5 mg/mL) were incubated at 37 °C under ambient oxygenation in the presence or absence of NADPH (2 mM). Total incubation volumes were 0.4 mL with a final organic concentration of 0.5%. Mixtures lacking substrate were preincubated at 37 °C for 5 min. Reactions were initiated by the addition of substrate, and at the designated times (0, 3, 7, 15, 30, and 45 min), a 25 μL aliquot of the incubation mixture was removed and precipitated by the addition of 4 volumes of ice-cold MeCN containing carbamazepine as an internal standard (50 nM). The mixtures were centrifuged at 3500 rcf (4 °C)

for 10 min. The resulting supernatants were diluted 1:3 (supernatant/water) into 96-well plates in preparation for LC-MS/MS analysis. All samples were analyzed via electrospray ionization on an AB Sciex API-6500 QTrap (Applied Biosystems, Foster City, CA) instrument that was coupled with LC-20ADXR pumps (Shimadzu, Columbia, MD) and a CTC PAL autosampler (Leap Technologies, Carrboro, NC). Analytes were separated by gradient elution using a Phenomenex Kinetix C18 column (2.1 mm × 50 mm, 1.7 μm; Phenomenex, Torrance, CA) thermostated at 40 °C. HPLC mobile phase A was 0.1% formic acid in water (pH unadjusted); mobile phase B was 0.1% formic acid in acetonitrile (pH unadjusted). The gradient started at 5% B after a 0.2 min hold and was linearly increased to 90% B over 1.0 min, held at 90% B for 1.0 min, and returned to 5% B in 0.1 min followed by a re-equilibration (0.5 min). The total run time was 2.5 min, and the HPLC flow rate was 0.5 mL/min. The source temperature was set at 500 °C, and mass spectral analyses were performed using multiple-reaction monitoring, with transitions and voltages specific for each compound using a Turbo Ion Spray source in positive ionization mode (4.5 kV spray voltage): **36**, m/z 443 > 124.9 CE 38; **40**, m/z 444 > 124.9 CE 46; **42**, m/z 403 > 120 CE 34; **43**, m/z 404 > 125 CE 36; verapamil, m/z 455.1 > 165.1 CE 40; carbamazepine, m/z 237.1 > 194.0 CE 25. All data were analyzed using AB Sciex Analyst version 1.5.1. Each compound was assayed in triplicate within the same 96-well plate. Hepatic intrinsic clearance (CL_{int}, milliliters per minute per kilogram) was extrapolated from hepatic S9 using the substrate depletion method and eq 1:[52]

$$CL_{int} = \frac{\ln 2}{t_{1/2(min)}} \times \frac{mL}{2.5 \text{ mg of protein}_{S9}} \times \frac{120.7 \text{ mg of protein}_{S9}}{\text{g of liver weight}}$$
$$\times \frac{21 \text{ g of liver weight}}{\text{kg of body weight}} \tag{1}$$

Hepatic clearance (CL_{HEP}, milliliters per minute per kilogram) was estimated using eq 2, according to the well-stirred model, uncorrected for the fraction unbound in plasma:[53]

$$CL_{HEP} = \frac{Q_H f_u CL_{int}}{Q_H + f_u CL_{int}} \tag{2}$$

where Q_H represents human hepatic blood flow (21 mL min⁻¹ kg⁻¹) and CL_{int} represents the intrinsic clearance calculated from eq 1.

***In Vitro* Biotransformation of Compounds in Hepatic S9 Fractions.** The *in vitro* metabolism of test articles was investigated using hepatic S9 fractions from Sprague-Dawley rats (62 males, pooled) and humans (150-donor UltraPool, BD Biosciences). A potassium phosphate-buffered reaction mixture (0.1 M, pH 7.4) of the test article (25 μM), hepatic S9 fractions (5 mg/mL), and $MgCl_2$ (3 mM) was incubated at 37 °C in borosilicate glass test tubes under ambient oxygenation for 1 h with select experiments being fortified with NADPH (2 mM). All S9 reactions were initiated by the addition of NADHP to the *in vitro* milieu. Protein was precipitated by the addition of 2 volumes of MeCN with subsequent centrifugation (3000 rcf, 10 min). The supernatant was dried under a stream of nitrogen and reconstituted in 85:15 (v/v) ammonium formate (10 mM, pH 4.1)/MeCN in preparation for LC-MS analysis.

Liquid Chromatography-UV-Mass Spectrometry Analysis of Metabolites. The LC-MS/MS system described in the hepatic S9 metabolic stability experiment was coupled to an Acquity BEH C18 column (2.1 μm, 2.1 mm × 100 mm; Waters, Billerica, MA). Solvent A was 10 mM (pH 4.1) ammonium formate, and solvent B was MeCN. The initial mobile phase was 85:15 A/B (v/v), held for 5 min, and by linear gradient transitioned to 20:80 A/B over 20 min. The flow rate was 0.400 mL/min. The HPLC eluent was first introduced into a Shimadzu SPD-20A UV detector (single wavelength selected, 254 nm) followed by electrospray ionization-assisted introduction into the 6500 QTrap mass spectrometer operated in positive ion mode. The electrospray voltage was set at 4.5 kV with a source temperature of 500 °C. The collision energy was 25 when the mass spectrometer was operated in MS/MS mode.

Compound Synthesis. *General Experimental.* All chemical reagents and reaction solvents were purchased from commercial suppliers and used as received. Normal phase chromatography was performed on a Teledyne ISCO CombiFlash NextGen300 system using Teledyne RediSep normal phase silica cartridges, with an average particle size range of 35–70 μm. Preparative reversed phase HPLC was performed using a Teledyne ACCQ-Prep HP150 instrument equipped with Phenomenex Kinetex C18 columns, using gradients of MeCN in H$_2$O with a 0.1% TFA additive. Compounds that are obtained as a TFA salt after purification were afforded as a free base, by dissolving the salt in EtOAc and washing with saturated aqueous K$_2$CO$_3$, or by elution through a Biotage ISOLUTE SCX-II cartridge, loading and washing with MeOH, and eluting with 2 N NH$_3$ in MeOH. Proton nuclear magnetic resonance (^{1}H NMR) spectra were recorded at 400 MHz on a Bruker spectrometer. For ^{1}H NMR spectra, chemical shifts are reported in parts per million and are reported relative to residual nondeuterated solvent signals. Coupling constants are reported in hertz. The following abbreviations (or a combination thereof) are used to describe splitting patterns: s, singlet; d, doublet; t, triplet; q, quartet; pent, pentet; m, multiplet; br, broad. Analytical thin layer chromatography (TLC) was performed on Kieselgel 60 F254 glass plates precoated with a 0.25 mm thickness of silica gel. TLC plates were visualized with UV light and iodine.

All compounds were ≥95% pure, unless otherwise noted, as measured by analytical reversed phase HPLC. Mass spectra were recorded on an Agilent 1290 series 6230 TOF spectrometer. Detection methods are diode array (DAD) at 210 and 254 nM and positive/negative electrospray ionization (ESI), with a mass range of *m/z* 100−1200. All methods use an Agilent InfinityLab Poroshell 120 EC-C18 column, with dimensions of 4.6 mm × 50 mm, 2.7 μM, fitted with a Poroshell 120 EC-C18, 2.1 mm, 1.9 μM guard. Mobile phase A was 0.1% TFA in H$_2$O, and mobile phase B was 0.1% TFA in MeCN.

Method A. Mobile phase B was 5% for 0.2 min, then a gradient from 5% to 95% B over 2.0 min, and then held for 0.45 min (0.4 mL/min flow rate), using positive ESI.

Method B. The gradient was from 40% to 95% B for 2.5 min and then held for 0.5 min (0.4 mL/min flow rate), using positive ESI.

2-(Benzotriazol-1-yl)-N-(4-phenylphenyl)-N-(3-thienylmethyl)-acetamide (6). The title compound was synthesized according to the published procedure:[21,54] ^{1}H NMR (400 MHz, DMSO-d_6) δ 8.03 (d, *J* = 8.4 Hz, 1H), 7.84−7.73 (m, 3H), 7.70 (d, *J* = 7.6 Hz, 2H), 7.60−7.51 (m, 4H), 7.48 (t, *J* = 7.6 Hz, 2H), 7.44−7.36 (m, 2H), 7.33 (s, 1H), 7.05−6.99 (m, 1H), 5.47 (s, 2H), 4.92 (s, 2H); ^{13}C NMR (101 MHz, DMSO) δ 165.6, 145.5, 140.6, 140.0, 139.4, 138.1, 134.3, 129.5, 129.2, 128.4, 128.3, 128.2, 127.6, 127.3, 127.1, 124.3, 123.8, 119.4, 111.6, 49.9, 48.7; purity ≥95% by LCMS (method A) t_R = 2.44 min, *m/z* 425.14 [M + H]$^+$; HRMS calcd for C$_{25}$H$_{21}$N$_4$OS [M + H]$^+$ 425.1431, found 425.1450.

2-(1H-Benzo[d][1,2,3]triazol-1-yl)-N-[4-(pyridin-3-yl)phenyl]-N-(thiophen-3-ylmethyl)acetamide (7). Step 1. 4-Bromo-N-(3-thienylmethyl)aniline. To a solution of **44** (493 mg, 4.4 mmol) and 4-bromoaniline (929 mg, 5.4 mmol) in DCE (44 mL) was added NaBH(OAc)$_3$ (1.42 g, 6.7 mmol), and the mixture was stirred for 1 h at rt. Saturated aqueous NH$_4$Cl (50 mL) was added, and the DCE layer separated. The aqueous layer was extracted with EtOAc (3 × 40 mL), concentrated, and purified by flash chromatography to afford a product (1.18 g, 4.4 mmol, 99%): LCMS (method A) t_R = 2.28 min, *m/z* 269.98 [M + H]$^+$.

Step 2. 2-(Benzotriazol-1-yl)-N-(4-bromophenyl)-N-(3-thienylmethyl)acetamide. To an ice-cold solution of **50** (1.27 g, 7.16 mmol) and Et$_3$N (2.00 mL, 14.32 mmol) in DCM (25 mL) was added HATU (2.72 g, 7.16 mmol), and the mixture was stirred for 30 min before the addition of 4-bromo-N-(3-thienylmethyl)aniline (1.28 g, 4.77 mmol) in a single portion. The mixture was stirred for 20 h at rt, washed with water and brine, concentrated, and purified by flash chromatography to afford a pale brown solid (1.13 g, 2.64 mmol, 55%): LCMS (method A) t_R = 2.34 min, *m/z* 429.02 [M + H]$^+$; ^{1}H NMR (400 MHz, CDCl$_3$) δ 8.05 (d, *J* = 8.4 Hz, 1H), 7.56 (d, *J* = 8.6 Hz, 2H), 7.53−7.45 (m, 2H), 7.42−7.33 (m, 1H), 7.30−7.27 (m, 1H), 7.03 (s, 1H), 7.00−6.93 (m, 3H), 5.15 (s, 2H), 4.86 (s, 2H).

Step 3. 2-(1H-Benzo[d][1,2,3]triazol-1-yl)-N-[4-(pyridin-3-yl)-phenyl]-N-(thiophen-3-ylmethyl)acetamide. A vial was charged with **47** (128 mg, 0.30 mmol), pyridine-3-boronic acid (59 mg, 0.48 mmol), and Pd(PPh$_3$)$_4$ (35 mg, 0.03 mmol). THF (3 mL) and water (0.6 mL) were added to the vial. The mixture was stirred and purged with Ar. The vial was capped and heated at 100 °C for 16 h. The reaction mixture was allowed to cool to ambient temperature, diluted with EtOAc, filtered with Celite, and purified by preparative RP-HPLC to afford a colorless solid (100 mg, 0.24 mmol, 78%): ^{1}H NMR (400 MHz, CD$_3$OD) δ 8.80 (d, *J* = 2.3 Hz, 1H), 8.55 (dd, *J* = 4.9, 1.6 Hz, 1H), 8.10 (dt, *J* = 8.2, 1.9 Hz, 1H), 7.97 (d, *J* = 8.4 Hz, 1H), 7.74 (d, *J* = 8.5 Hz, 2H), 7.66 (d, *J* = 8.4 Hz, 1H), 7.58−7.50 (m, 2H), 7.46−7.35 (m, 4H), 7.18 (s, 1H), 7.04 (d, *J* = 5.0 Hz, 1H), 5.45 (s, 2H), 4.98 (s, 2H); ^{13}C NMR (101 MHz, CDCl$_3$) δ 165.08, 149.46, 148.49, 146.25, 140.41, 139.05, 137.06, 135.43, 134.78, 133.98, 129.31, 129.20, 128.55, 128.00, 126.66, 124.87, 124.27, 124.05, 120.37, 110.05, 50.25, 48.84; purity ≥95% by LCMS (method A) t_R = 1.68 min, *m/z* 426.14 [M + H]$^+$; HRMS calcd for C$_{24}$H$_{19}$N$_5$OS [M + H]$^+$ 426.1394, found 426.1396.

2-(1H-Benzo[d][1,2,3]triazol-1-yl)-N-phenyl-N-(thiophen-3-ylmethyl)acetamide (9). Step 1. N-(Thiophen-3-ylmethyl)aniline. To a stirring solution of thiophene-3-carbaldehyde, **44** (88 μL, 1.0 mmol), and aniline (112 μL, 1.23 mmol) in DCE (10 mL) was added sodium triacetoxyborohydride (323 mg, 1.52 mmol). The mixture was stirred at rt for 2 h, saturated aqueous NH$_4$Cl (20 mL) added, and the DCE layer separated. The aqueous portion was extracted with DCM (3 × 30 mL), and the combined organics were dried (Na$_2$SO$_4$), concentrated, and purified by flash chromatography to afford a colorless solid (188 mg, 1.1 mmol, 99%): LCMS (method A) t_R = 1.57 min, *m/z* 190.06 [M + H]$^+$; ^{1}H NMR (400 MHz, CDCl$_3$) δ 7.34−7.28 (m, 1H), 7.23−7.15 (m, 3H), 7.12−7.06 (m, 1H), 6.74 (t, *J* = 7.4 Hz, 1H), 6.67 (d, *J* = 7.9 Hz, 2H), 4.34 (s, 2H), 4.20 (d, *J* = 20.9 Hz, 1H).

Step 2. 2-(1H-Benzo[d][1,2,3]triazol-1-yl)-N-phenyl-N-(thiophen-3-ylmethyl)acetamide. To a stirred solution of N-(thiophen-3-ylmethyl)aniline (208 mg, 1.1 mmol) and benzotriazol-1-yl-acetic acid (195 mg, 1.1 mmol) in DMF (5.5 mL) was added T3P (50% in EtOAc) (1.31 mL, 2.2 mmol), followed by pyridine (266 μL, 3.3 mmol). The mixture was stirred at rt for 18 h, and then saturated aqueous NaHCO$_3$ (20 mL) was added. The aqueous portion was extracted with DCM (3 × 30 mL), and the combined organics were dried (Na$_2$SO$_4$), concentrated, and purified by flash chromatography to afford a colorless solid (325 mg, 1.1 mmol, 85%): ^{1}H NMR (400 MHz, CD$_3$OD) δ 7.98 (d, *J* = 8.4 Hz, 1H), 7.66 (d, *J* = 8.4 Hz, 1H), 7.60−7.52 (m, 1H), 7.52−7.40 (m, 4H), 7.36 (dd, *J* = 5.0, 2.9 Hz, 1H), 7.30 (d, *J* = 6.7 Hz, 2H), 7.13 (s, 1H), 6.99 (d, *J* = 4.9 Hz, 1H), 5.35 (s, 2H), 4.93 (s, 2H); ^{13}C NMR (101 MHz, CDCl$_3$) δ 165.09, 146.25, 140.56, 137.18, 134.04, 130.62, 129.53, 128.68, 128.64, 128.01, 126.50, 124.84, 124.27, 120.38, 110.10, 50.23, 48.78; purity ≥95% by LCMS (method A) t_R = 2.18 min, *m/z* 349.11 [M + H]$^+$; HRMS calcd for C$_{19}$H$_{16}$N$_4$OS [M + H]$^+$ 349.1129, found 349.1139.

4-{[2-(Benzotriazol-1-yl)acetyl]-(3-thienylmethyl)amino}-benzamide (10). Step 1. Ethyl 4-(3-Thienylmethylamino)benzoate. To a stirring solution of **44** (1.75 mL, 20 mmol) and ethyl 4-aminobenzoate (3.63 g, 22 mmol) in DCE (100 mL) was added sodium triacetoxyborohydride (5.09 g, 24 mmol). The mixture was stirred at rt for 12 h, saturated aqueous NaHCO$_3$ (100 mL) added, and the DCE layer separated. The aqueous portion was extracted with DCM (3 × 50 mL), and the combined organics were dried (MgSO$_4$), concentrated, and purified by flash chromatography to afford a colorless solid (1.67 g, 6.4 mmol, 32%): LCMS (method A) t_R = 2.02 min, *m/z* 262.09 [M + H]$^+$; ^{1}H NMR (400 MHz, CDCl$_3$) δ 7.89 (d, *J* = 8.3 Hz, 1H), 7.32 (dd, *J* = 5.0, 2.9 Hz, 1H), 7.22−7.18 (m, 1H), 7.07 (dd, *J* = 5.0, 1.4 Hz, 1H), 6.65 (d, *J* = 8.3 Hz, 1H), 4.40 (s, 1H), 4.32 (q, *J* = 7.1 Hz, 1H), 1.36 (t, *J* = 7.1 Hz, 2H).

Step 2. Ethyl 4-{[2-(Benzotriazol-1-yl)acetyl]-(3-thienylmethyl)-amino}benzoate. To a stirred solution of ethyl 4-(3-thienylmethylamino)benzoate (1.67 g, 6.4 mmol) and benzotriazol-1-yl-acetic acid (1.24 g, 7.0 mmol) in EtOAc (12.75 mL) was added T3P (50% in EtOAc) (7.6 mL, 12.75 mmol), followed by pyridine

(1.54 mL, 19.12 mmol). The mixture was stirred at rt for 16 h and then washed with water (20 mL) and brine (20 mL). Purification by flash column chromatography afforded a cream-colored solid (2.52 g, 6.0 mmol, 94%): LCMS (method A) t_R = 2.00 min, m/z 421.04 [M + H]$^+$.

Step 3. 4-{[2-(Benzotriazol-1-yl)acetyl]-(3-thienylmethyl)amino}-benzoic Acid (45). To a solution of ethyl 4-{[2-(benzotriazol-1-yl)acetyl]-(3-thienylmethyl)amino}benzoate (2.52 g, 6.0 mmol) in THF (30 mL) was added 2 M LiOH (15 mL, 30 mmol), and the mixture was stirred at rt for 18 h. The mixture was acidified with 2 M HCl (20 mL), extracted with EtOAc, washed with brine, and concentrated. The crude material was purified by preparative RP-HPLC to afford a colorless solid (1.11 g, 2.83 mmol, 47%): LCMS (method A) t_R = 1.89 min, m/z 393.10 [M + H]$^+$.

Step 4. 4-{[2-(Benzotriazol-1-yl)acetyl]-(3-thienylmethyl)amino}-benzamide. To **45** (100 mg, 0.25 mmol) in THF (1.3 mL) were added 1-ethyl-3-[3-(dimethylamino)propyl]carbodiimide (98 mg, 0.51 mmol) and HOBt (41 mg, 0.31 mmol), and the mixture was stirred at rt for 20 min before the addition of NH$_4$Cl (68 mg, 1.27 mmol) and Et$_3$N (0.35 mL, 2.55 mmol). The mixture was stirred for 18 h, diluted with EtOAc, and washed with saturated aqueous NaCl. Purification by ISCO automated flash chromatography afforded the title compound as a colorless solid (27 mg, 27%): ^{1}H NMR (400 MHz, CD$_3$OD) δ 7.88 (d, J = 8.4 Hz, 1H), 7.84 (d, J = 8.1 Hz, 1H), 7.56 (d, J = 8.4 Hz, 1H), 7.45 (t, J = 7.7 Hz, 1H), 7.34 (d, J = 7.7 Hz, 1H), 7.31−7.24 (m, 3H), 7.05 (br s, 1H), 6.90 (d, J = 4.9 Hz, 1H), 5.30 (s, 2H), 4.87 (s, 2H); ^{13}C NMR (101 MHz, CD$_3$OD) δ 169.59, 165.61, 145.11, 142.97, 136.79, 134.17, 133.89, 129.10, 128.27, 127.53, 125.98, 124.20, 123.85, 118.49, 110.21, 49.45; purity ≥95% by LCMS (method A) t_R = 1.74 min, m/z 392.12 [M + H]$^+$; HRMS calcd for C$_{20}$H$_{17}$N$_5$O$_2$S [M + H]$^+$ 392.1176, found 392.1163.

4-{[2-(Benzotriazol-1-yl)acetyl]-(3-thienylmethyl)amino}-N-cyclopropylbenzamide (11). To a stirred solution of **45** (78 mg, 0.2 mmol) and cyclopropylamine (21 μL, 0.3 mmol) in DCM (1 mL) were added COMU (128 mg, 0.3 mmol) and DIPEA (105 μL, 0.6 mmol). The mixture was stirred at rt for 2 h, washed with water, and concentrated. Purification by RP-HPLC affords a colorless solid (15 mg, 35%): ^{1}H NMR (400 MHz, CD$_3$OD) δ 8.00 (d, J = 8.4 Hz, 1H), 7.88 (d, J = 8.2 Hz, 2H), 7.71−7.66 (m, 1H), 7.61−7.54 (m, 1H), 7.49−7.42 (m, 1H), 7.39 (d, J = 8.2 Hz, 2H), 7.15 (s, 1H), 7.01 (d, J = 4.9 Hz, 1H), 5.41 (s, 2H), 4.98 (s, 2H), 2.87 (dq, J = 7.2, 3.7 Hz, 1H), 0.83 (dt, J = 7.1, 3.6 Hz, 2H), 0.74−0.58 (m, 2H); ^{13}C NMR (101 MHz, CD$_3$OD) δ 169.08, 165.59, 145.11, 142.73, 136.78, 134.64, 133.88, 128.72, 127.54, 125.97, 124.20, 123.85, 118.50, 110.22, 60.13, 49.44, 22.68, 5.15; purity ≥95% by LCMS (method A) t_R = 1.91 min, m/z 432.15 [M + H]$^+$; HRMS calcd for C$_{23}$H$_{21}$N$_5$O$_2$S [M + H]$^+$ 432.1489, found 432.1506.

2-(1H-Benzo[d][1,2,3]triazol-1-yl)-N-[4-(methylsulfonamido)-phenyl]-N-(thiophen-3-ylmethyl)acetamide (12). Step 1. tert-Butyl N-[4-(3-Thienylmethylamino)phenyl]carbamate. To a solution of **44** (493 mg, 4.4 mmol) and 4-(tert-butoxycarbonylamino)aniline (1125 mg, 5.4 mmol) in DCE (44 mL) was added NaBH(OAc)$_3$ (1.42 g, 6.7 mmol), and the mixture was stirred for 1 h at rt. Saturated aqueous NH$_4$Cl (50 mL) was added, and the DCE layer separated. The aqueous layer was extracted with EtOAc (3 × 40 mL), concentrated, and purified by flash chromatography to afford a colorless solid (1.23 g, 4.0 mmol, 92%): LCMS (method A) t_R = 1.81 min, m/z 305.13 [M + H]$^+$.

Step 2. tert-Butyl N-(4-{[2-(Benzotriazol-1-yl)acetyl]-(3-thienylmethyl)amino}phenyl)carbamate. To an ice-cold solution of 2-(benzotriazol-1-yl)acetic acid (700 mg, 3.95 mmol) and Et$_3$N (1.10 mL, 7.90 mmol) in DCM (20 mL) was added HATU (1.50 g, 3.95 mmol), and the mixture was stirred for 30 min before the addition of tert-butyl N-[4-(3-thienylmethylamino)phenyl]carbamate (802 mg, 2.63 mmol) in a single portion. The mixture was stirred for 16 h at rt, washed with water and brine, and concentrated. Purification by flash chromatography afforded the title compound as a pale brown solid (1.08 g, 2.34 mmol, 89%): LCMS (method A) t_R = 2.34 min, m/z 464.18 [M + H]$^+$; ^{1}H NMR (400 MHz, CDCl$_3$) δ 8.05 (d, J = 8.4 Hz, 1H), 7.50−7.47 (m, 2H), 7.44 (d, J = 8.7 Hz, 2H), 7.36 (ddd, J =

8.1, 5.6, 2.3 Hz, 1H), 7.26−7.23 (m, 1H), 7.05−6.99 (m, 3H), 6.97 (dd, J = 5.0, 1.3 Hz, 1H), 6.62 (s, 1H), 5.15 (s, 2H), 4.84 (s, 2H), 1.53 (s, 9H).

Step 3. N-(4-Aminophenyl)-2-(benzotriazol-1-yl)-N-(3-thienylmethyl)acetamide (46). To a solution of tert-butyl N-(4-{[2-(benzotriazol-1-yl)acetyl]-(3-thienylmethyl)amino}phenyl)-carbamate (588 mg, 1.27 mmol) in DCM (3 mL) was added TFA (2 mL), and the mixture was stirred for 1 h, diluted with DCM (10 mL), and washed with saturated aqueous K$_2$CO$_3$ (20 mL), water, and saturated aqueous NaCl, affording a cream-colored solid that was used without purification (436 mg, 1.20 mmol, 95%): LCMS (method A) t_R = 1.70 min, m/z 364.14 [M + H]$^+$; ^{1}H NMR (400 MHz, CDCl$_3$) δ 8.05 (d, J = 8.4 Hz, 1H), 7.50−7.46 (m, 2H), 7.36 (ddd, J = 8.1, 5.1, 2.8 Hz, 1H), 7.25−7.22 (m, 1H), 7.04 (d, J = 2.9 Hz, 1H), 6.98 (dd, J = 5.0, 1.2 Hz, 1H), 6.86 (d, J = 8.6 Hz, 2H), 6.67 (d, J = 8.6 Hz, 2H), 5.17 (s, 2H), 4.82 (s, 2H), 3.84 (s, 2H).

Step 4. 2-(Benzotriazol-1-yl)-N-[4-(methanesulfonamido)-phenyl]-N-(3-thienylmethyl)acetamide. To a solution of **46** (87 mg, 0.24 mmol) in DCM (2 mL) were added methanesulfonyl chloride (28 μL, 0.36 mmol) and Et$_3$N (509 μL, 3.6 mmol), and the mixture was stirred for 2 h at rt. The mixture was washed with saturated aqueous NH$_4$Cl, concentrated, and purified by flash chromatography to afford a colorless solid (26 mg, 0.06 mmol, 25%): ^{1}H NMR (400 MHz, CDCl$_3$) δ 8.04 (d, J = 8.4 Hz, 1H), 7.51 (d, J = 3.9 Hz, 2H), 7.41−7.35 (m, 1H), 7.22 (d, J = 8.7 Hz, 2H), 7.05−6.98 (m, 3H), 6.97 (d, J = 4.9 Hz, 1H), 6.69 (s, 1H), 5.19 (s, 2H), 4.85 (s, 2H), 3.11 (s, 3H); ^{13}C NMR (101 MHz, CDCl$_3$) δ 165.16, 146.24, 137.90, 137.02, 136.94, 133.90, 129.96, 128.51, 128.18, 126.74, 124.91, 124.45, 121.25, 120.40, 110.09, 50.55, 48.88, 40.46; purity ≥95% by LCMS (method A) t_R = 1.92 min, m/z 442.12 [M + H]$^+$; HRMS calcd for C$_{20}$H$_{19}$N$_5$O$_3$S$_2$ [M + H]$^+$ 442.1013, found 442.1009.

2-(1H-Benzo[d][1,2,3]triazol-1-yl)-N-[4-(cyclopropanesulfonamido)phenyl]-N-(thiophen-3-ylmethyl)-acetamide (13). To a solution of **46** (36 mg, 0.1 mmol) in DCM (1 mL) were added cyclopropanesulfonyl chloride (12 μL, 0.12 mmol) and Et$_3$N (509 μL, 3.6 mmol), and the mixture was stirred at rt for 1 h. The mixture was washed with saturated aqueous NH$_4$Cl, concentrated, purified by preparative RP-HPLC, washed with aqueous K$_2$CO$_3$ to remove TFA, and concentrated to afford a colorless solid (8 mg, 0.02 mmol, 7%): ^{1}H NMR (400 MHz, CD$_3$OD) δ 7.98 (d, J = 8.4 Hz, 1H), 7.67 (d, J = 8.4 Hz, 1H), 7.56 (t, J = 7.7 Hz, 1H), 7.44 (t, J = 7.6 Hz, 1H), 7.39−7.29 (m, 3H), 7.22 (d, J = 8.8 Hz, 2H), 7.15 (s, 1H), 6.99 (d, J = 4.7 Hz, 1H), 5.38 (s, 2H), 4.91 (s, 2H), 2.65−2.56 (m, 1H), 1.10−1.03 (m, 2H), 1.00−0.93 (m, 2H); ^{13}C NMR (101 MHz, CDCl$_3$) δ 165.19, 146.22, 138.22, 136.96 (two peaks overlap), 133.98, 129.77, 128.52, 128.18, 126.69, 124.89, 124.45, 122.32, 120.38, 110.15, 50.40, 48.84, 30.73, 6.20; purity ≥95% by LCMS (method A) t_R = 2.05 min, m/z 468.12 [M + H]$^+$; HRMS calcd for C$_{22}$H$_{21}$N$_5$O$_3$S$_2$ [M + H]$^+$ 468.1170, found 468.1166.

2-(1H-Benzo[d][1,2,3]triazol-1-yl)-N-[4-(pyridin-4-yl)phenyl]-N-(thiophen-3-ylmethyl)acetamide (14). An argon-purged vial was charged with **47** (85 mg, 0.20 mmol), pyridine-4-boronic acid (39 mg, 0.32 mmol), and Pd(PPh$_3$)$_4$ (23 mg, 0.02 mmol). THF (2 mL) and water (0.4 mL) were added to the vial. The vial was capped and heated at 100 °C for 16 h. The reaction mixture was allowed to cool to ambient temperature, diluted with EtOAc, filtered with Celite, and purified by preparative RP-HPLC to afford the title compound as a colorless solid (52 mg, 0.12 mmol, 61%): ^{1}H NMR (400 MHz, CDCl$_3$) δ 8.72 (d, J = 6.3 Hz, 2H), 8.05 (d, J = 8.4 Hz, 1H), 7.69 (d, J = 8.6 Hz, 2H), 7.58−7.46 (m, 4H), 7.40−7.34 (m, 1H), 7.31−7.27 (m, 1H), 7.23 (d, J = 8.0 Hz, 2H), 7.07 (s, 1H), 7.00 (dd, J = 5.0, 1.3 Hz, 1H), 5.22 (s, 2H), 4.93 (s, 2H); ^{13}C NMR (101 MHz, CDCl$_3$) δ 165.05, 150.62, 147.26, 146.29, 141.29, 139.31, 137.00, 133.99, 129.39, 129.18, 128.54, 128.07, 126.75, 124.94, 124.33, 121.99, 120.43, 110.06, 50.29, 48.86; purity ≥95% by LCMS (method A) t_R = 1.67 min, m/z 426.13 [M + H]$^+$; HRMS calcd for C$_{24}$H$_{19}$N$_5$OS [M + H]$^+$ 426.1394, found 426.1390.

2-(1H-Benzo[d][1,2,3]triazol-1-yl)-N-[4-(pyridin-2-yl)phenyl]-N-(thiophen-3-ylmethyl)acetamide (15). A vial was charged with **47**

(86 mg, 0.20 mmol), 2-pyridinylboronic acid (49 mg, 0.40 mmol), CsCO$_3$ (261 mg, 0.80 mmol), CuCl (20 mg, 0.20 mmol), Pd(OAc)$_2$ (2 mg, 0.01 mmol), and 1,1-bis(diphenylphosphino)ferrocene (11 mg, 0.02 mmol). DMF (2 mL) was added to the vial. The mixture was stirred and purged with Ar. The vial was capped and heated at 100 °C for 15 h. The reaction mixture was allowed to cool to ambient temperature, diluted with EtOAc, filtered with Celite, and purified by flash chromatography to afford the title compound as a colorless solid (55 mg, 0.13 mmol, 65%): ^{1}H NMR (400 MHz, CD$_3$OD) δ 8.64 (d, J = 4.8 Hz, 1H), 8.05 (d, J = 8.1 Hz, 2H), 7.98 (d, J = 8.4 Hz, 1H), 7.95−7.85 (m, 2H), 7.68 (d, J = 8.4 Hz, 1H), 7.55 (t, J = 7.7 Hz, 1H), 7.46−7.34 (m, 5H), 7.18 (s, 1H), 7.03 (d, J = 4.9 Hz, 1H), 5.44 (s, 2H), 4.98 (s, 2H); ^{13}C NMR (101 MHz, CDCl$_3$) δ 165.05, 156.12, 150.20, 146.25, 140.96, 140.56, 137.37, 137.05, 134.03, 129.06, 128.99, 128.60, 127.97, 126.55, 124.92, 124.21, 123.13, 121.03, 120.34, 110.04, 50.12, 48.71; purity ≥95% by LCMS (method A) t_R = 1.76 min, m/z 426.14 [M + H]$^+$; HRMS calcd for C$_{24}$H$_{19}$N$_5$OS [M + H]$^+$ 426.1394, found 426.1397.

2-(1H-Benzo[d][1,2,3]triazol-1-yl)-N-[4-(2-methoxypyridin-3-yl)-phenyl]-N-(thiophen-3-ylmethyl)acetamide (16). A vial was charged with **47** (85 mg, 0.20 mmol), (2-methoxy-3-pyridyl)boronic acid (49 mg, 0.32 mmol), and Pd(PPh$_3$)$_4$ (23 mg, 0.02 mmol). THF (2 mL) and water (0.4 mL) were added to the vial. The mixture was stirred and purged with Ar. The vial was capped and heated at 100 °C for 16 h. The reaction mixture was allowed to cool to ambient temperature, diluted with EtOAc, filtered with Celite, and purified by flash chromatography to afford a colorless solid (90 mg, 0.20 mmol, 99%): ^{1}H NMR (400 MHz, CDCl$_3$) δ 8.21 (dd, J = 5.0, 1.9 Hz, 1H), 8.06 (d, J = 8.5 Hz, 1H), 7.69−7.60 (m, 3H), 7.53−7.47 (m, 2H), 7.41−7.33 (m, 1H), 7.31−7.27 (m, 1H), 7.18 (d, J = 8.3 Hz, 2H), 7.10 (s, 1H), 7.07−6.98 (m, 2H), 5.23 (s, 2H), 4.92 (s, 2H), 4.01 (s, 3H); ^{13}C NMR (101 MHz, CDCl$_3$) δ 164.86, 160.71, 146.50, 145.98, 139.40, 138.66, 137.80, 136.98, 133.75, 130.97, 128.31, 128.03, 127.67, 126.21, 124.48, 123.91, 122.95, 120.07, 117.25, 109.77, 53.65, 49.94, 48.55; purity ≥95% by LCMS (method A) t_R = 2.23 min, m/z 456.15 [M + H]$^+$; HRMS calcd for C$_{25}$H$_{21}$N$_5$O$_2$S [M + H]$^+$ 445.1489, found 456.1499.

2-(1H-Benzo[d][1,2,3]triazol-1-yl)-N-[4-(2-oxo-1,2-dihydropyridin-3-yl)phenyl]-N-(thiophen-3-ylmethyl)acetamide (17). Step 1. 2-(Benzotriazol-1-yl)-N-[4-(2-fluoro-3-pyridyl)phenyl]-N-(3-thienylmethyl)acetamide (48). A vial was charged with **47** (85 mg, 0.20 mmol), 2-fluoropyridine-3-boronic acid (45 mg, 0.32 mmol), and Pd(PPh$_3$)$_4$ (23 mg, 0.02 mmol). THF (2 mL) and water (0.4 mL) were added to the vial. The mixture was stirred and purged with Ar. The vial was capped and heated at 100 °C for 16 h. The reaction mixture was allowed to cool to ambient temperature, diluted with EtOAc, filtered with Celite, and purified by RP-HPLC and flash chromatography to afford a colorless solid (80 mg, 0.18 mmol, 90%): LCMS (method A) t_R = 2.16 min, m/z 444.13 [M + H]$^+$; ^{1}H NMR (400 MHz, CDCl$_3$) δ 8.25 (dt, J = 4.8, 1.6 Hz, 1H), 8.09−8.02 (m, 1H), 7.88 (ddd, J = 9.6, 7.5, 1.9 Hz, 1H), 7.67−7.60 (m, 2H), 7.53−7.47 (m, 2H), 7.41−7.31 (m, 2H), 7.30−7.27 (m, 1H), 7.21 (d, J = 8.1 Hz, 2H), 7.08 (s, 1H), 7.01 (dd, J = 5.0, 1.3 Hz, 1H), 5.23 (s, 2H), 4.93 (s, 2H).

Step 2. 2-(1H-Benzo[d][1,2,3]triazol-1-yl)-N-[4-(2-oxo-1,2-dihydropyridin-3-yl)phenyl]-N-(thiophen-3-ylmethyl)acetamide. To a solution of **48** (44 mg, 0.10 mmol) in dioxane (1 mL) was added concentrated aqueous HCl (0.08 mL, 1 mmol), and the mixture was stirred for 16 h at 80 °C. The reaction mixture was allowed to cool to room temperature, concentrated, and purified by flash chromatography to afford a colorless solid (9.0 mg, 0.02 mmol, 20%): ^{1}H NMR (400 MHz, CDCl$_3$) δ 8.06 (d, J = 8.4 Hz, 1H), 7.83 (d, J = 8.3 Hz, 2H), 7.66 (dd, J = 7.1, 2.0 Hz, 1H), 7.53−7.47 (m, 2H), 7.43 (dd, J = 6.5, 2.0 Hz, 1H), 7.40−7.33 (m, 1H), 7.30−7.26 (m, 1H), 7.20 (d, J = 8.1 Hz, 2H), 7.09 (s, 1H), 7.03 (dd, J = 5.0, 1.3 Hz, 1H), 6.44 (t, J = 6.8 Hz, 1H), 5.22 (s, 2H), 4.91 (s, 2H); ^{13}C NMR (101 MHz, CDCl$_3$) δ 165.20, 163.62, 146.30, 140.61, 140.03, 137.63, 137.30, 134.75, 134.08, 130.61, 130.28, 128.64, 128.46, 128.01, 126.53, 124.81, 124.25, 120.40, 110.11, 107.71, 50.26, 48.90; purity ≥95% by

LCMS (method A) t_R = 1.65 min, m/z 442.13 [M + H]$^+$; HRMS calcd for C$_{24}$H$_{19}$N$_5$O$_2$S [M + H]$^+$ 442.1343, found 442.1342.

2-(Benzotriazol-1-yl)-N-[4-(1-methylpyrazol-4-yl)phenyl]-N-(3-thienylmethyl)acetamide (18). A vial was charged with **47** (128 mg, 0.30 mmol), 1-methyl-1H-pyrazole-4-boronic acid, pinacol ester (75 mg, 0.36 mmol), 2 M aqueous K$_2$CO$_3$ (0.3 mL, 0.60 mmol), and Pd(dppf)Cl$_2$·DCM (12 mg, 0.02 mmol). 1,4-Dioxane (1.5 mL) was added, and the mixture degassed under a stream of Ar for 15 min and then heated at 100 °C for 16 h. The reaction mixture was diluted with DCM, washed with water, dried (Na$_2$SO$_4$), and concentrated *in vacuo*. The residue was purified by preparative RP-HPLC (5−95% MeCN in H$_2$O, 0.1% TFA), and pure fractions were combined and concentrated *in vacuo*. The free base was obtained by SCX-II chromatography (load/wash MeOH, elution with 2 N NH$_3$ in MeOH) to afford the title compound as a colorless solid (57 mg, 0.13 mmol, 44%): ^{1}H NMR (400 MHz, CD$_3$OD) δ 8.02−7.94 (m, 2H), 7.84 (s, 1H), 7.69−7.59 (m, 3H), 7.54 (t, J = 7.6 Hz, 1H), 7.46−7.39 (m, 1H), 7.37 (dd, J = 5.0, 2.9 Hz, 1H), 7.29−7.21 (m, 2H), 7.15 (d, J = 3.0 Hz, 1H), 7.04−6.98 (m, 1H), 5.40 (s, 2H), 4.93 (s, 2H), 3.93 (s, 3H); ^{13}C NMR (101 MHz, DMSO-d_6) δ 165.62, 145.46, 138.26, 138.06, 136.79, 134.27, 133.35, 129.17, 128.66, 128.22, 127.62, 127.00, 126.54, 124.25, 123.88, 121.43, 119.41, 111.58, 49.82, 48.48, 39.19; purity ≥95% by LCMS (method A) t_R = 1.84 min, m/z 429.15 [M + H]$^+$; HRMS calcd for C$_{23}$H$_{20}$N$_6$OS [M + H]$^+$ 429.1492, found 429.1497.

2-(Benzotriazol-1-yl)-N-[4-(1H-pyrazol-4-yl)phenyl]-N-(3-thienylmethyl)acetamide (19). A vial was charged with **46** (128 mg, 0.30 mmol), 4-(4,4,5,5-tetramethyl-1,3,2-dioxaborolan-2-yl)-1H-pyrazole (70 mg, 0.36 mmol), 2 M K$_2$CO$_3$ (0.3 mL, 0.60 mmol), and Pd(dppf)Cl$_2$·DCM (12 mg, 0.02 mmol). 1,4-Dioxane (1.5 mL, 0.2 M) was added, and the mixture degassed under a stream of Ar for 15 min and then heated at 110 °C for 4 h. The reaction mixture was filtered through Celite with EtOAc. The filtrate was washed with water, dried (Na$_2$SO$_4$), and concentrated *in vacuo*. The residue was purified by preparative RP-HPLC (5−95% MeCN in H$_2$O, 0.1% TFA). The pure fractions were combined and concentrated *in vacuo*. The free base was obtained by SCX-II chromatography (load/wash MeOH, elution with 2 N NH$_3$ in MeOH) to afford the title compound as a colorless solid (63 mg, 0.15 mmol, 51%): ^{1}H NMR (400 MHz, CD$_3$OD) δ 8.01−7.76 (m, 3H), 7.45 (t, J = 7.6 Hz, 1H), 7.33 (t, J = 7.7 Hz, 1H), 7.27 (dd, J = 5.0, 2.9 Hz, 1H), 7.20−7.13 (m, 2H), 7.06 (d, J = 3.0 Hz, 1H), 6.92 (d, J = 4.9 Hz, 1H), 5.31 (s, 2H), 4.84 (s, 2H); ^{13}C NMR (101 MHz, CD$_3$OD) δ 165.91, 153.23, 145.12, 137.87, 137.05, 133.91, 128.58, 127.67, 127.48, 126.61, 125.82, 124.17, 123.80, 121.07, 118.46, 110.23, 49.39; purity ≥95% by LCMS (method A) t_R = 1.71 min, m/z 415.13 [M + H]$^+$; HRMS calcd for C$_{22}$H$_{18}$N$_6$OS [M + H]$^+$ 415.1336, found 415.1328.

2-(Benzotriazol-1-yl)-N-[4-(1-methylimidazol-4-yl)phenyl]-N-(3-thienylmethyl)acetamide (20). Step 1. 2-(Benzotriazol-1-yl)-N-[4-(4,4,5,5-tetramethyl-1,3,2-dioxaborolan-2-yl)phenyl]-N-(3-thienylmethyl)acetamide. Compound **47** (717 mg, 1.68 mmol), bis(pinacolato)diboron (511 mg, 2.01 mmol), Pd(dppf)Cl$_2$·DCM (68 mg, 0.08 mmol), and KOAc (494 mg, 5.03 mmol) were combined in dioxane (8 mL) and heated to 100 °C for 16 h. Upon cooling, the mixture was filtered, concentrated, and purified by ISCO flash chromatography (0−100% EtOAc in hexanes) to afford a pale brown solid (650 mg, 1.37 mmol, 82%): LCMS (method A) t_R = 2.22 min, m/z 475.09 [M + H]$^+$; ^{1}H NMR (400 MHz, CDCl$_3$) δ 8.05 (d, J = 8.2 Hz, 1H), 7.88 (d, J = 7.2 Hz, 2H), 7.53−7.44 (m, 2H), 7.36 (t, J = 7.0 Hz, 1H), 7.30−7.21 (m, 1H), 7.14 (d, J = 7.5 Hz, 2H), 7.02 (d, J = 2.9 Hz, 1H), 6.96 (d, J = 4.9 Hz, 1H), 5.14 (s, 2H), 4.89 (s, 2H), 1.36 (s, 12H).

Step 2. 2-(Benzotriazol-1-yl)-N-[4-(1-methylimidazol-4-yl)-phenyl]-N-(3-thienylmethyl)acetamide. 2-(Benzotriazol-1-yl)-N-[4-(4,4,5,5-tetramethyl-1,3,2-dioxaborolan-2-yl)phenyl]-N-(3-thienylmethyl)acetamide (100 mg, 0.21 mmol), 4-bromo-1-methyl-1H-pyrazole (41 mg, 0.25 mmol), 2 M aqueous K$_2$CO$_3$ (0.21 mL, 0.42 mmol), and Pd(dppf)Cl$_2$·DCM (9 mg, 0.01 mmol) were combined in 1,4-dioxane (1 mL), degassed under a stream of Ar for 15 min, and then heated at 100 °C for 18 h. The reaction mixture was

filtered through Celite and washed with EtOAc. The filtrate was washed with water, dried (Na$_2$SO$_4$), and concentrated *in vacuo*. The residue was purified by preparative RP-HPLC (5−95% MeCN in H$_2$O, 0.1% TFA), and pure fractions were combined and concentrated *in vacuo*. The free base was obtained by SCX-II chromatography (load/wash MeOH, elution with 2 N NH$_3$ in MeOH) to afford the title compound as a colorless solid (36 mg, 0.08 mmol, 40%): ^{1}H NMR (400 MHz, CD$_3$OD) δ 7.98 (d, *J* = 8.4 Hz, 1H), 7.80 (d, *J* = 8.4 Hz, 2H), 7.71 (s, 1H), 7.67 (d, *J* = 8.4 Hz, 1H), 7.59−7.51 (m, 2H), 7.43 (t, *J* = 7.7 Hz, 1H), 7.37 (dd, *J* = 5.0, 2.9 Hz, 1H), 7.28 (d, *J* = 8.6 Hz, 2H), 7.16 (s, 1H), 7.01 (d, *J* = 5.0 Hz, 1H), 5.41 (s, 2H), 4.94 (s, 2H), 3.78 (s, 3H); ^{13}C NMR (101 MHz, DMSO-*d$_6$*) δ 165.61, 145.47, 139.90, 139.18, 138.51, 138.05, 134.29, 128.90, 128.22, 127.64, 126.99, 125.78, 124.25, 123.88, 119.42, 118.22, 111.59, 49.80, 48.48, 33.68; purity ≥95% by LCMS (method A) *t*$_R$ = 1.43 min, *m/z* 429.03 [M + H]$^+$; HRMS calcd for C$_{23}$H$_{20}$N$_6$OS [M + H]$^+$ 429.1492, found 429.1497.

2-(Benzotriazol-1-yl)-N-[4-(1H-imidazol-4-yl)phenyl]-N-(3-thienylmethyl)acetamide (21). Step 1. 2-(Benzotriazol-1-yl)-N-(3-thienylmethyl)-N-[4-(1-tritylimidazol-4-yl)phenyl]acetamide. Compound 49 {2-(benzotriazol-1-yl)-*N*-[4-(4,4,5,5-tetramethyl-1,3,2-dioxaborolan-2-yl)phenyl]-*N*-(3-thienylmethyl)acetamide (122 mg, 0.31 mmol)}, 4-bromo-1-trityl-imidazole (178 mg, 0.38 mmol), 2 M aqueous K$_2$CO$_3$ (0.31 mL, 0.63 mmol), and Pd(dppf)Cl$_2$·DCM (13 mg, 0.02 mmol) were combined in 1,4-dioxane (1.6 mL), degassed under a stream of Ar for 15 min, and then heated at 100 °C for 18 h. The reaction mixture was filtered through Celite and washed with EtOAc. The filtrate was washed with water, dried (Na$_2$SO$_4$), and concentrated *in vacuo*. The residue was purified by ISCO flash chromatography (24 g, 0−60% EtOAc in hexanes) to afford the title compound (117 mg, 0.18 mmol, 57%): purity 85% by LCMS (210, 254 nm) *t*$_R$ = 1.78 min, *m/z* 657.24 [M + H]$^+$.

Step 2. 2-(Benzotriazol-1-yl)-N-[4-(1H-imidazol-4-yl)phenyl]-N-(3-thienylmethyl)acetamide. Compound 49 (50 mg, 0.08 mmol) was dissolved in MeOH (380 μL), acetic acid (95 μL, 0.08 mmol) added, and the reaction mixture stirred at 65 °C for 2 h. The mixture was concentrated *in vacuo* and then purified by preparative RP-HPLC (5−40% MeCN in H$_2$O, 0.1% TFA). The free base was obtained by SCX-II chromatography (load/wash MeOH, elution with 2 N NH$_3$ in MeOH) to afford the title compound as a colorless solid (11 mg, 0.03 mmol, 35%): ^{1}H NMR (400 MHz, CD$_3$OD) δ 9.04−9.00 (m, 1H), 8.01−7.94 (m, 2H), 7.80 (d, *J* = 8.1 Hz, 2H), 7.67 (s, 1H), 7.56 (t, *J* = 7.7 Hz, 1H), 7.46−7.35 (m, 4H), 7.16 (s, 1H), 7.02 (d, *J* = 4.9 Hz, 1H), 5.44 (s, 2H), 4.98 (s, 2H); ^{13}C NMR (101 MHz, CD$_3$OD) δ 165.61, 145.47, 138.38, 138.04, 136.75, 134.29, 128.90, 128.24, 127.64, 126.99, 125.86, 124.25, 123.92, 119.42, 111.59, 49.80, 48.45; purity ≥95% by LCMS (method A) *t*$_R$ = 1.65 min, *m/z* 415.13 [M + H]$^+$; HRMS calcd for C$_{22}$H$_{18}$N$_6$OS [M + H]$^+$ 415.1336, found 415.1341.

2-(1H-Benzo[d][1,2,3]triazol-1-yl)-N-isopentyl-N-[4-(pyridin-3-yl)phenyl]acetamide (22). Step 1. 4-(3-Pyridyl)aniline (51). To a vial containing 4-bromoaniline (1.72 g, 10 mmol), pyridine-3-boronic acid (1.47 g, 12 mmol), Pd(dppf)Cl$_2$·DCM (203.66 mg, 0.25 mmol), and K$_2$CO$_3$ (2.76 g, 20 mmol) were added dioxane (25 mL) and water (5 mL). The mixture was heated to 100 °C for 18 h. The mixture was diluted with EtOAc, washed with water and brine, dried over MgSO$_4$, and concentrated. The crude material was purified by flash chromatography to afford a pale brown solid (1.45 g, 8.54 mmol, 85%): LCMS (method A) *t*$_R$ = 0.53 min, *m/z* 171.03 [M + H]$^+$.

Step 2. N-Isopentyl-4-(3-pyridyl)aniline. To a solution of isovaleraldehyde (0.05 mL, 0.50 mmol) and 51 (104 mg, 0.61 mmol) in DCE (5 mL) was added NaBH(OAc)$_3$ (161 mg, 0.76 mmol), and the mixture stirred for 2 h at rt. Saturated aqueous NH$_4$Cl (30 mL) was added, and the DCE layer separated. The aqueous layer was extracted with DCM (3 × 10 mL) and concentrated to dryness. Purification by flash chromatography afforded a yellow solid (107 mg, 0.45 mmol, 89%): ^{1}H NMR (400 MHz, CDCl$_3$) δ 8.80 (s, 1H), 8.48 (dd, *J* = 5.0, 1.6 Hz, 1H), 7.82 (dt, *J* = 8.1, 1.9 Hz, 1H), 7.43 (d, *J* = 8.7 Hz, 2H), 7.31 (dd, *J* = 8.0, 4.9 Hz, 1H), 6.69 (d, *J* = 8.7 Hz, 2H),

3.18 (t, *J* = 7.4 Hz, 2H), 1.81−1.67 (m, 1H), 1.55 (q, *J* = 7.2 Hz, 2H), 0.97 (d, *J* = 6.6 Hz, 6H).

Step 3. 2-(1H-Benzo[d][1,2,3]triazol-1-yl)-N-isopentyl-N-[4-(pyridin-3-yl)phenyl]acetamide. To a stirred solution of *N*-isopentyl-4-(3-pyridyl)aniline (48 mg, 0.2 mmol) and 50 (35 mg, 0.2 mmol) in DMF (0.5 mL) was added T3P (50% in EtOAc, 238 μL, 0.4 mmol), followed by pyridine (48 μL, 0.6 mmol). The mixture was stirred at rt for 16 h and then directly purified by RP-HPLC to afford a colorless solid (30 mg, 0.08 mmol, 38%): ^{1}H NMR (400 MHz, CDCl$_3$) δ 8.88 (d, *J* = 2.4 Hz, 1H), 8.66 (dd, *J* = 4.9, 1.7 Hz, 1H), 8.04 (d, *J* = 8.4 Hz, 1H), 7.92 (dt, *J* = 7.9, 2.0 Hz, 1H), 7.71 (d, *J* = 8.1 Hz, 2H), 7.55−7.31 (m, 6H), 5.21 (s, 2H), 3.84−3.75 (m, 2H), 1.65−1.52 (m, 1H), 1.52−1.43 (m, 2H), 0.89 (d, *J* = 6.6 Hz, 6H); ^{13}C NMR (101 MHz, CDCl$_3$) δ 164.95, 149.43, 148.49, 146.28, 140.92, 138.92, 135.58, 134.90, 134.06, 129.39, 129.25, 128.00, 124.25, 124.12, 120.36, 110.17, 50.34, 49.09, 36.63, 26.37, 22.79; purity ≥95% by LCMS (method A) *t*$_R$ = 1.76 min, *m/z* 400.21 [M + H]$^+$; HRMS calcd for C$_{24}$H$_{25}$N$_5$O [M + H]$^+$ 400.2143, found 400.2131.

2-(1H-Benzo[d][1,2,3]triazol-1-yl)-N-isopentyl-N-[4-(pyridin-3-yl)phenyl]acetamide (23). Step 1. N-(Cyclopropylmethyl)-4-(3-pyridyl)aniline. To a solution of cyclopropanecarbaldehyde (0.04 mL, 0.50 mmol) and 51 (104 mg, 0.61 mmol) in DCE (5 mL) was added NaBH(OAc)$_3$ (161.4 mg, 0.76 mmol), and the mixture was stirred for 1.5 h at rt. Saturated aqueous NH$_4$Cl (30 mL) was added, and the DCE layer separated. The aqueous layer was extracted with EtOAc (3 × 10 mL) and concentrated. Purification by flash chromatography afforded a pale cream-colored solid (100 mg, 0.45 mmol, 89%): ^{1}H NMR (400 MHz, CDCl$_3$) δ 8.80 (s, 1H), 8.52−8.46 (m, 1H), 7.81 (dt, *J* = 7.9, 2.0 Hz, 1H), 7.43 (d, *J* = 8.6 Hz, 2H), 7.30 (dd, *J* = 7.9, 4.8 Hz, 1H), 6.70 (d, *J* = 8.6 Hz, 2H), 4.03 (s, 1H), 3.01 (d, *J* = 6.9 Hz, 2H), 1.19−1.05 (m, 1H), 0.63−0.54 (m, 2H), 0.31−0.23 (m, 2H).

Step 2. 2-(1H-Benzo[d][1,2,3]triazol-1-yl)-N-isopentyl-N-[4-(pyridin-3-yl)phenyl]acetamide. To a stirred solution of *N*-(cyclopropylmethyl)-4-(3-pyridyl)aniline (45 mg, 0.2 mmol) and 50 (35 mg, 0.2 mmol) in DMF (0.5 mL) was added T3P (50% in EtOAc, 238 μL, 0.4 mmol), followed by pyridine (48 μL, 0.6 mmol). The mixture was stirred at rt for 14 h and then directly purified by RP-HPLC to afford a colorless solid (50 mg, 0.13 mmol, 65%): ^{1}H NMR (400 MHz, CDCl$_3$) δ 8.88 (d, *J* = 2.4 Hz, 1H), 8.66 (dd, *J* = 4.8, 1.6 Hz, 1H), 8.04 (d, *J* = 8.4 Hz, 1H), 7.92 (dt, *J* = 7.9, 2.0 Hz, 1H), 7.70 (d, *J* = 8.3 Hz, 2H), 7.55−7.40 (m, 5H), 7.36 (ddd, *J* = 8.1, 6.5, 1.4 Hz, 1H), 5.23 (s, 2H), 3.67 (d, *J* = 7.3 Hz, 2H), 1.08−0.96 (m, 1H), 0.54−0.45 (m, 2H), 0.23−0.14 (m, 2H); ^{13}C NMR (101 MHz, CDCl$_3$) δ 165.02, 149.46, 148.54, 146.28, 141.00, 138.96, 135.57, 134.84, 134.04, 129.54, 129.24, 127.95, 124.23, 124.09, 120.34, 110.19, 54.68, 50.36, 10.04, 4.18; purity ≥95% by LCMS (method A) *t*$_R$ = 1.59 min, *m/z* 384.18 [M + H]$^+$; HRMS calcd for C$_{23}$H$_{21}$N$_5$O [M + H]$^+$ 384.1830, found 384.1813.

2-(1H-Benzo[d][1,2,3]triazol-1-yl)-N-(cyclobutylmethyl)-N-[4-(pyridin-3-yl)phenyl]acetamide (24). Step 1. N-(Cyclobutylmethyl)-4-(3-pyridyl)aniline. To a solution of cyclobutanecarbaldehyde (0.04 mL, 0.50 mmol) and 51 (104 mg, 0.61 mmol) in DCE (5 mL) was added NaBH(OAc)$_3$ (161 mg, 0.76 mmol), and the mixture was stirred for 1 h at rt. Saturated aqueous NH$_4$Cl (30 mL) was added, and the DCE layer separated. The aqueous layer was extracted with DCM (3 × 10 mL), concentrated, and purified by flash chromatography to afford a light-yellow solid (110 mg, 0.46 mmol, 92%): ^{1}H NMR (400 MHz, CDCl$_3$) δ 8.80 (s, 1H), 8.48 (dd, *J* = 4.9, 1.7 Hz, 1H), 7.82 (dt, *J* = 8.1, 1.9 Hz, 1H), 7.42 (d, *J* = 8.7 Hz, 2H), 7.31 (dd, *J* = 7.9, 4.9 Hz, 1H), 6.69 (d, *J* = 8.7 Hz, 2H), 3.18 (d, *J* = 7.3 Hz, 2H), 2.68−2.54 (m, 1H), 2.21−2.09 (m, 2H), 2.02−1.87 (m, 3H), 1.83−1.70 (m, 3H).

Step 2. 2-(1H-Benzo[d][1,2,3]triazol-1-yl)-N-(cyclobutylmethyl)-N-[4-(pyridin-3-yl)phenyl]acetamide. To a stirred solution of *N*-(cyclobutylmethyl)-4-(3-pyridyl)aniline (48 mg, 0.2 mmol) and 50 (35 mg, 0.2 mmol) in DMF (0.5 mL) was added T3P (50% in EtOAc, 238 μL, 0.4 mmol), followed by pyridine (48 μL, 0.6 mmol). The mixture was stirred at rt for 13 h and then directly purified by RP-HPLC to afford a colorless solid (30 mg, 0.08 mmol, 38%): ^{1}H NMR

(400 MHz, MeOD) δ 8.85 (d, J = 2.4 Hz, 1H), 8.60−8.54 (m, 1H), 8.15 (dt, J = 8.2, 2.0 Hz, 1H), 7.97 (d, J = 8.4 Hz, 1H), 7.83 (d, J = 8.1 Hz, 2H), 7.64 (d, J = 8.4 Hz, 1H), 7.61−7.49 (m, 4H), 7.41 (t, J = 7.7 Hz, 1H), 5.39 (s, 2H), 3.87 (d, J = 7.6 Hz, 2H), 2.64−2.51 (m, 1H), 2.10−1.97 (m, 2H), 1.97−1.81 (m, 2H), 1.78−1.67 (m, 2H); ^{13}C NMR (101 MHz, CDCl$_3$) δ 165.20, 149.33, 148.40, 146.29, 140.92, 138.85, 135.62, 134.97, 134.03, 129.28 (two peaks overlap), 127.96, 124.24, 124.15, 120.35, 110.21, 55.14, 50.38, 34.01, 26.54, 18.64; purity ≥95% by LCMS (method A) t_R = 1.70 min, m/z 398.20 [M + H]$^+$; HRMS calcd for C$_{24}$H$_{23}$N$_5$O [M + H]$^+$ 398.1986, found 398.1969.

2-(1H-Benzo[d][1,2,3]triazol-1-yl)-N-(cyclopentylmethyl)-N-[4-(pyridin-3-yl)phenyl]acetamide (25). Step 1. N-(Cyclobutylmethyl)-4-(3-pyridyl)aniline. To a solution of cyclopentanecarbaldehyde (0.05 mL, 0.50 mmol) and **51** (104 mg, 0.61 mmol) in DCE (5 mL) was added NaBH(OAc)$_3$ (161 mg, 0.76 mmol), and the mixture was stirred for 1 h at rt. Saturated aqueous NH$_4$Cl (30 mL) was added, and the DCE layer separated. The aqueous layer was extracted with EtOAc (3 × 10 mL) and concentrated. Purification by flash chromatography afforded a light yellow solid (126 mg, 0.20 mmol, 99%): LCMS (method A) t_R = 1.55 min, m/z 253.09 [M + H]$^+$.

Step 2. 2-(1H-Benzo[d][1,2,3]triazol-1-yl)-N-(cyclopentylmethyl)-N-[4-(pyridin-3-yl)phenyl]acetamide. To an ice-cold solution of **50** (53 mg, 0.30 mmol) and Et$_3$N (0.08 mL, 0.60 mmol) in DCM (1 mL) was added HATU (114 mg, 0.30 mmol), and the mixture was stirred for 30 min before the addition of *N*-(cyclopentylmethyl)-4-(3-pyridyl)aniline (51 mg, 0.20 mmol) in a single portion. The mixture was stirred for 20 h at rt, washed with water and brine, and concentrated. Purification by flash chromatography afforded the title compound as a colorless solid (69.1 mg, 0.17 mmol, 84%): ^{1}H NMR (400 MHz, MeOD) δ 8.85 (d, J = 2.4 Hz, 1H), 8.60−8.54 (m, 1H), 8.15 (dt, J = 8.0, 2.0 Hz, 1H), 7.97 (d, J = 8.4 Hz, 1H), 7.84 (d, J = 8.4 Hz, 2H), 7.69−7.59 (m, 3H), 7.60−7.50 (m, 2H), 7.41 (t, J = 7.7 Hz, 1H), 5.42 (s, 2H), 3.79 (d, J = 7.7 Hz, 2H), 2.19−2.06 (m, 1H), 1.82−1.71 (m, 2H), 1.69−1.50 (m, 4H), 1.35−1.24 (m, 2H); ^{13}C NMR (101 MHz, CDCl$_3$) δ 165.29, 149.47, 148.54, 146.25, 140.96, 138.86, 135.54, 134.81, 134.03, 129.30, 129.23, 127.95, 124.22, 124.08, 120.31, 110.19, 54.82, 50.40, 38.25, 30.65, 25.52; purity ≥95% by LCMS (method A) t_R = 1.81 min, m/z 412.21 [M + H]$^+$; HRMS calcd for C$_{25}$H$_{25}$N$_5$O [M + H]$^+$ 412.2143, found 412.2125.

2-(1H-Benzo[d][1,2,3]triazol-1-yl)-N-[4-(pyridin-3-yl)phenyl]-N-[(tetrahydrofuran-3-yl)methyl]acetamide (26). Step 1. 4-(3-Pyridyl)-N-(tetrahydrofuran-3-ylmethyl)aniline. To a solution of tetrahydrofuran-3-carbaldehyde (50% aqueous, 91 μL, 0.50 mmol) and **51** (98 mg, 0.58 mmol) in DCE (5 mL) was added NaBH(OAc)$_3$ (148 mg, 0.70 mmol), and the mixture was stirred for 1 h at rt. Saturated aqueous NH$_4$Cl (30 mL) was added, and the DCE layer separated. The aqueous layer was extracted with EtOAc (3 × 10 mL) and concentrated. Purification by flash chromatography afforded a yellow oil (114 mg, 0.45 mmol, 90%): LCMS (method A) t_R = 1.15 min, m/z 255.08 [M + H]$^+$.

Step 2. 2-(1H-Benzo[d][1,2,3]triazol-1-yl)-N-[4-(pyridin-3-yl)phenyl]-N-[(tetrahydrofuran-3-yl)methyl]acetamide. To a stirred solution of 4-(3-pyridyl)-*N*-(tetrahydrofuran-3-ylmethyl)aniline (51 mg, 0.2 mmol) and **50** (35 mg, 0.2 mmol) in DMF (0.5 mL) was added T3P (50% in EtOAc, 238 μL, 0.4 mmol), followed by pyridine (48 μL, 0.6 mmol). The mixture was stirred at rt for 16 h and then washed with water (20 mL) and brine (20 mL). Purification by flash chromatography afforded a colorless solid (47 mg, 0.11 mmol, 57%): ^{1}H NMR (400 MHz, CDCl$_3$) δ 8.88 (s, 1H), 8.67 (d, J = 4.8 Hz, 1H), 8.05 (d, J = 8.4 Hz, 1H), 7.95 (d, J = 8.1 Hz, 1H), 7.71 (d, J = 8.3 Hz, 2H), 7.53−7.45 (m, 3H), 7.42 (d, J = 8.1 Hz, 2H), 7.40−7.33 (m, 1H), 5.29−5.17 (m, 2H), 3.99 (dd, J = 13.5, 7.7 Hz, 1H), 3.90−3.68 (m, 4H), 3.51−3.43 (m, 1H), 2.59−2.48 (m, 1H), 2.06−1.94 (m, 1H), 1.68−1.64 (m, 1H); ^{13}C NMR (101 MHz, CDCl$_3$) δ 165.61, 149.54, 148.48, 146.26, 140.75, 139.18, 135.41, 134.88, 133.98, 129.54, 129.09, 128.06, 124.32, 124.14, 120.40, 110.04, 71.59, 68.00, 52.86, 50.32, 38.45, 30.46; purity ≥95% by LCMS (method A) t_R = 1.44 min, m/z 414.19 [M + H]$^+$; HRMS calcd for C$_{24}$H$_{23}$N$_5$O$_2$ [M + H]$^+$ 414.1935, found 414.1936.

2-(Benzotriazol-1-yl)-N-[4-(3-pyridyl)phenyl]-N-(thiazol-4-ylmethyl)acetamide (27). Step 1. 4-(3-Pyridyl)-N-(thiazol-4-ylmethyl)aniline. To a solution of **51** (34 mg, 0.20 mmol) and thiazole-4-carbaldehyde (25 mg, 0.22 mmol) in DCM (1 mL) was added AcOH (50 μL), and the mixture was stirred for 30 min before the addition of NaBH(OAc)$_3$ (64 mg, 0.30 mmol). The mixture was stirred for 16 h, diluted with DCM, washed with saturated aqueous NaHCO$_3$, concentrated, and purified by ISCO flash chromatography (0−100% EtOAc in hexanes) to afford a cream-colored solid (47 mg, 0.18 mmol, 88%): LCMS (method A) t_R = 1.13 min, m/z 268.01 [M + H]$^+$.

Step 2. 2-(Benzotriazol-1-yl)-N-[4-(3-pyridyl)phenyl]-N-(thiazol-4-ylmethyl)acetamide. To a solution of 4-(3-pyridyl)-*N*-(thiazol-4-ylmethyl)aniline (47 mg, 0.18 mmol) and **50** (31 mg, 0.18 mmol) in DMF (1 mL) were added T3P (50% in DMF, 0.21 mL, 0.35 mmol) and pyridine (43 μL, 0.53 mmol). The mixture was stirred at rt for 16 h, filtered, and purified by preparative RP-HPLC. The free base was obtained by SCX-II chromatography (eluent, 2 N NH$_3$/MeOH) affording a colorless solid (27 mg, 0.06 mmol, 36%): ^{1}H NMR (400 MHz, MeOH-d_4) δ 8.99 (s, 1H), 8.82 (s, 1H), 8.61−8.52 (m, 1H), 8.12 (d, J = 8.0 Hz, 1H), 7.99 (d, J = 8.4 Hz, 1H), 7.77 (d, J = 8.0 Hz, 2H), 7.71 (d, J = 8.4 Hz, 1H), 7.60−7.47 (m, 6H), 7.43 (t, J = 7.7 Hz, 1H), 5.50 (s, 2H), 5.18 (s, 2H); ^{13}C NMR (101 MHz, DMSO-d_6) δ 165.61, 154.83, 152.81, 149.31, 148.20, 145.46, 140.95, 134.92, 134.70, 134.19, 129.38, 128.66, 127.61, 124.37, 124.26, 119.42, 117.47, 111.58, 50.00, 49.50; purity ≥95% by LCMS (method A) t_R = 1.24 min, m/z 427.13 [M + H]$^+$; HRMS calcd for C$_{23}$H$_{18}$N$_6$OS [M + H]$^+$ 427.1336, found 427.1339.

2-(Benzotriazol-1-yl)-N-[(3-chlorophenyl)methyl]-N-[4-(3-pyridyl)phenyl]acetamide (28). Step 1. N-[(3-Chlorophenyl)-methyl]-4-(3-pyridyl)aniline. To a solution of **51** (34 mg, 0.20 mmol) and 3-chlorobenzaldehyde (25 μL, 0.22 mmol) in DCM (1 mL) was added AcOH (50 μL), and the mixture was stirred for 30 min before the addition of NaBH(OAc)$_3$ (64 mg, 0.30 mmol). The mixture was stirred for 16 h, diluted with DCM, and washed with saturated aqueous NaHCO$_3$. Concentration and purification by ISCO flash chromatography (0−100% EtOAc in hexanes) afforded a cream-colored solid (51 mg, 0.17 mmol, 86%): LCMS (method A) t_R = 1.63 min, m/z 295.02 [M + H]$^+$.

Step 2. 2-(Benzotriazol-1-yl)-N-[(3-chlorophenyl)methyl]-N-[4-(3-pyridyl)phenyl]acetamide. To a solution of *N*-[(3-chlorophenyl)-methyl]-4-(3-pyridyl)aniline (51 mg, 0.17 mmol) and **50** (30 mg, 0.17 mmol) in DMF (1 mL) were added T3P (50% in DMF, 206 μL, 0.35 mmol) and pyridine (42 μL, 0.52 mmol). The mixture was stirred at rt for 16 h, filtered, and purified by preparative RP-HPLC. The free base was obtained after SCX-II chromatography (eluent, 2 N NH$_3$/MeOH) affording a colorless solid (48 mg, 0.11 mmol, 61%): ^{1}H NMR (400 MHz, DMSO-d_6) δ 8.93 (s, 1H), 8.59 (d, J = 4.8 Hz, 1H), 8.11 (d, J = 8.0 Hz, 1H), 8.04 (d, J = 8.4 Hz, 1H), 7.86 (d, J = 8.1 Hz, 2H), 7.82 (d, J = 8.4 Hz, 1H), 7.64 (d, J = 8.0 Hz, 2H), 7.55 (t, J = 7.7 Hz, 1H), 7.50 (dd, J = 7.9, 4.8 Hz, 1H), 7.44−7.31 (m, 4H), 7.26 (d, J = 6.1 Hz, 1H), 5.55 (s, 2H), 4.98 (s, 2H); ^{13}C NMR (101 MHz, DMSO-d_6) δ 166.19, 149.33, 148.20, 145.44, 140.58, 139.92, 137.49, 134.83, 134.69, 134.20, 133.58, 130.80, 129.24, 128.74, 128.17, 127.83, 127.63, 127.07, 124.36, 124.28, 119.43, 111.57, 52.49, 49.98; purity ≥95% by LCMS (method A) t_R = 1.60 min, m/z 454.14 [M + H]$^+$; HRMS calcd for C$_{26}$H$_{20}$ClN$_5$O [M + H]$^+$ 454.1429, found 454.1445.

2-(Benzotriazol-1-yl)-N-[(3-chloro-4-fluorophenyl)methyl]-N-[4-(3-pyridyl)phenyl]acetamide (29). Step 1. N-[(3-Chloro-4-fluorophenyl)methyl]-4-(3-pyridyl)aniline. 3-Chloro-4-fluoro-benzaldehyde (35 mg, 0.22 mmol) and **51** (34 mg, 0.20 mmol) were dissolved in a DCM/AcOH solvent (0.2 M, 20:1) and stirred for 30 min at 23 °C. To the mixture was added NaBH(OAc)$_3$ (63.6 mg, 0.30 mmol), and the mixture was stirred at 23 °C for 18 h. The reaction mixture was diluted with DCM and washed with saturated aqueous NaHCO$_3$. The organic layer was dried (Na$_2$SO$_4$), filtered, and concentrated *in vacuo*. The resulting residue was purified by ISCO automated flash chromatography (4 g, 0−100% EtOAc in hexanes) to afford a cream-colored solid (19 mg, 0.06 mmol, 30%): LCMS (method A) t_R = 1.86 min, m/z 313.09 [M + H]$^+$.

Step 2. 2-(Benzotriazol-1-yl)-N-[(3-chloro-4-fluorophenyl)-methyl]-N-[4-(3-pyridyl)phenyl]acetamide. Pyridine (14 μL, 0.17 mmol) and T3P (50% in DMF, 78 μL, 0.12 mmol) were added to a solution of *N*-[(3-chloro-4-fluorophenyl)methyl]-4-(3-pyridyl)aniline (18 mg, 0.06 mmol) and **50** (11 mg, 0.06 mmol) in DMF (0.5 mL, 0.2 M), and the mixture was stirred at 23 °C for 18 h. The concentrated reaction mixture was purified by preparative RP-HPLC (5−50% MeCN in H$_2$O, 0.1% TFA), and pure fractions were combined and concentrated *in vacuo*. The free base was obtained by SCX-II chromatography (load/wash MeOH, elution with 2 N NH$_3$ in MeOH) to afford the title compound as a colorless solid (7.5 mg, 0.02 mmol, 28%): ^{1}H NMR (400 MHz, CD$_3$OD) δ 9.02 (d, *J* = 2.3 Hz, 1H), 8.74 (dd, *J* = 5.5, 1.5 Hz, 1H), 8.61−8.54 (m, 1H), 7.98 (d, *J* = 8.5 Hz, 1H), 7.91 (dd, *J* = 8.1, 5.5 Hz, 1H), 7.83 (d, *J* = 8.4 Hz, 2H), 7.69 (d, *J* = 8.4 Hz, 1H), 7.59−7.52 (m, 1H), 7.50−7.34 (m, 4H), 7.24−7.13 (m, 2H), 5.49 (s, 2H), 4.99 (s, 2H); ^{13}C NMR (101 MHz, DMSO-d_6) δ 165.71, 157.68, 155.23, 148.85, 147.71, 144.97, 139.96, 137.06, 134.86, 134.82, 134.33, 134.21, 133.71, 130.02, 128.81, 128.28, 127.15, 123.88, 119.46, 119.28, 118.95, 116.97, 116.76, 111.09, 51.42, 49.51; ^{19}F NMR (376 MHz, CD$_3$OD) δ −112.43; purity ≥95% by LCMS (method A) t_R = 1.86 min, *m/z* 472.13 [M + H]$^+$; HRMS calcd for C$_{26}$H$_{19}$ClFN$_5$O [M + H]$^+$ 472.1335, found 472.1345.

*2-(Benzotriazol-1-yl)-N-[(3,4-dichlorophenyl)methyl]-N-[4-(3-pyridyl)phenyl]acetamide (**30**). Step 1. N-[(3,4-Dichlorophenyl)-methyl]-4-(3-pyridyl)aniline.* 3,4-Dichlorobenzaldehyde (39 mg, 0.22 mmol) and **51** (34 mg, 0.20 mmol) were dissolved in a DCM/AcOH solvent (0.2 M, 20:1) and stirred for 30 min at rt. To the mixture was added NaBH(OAc)$_3$ (63.6 mg, 0.30 mmol), and the mixture was stirred at rt for 18 h. The reaction mixture was diluted with DCM and washed with saturated aqueous NaHCO$_3$. The organic layer was dried (Na$_2$SO$_4$), filtered, and concentrated *in vacuo*. The resulting residue was purified by ISCO flash chromatography (4 g, 0−100% EtOAc in hexanes) to afford *N*-[(3,4-dichlorophenyl)methyl]-4-(3-pyridyl)-aniline as a cream-colored solid (40 mg, 0.12 mmol, 61%): LCMS (method A) t_R = 1.93 min, *m/z* 329.06 [M + H]$^+$.

Step 2. 2-(Benzotriazol-1-yl)-N-[(3,4-dichlorophenyl)methyl]-N-[4-(3-pyridyl)phenyl]acetamide. Pyridine (29 μL, 0.36 mmol) and T3P (50% in DMF, 160 μL, 0.24 mmol) were added to a solution of *N*-[(3,4-dichlorophenyl)methyl]-4-(3-pyridyl)aniline (39 mg, 0.12 mmol) and **50** (23 mg, 0.13 mmol, 1.1 equiv) in DMF (0.6 mL, 0.2 M) and stirred at rt for 18 h. The reaction mixture was purified directly by preparative RP-HPLC (5−50% MeCN in H$_2$O, 0.1% TFA). The product-containing fractions were combined and concentrated *in vacuo*. The free base was obtained by SCX-II chromatography (load/wash MeOH, elution with 2 N NH$_3$ in MeOH) to afford the title compound as a colorless solid (36 mg, 0.07 mmol, 62%): ^{1}H NMR (400 MHz, CD$_3$OD) δ 9.02 (d, *J* = 2.3 Hz, 1H), 8.74 (dd, *J* = 5.5, 1.5 Hz, 1H), 8.57 (dd, *J* = 6.1, 4.1 Hz, 1H), 7.98 (d, *J* = 8.4 Hz, 1H), 7.92 (dd, *J* = 8.1, 5.4 Hz, 1H), 7.87−7.80 (m, 2H), 7.69 (d, *J* = 8.4 Hz, 1H), 7.58−7.53 (m, 1H), 7.51−7.39 (m, 5H), 7.20 (d, *J* = 8.3 Hz, 1H), 5.50 (s, 2H), 5.00 (s, 2H); ^{13}C NMR (101 MHz, DMSO-d_6) δ 166.23, 158.89, 158.53, 146.78, 145.79, 145.45, 140.92, 138.57, 137.69, 135.88, 134.17, 131.54, 131.10, 130.45, 130.41, 129.32, 128.98, 128.82, 127.65, 125.47, 124.30, 119.44, 111.58, 51.91, 50.00; purity ≥95% by LCMS (method A) t_R = 1.93 min, *m/z* 488.10 [M + H]$^+$; HRMS calcd for C$_{26}$H$_{19}$Cl$_2$N$_5$O [M + H]$^+$ 488.1039, found 488.1048.

*2-(Benzotriazol-1-yl)-N-[(3-chloro-5-fluorophenyl)methyl]-N-[4-(3-pyridyl)phenyl]acetamide (**31**). Step 1. N-[(3-Chloro-5-fluorophenyl)methyl]-4-(3-pyridyl)aniline.* 3-Chloro-5-fluoro-benzaldehyde (35 mg, 0.22 mmol) and **51** (34 mg, 0.20 mmol) were dissolved in a DCM/AcOH solvent (0.2 M, 20:1) and stirred for 30 min at 23 °C. To the mixture was added NaBH(OAc)$_3$ (64 mg, 0.30 mmol), and the mixture was stirred at rt for 18 h. The reaction mixture was diluted with DCM and washed with saturated aqueous NaHCO$_3$. The organic layers were dried (Na$_2$SO$_4$), filtered, and concentrated *in vacuo*. The resulting residue was purified by ISCO automated flash chromatography (4 g, 0−100% EtOAc in hexanes) to

afford a colorless solid (56 mg, 0.18 mmol, 90%): LCMS (method A) t_R = 1.87 min, *m/z* 313.09 [M + H]$^+$.

Step 2. 2-(Benzotriazol-1-yl)-N-[(3-chloro-5-fluorophenyl)-methyl]-N-[4-(3-pyridyl)phenyl]acetamide. Pyridine (40 μL, 0.50 mmol) and T3P (50% in DMF, 224 μL, 0.33 mmol) were added to a solution of *N*-[(3-chloro-5-fluorophenyl)methyl]-4-(3-pyridyl)aniline (52 mg, 0.17 mmol) and **50** (32 mg, 0.18 mmol) in DMF (0.8 mL) and stirred at rt for 18 h. The reaction mixture was purified directly by preparative RP-HPLC (5−50% MeCN in H$_2$O, 0.1% TFA). The product-containing fractions were combined and concentrated *in vacuo*. The free base was obtained by SCX-II chromatography (load/wash MeOH, elution with 2 N NH$_3$ in MeOH) to afford the title compound as a colorless solid (26 mg, 0.06 mmol, 33%): ^{1}H NMR (400 MHz, CD$_3$OD) δ 8.81 (s, 1H), 8.56 (d, *J* = 4.8 Hz, 1H), 8.11 (dt, *J* = 7.9, 2.0 Hz, 1H), 7.98 (d, *J* = 8.4 Hz, 1H), 7.76 (d, *J* = 8.4 Hz, 2H), 7.68 (d, *J* = 8.4 Hz, 1H), 7.54 (dd, *J* = 8.3, 5.9 Hz, 2H), 7.49−7.38 (m, 3H), 7.17−7.09 (m, 2H), 7.02 (d, *J* = 9.3 Hz, 1H), 5.51 (s, 2H), 5.00 (s, 2H); ^{13}C NMR (101 MHz, DMSO-d_6) δ 166.38, 163.87, 161.41, 149.15, 148.04, 145.45, 142.12, 142.04, 140.55, 137.47, 134.91, 134.47, 134.36, 134.17, 129.17, 128.80, 127.62, 124.44, 124.28, 119.43, 115.53, 115.28, 114.22, 114.00, 111.59, 52.19, 50.01; ^{19}F NMR (376 MHz, CD$_3$OD) δ −110.58; purity ≥95% by LCMS (method A) t_R = 1.87 min, *m/z* 472.13 [M + H]$^+$; HRMS calcd for C$_{26}$H$_{19}$ClFN$_5$O [M + H]$^+$ 472.1335, found 472.1343.

*2-(Benzotriazol-1-yl)-N-[(3,5-dichlorophenyl)methyl]-N-[4-(3-pyridyl)phenyl]acetamide (**32**). Step 1. N-[(3,5-Dichlorophenyl)-methyl]-4-(3-pyridyl)aniline.* Compound **51** (34 mg, 0.20 mmol) and 3,5-dichlorobenzaldehyde (39 mg, 0.22 mmol) were dissolved in a DCM/AcOH solvent (0.2 M, 20:1) and stirred for 30 min at 23 °C. To the mixture was added NaHB(OAc)$_3$ (64 mg, 0.30 mmol), and the mixture was stirred at rt for 18 h. The reaction mixture was diluted with DCM and washed with saturated aqueous NaHCO$_3$. The organic layers were dried (Na$_2$SO$_4$), filtered, and concentrated *in vacuo*. The resulting residue was purified by ISCO automated flash chromatography (4 g, 0−100% EtOAc in hexanes) to afford a colorless solid (65 mg, 0.20 mmol, 99%): LCMS (method A) t_R = 1.95 min, *m/z* 329.06 [M + H]$^+$.

Step 2. 2-(Benzotriazol-1-yl)-N-[(3,5-dichlorophenyl)methyl]-N-[4-(3-pyridyl)phenyl]acetamide. Pyridine (46 μL, 0.57 mmol) and T3P (50% in DMF, 258 μL, 0.38 mmol) were added to a solution of *N*-[(3,5-dichlorophenyl)methyl]-4-(3-pyridyl)aniline (63 mg, 0.19 mmol) and **50** (37 mg, 0.21 mmol) in DMF (1 mL) and stirred at rt for 1 h. The reaction mixture was purified directly by preparative RP-HPLC (5−50% MeCN in H$_2$O, 0.1% TFA). The product-containing fractions were combined and concentrated *in vacuo*. The free base was obtained by SCX-II chromatography (load/wash MeOH, elution with 2 N NH$_3$ in MeOH) to afford the title compound as a beige powder (76 mg, 0.16 mmol, 81%): ^{1}H NMR (400 MHz, DMSO-d_6) δ 8.93 (d, *J* = 2.4 Hz, 1H), 8.59 (dd, *J* = 4.6, 1.7 Hz, 1H), 8.11 (d, *J* = 7.7 Hz, 1H), 8.03 (d, *J* = 8.4 Hz, 2H), 7.87 (d, *J* = 8.0 Hz, 2H), 7.80 (d, *J* = 8.4 Hz, 1H), 7.67 (d, *J* = 8.0 Hz, 2H), 7.58−7.46 (m, 3H), 7.43−7.35 (m, 3H), 5.56 (s, 2H), 4.98 (s, 2H); ^{13}C NMR (101 MHz, DMSO-d_6) δ 166.42, 149.34, 148.21, 145.45, 141.80, 140.49, 134.81, 134.70, 134.57, 134.15, 129.14, 128.79, 127.62, 127.53, 127.05, 124.37, 124.29, 119.44, 111.57, 52.09, 50.03; purity ≥95% by LCMS (method A) t_R = 1.95 min, *m/z* 488.10 [M + H]$^+$; HRMS calcd for C$_{26}$H$_{19}$Cl$_2$N$_5$O [M + H]$^+$ 488.1039, found 488.1049.

*2-(Benzotriazol-1-yl)-N-[(3-chloro-5-methylphenyl)methyl]-N-[4-(3-pyridyl)phenyl]acetamide (**33**). Step 1. N-[(3-Chloro-5-methylphenyl)methyl]-4-(3-pyridyl)aniline.* Compound **51** (34 mg, 0.20 mmol) and 3-chloro-5-methyl-benzaldehyde (28 μL, 0.22 mmol) were added to DCM (1 mL) and acetic acid (0.05 mL) and stirred for 30 min before the addition of NaHB(OAc)$_3$ (64 mg, 0.30 mmol) and then stirred for 18 h at rt. The mixture was diluted with DCM and washed with saturated aqueous NaHCO$_3$. The organic layers were separated and concentrated to dryness. Purification by ISCO automated flash chromatography (4 g, 0−100% EtOAc in hexanes) afforded a straw-colored oil (54 mg, 0.17 mmol, 87%): LCMS (method A) t_R = 1.94 min, *m/z* 309.12 [M + H]$^+$.

R

Step 2. 2-(Benzotriazol-1-yl)-N-[(3-chloro-5-methylphenyl)-methyl]-N-[4-(3-pyridyl)phenyl]acetamide. To a solution of *N*-[(3-chloro-5-methylphenyl)methyl]-4-(3-pyridyl)aniline (54 mg, 0.17 mmol) and **50** (31 mg, 0.17 mmol) in DMF (1 mL) were added T3P (50% in EtOAc, 0.21 mL, 0.35 mmol) and pyridine (43 μL, 0.53 mmol). The mixture was stirred at rt for 16 h, filtered, and purified by preparative RP-HPLC. The free base was obtained by SCX-II chromatography (eluent, 2 N NH$_3$/MeOH) affording a colorless solid (39 mg, 0.08 mmol, 48%): ^{1}H NMR (400 MHz, DMSO-d_6) δ 8.93 (s, 1H), 8.60 (d, *J* = 4.9 Hz, 1H), 8.12 (d, *J* = 8.0 Hz, 1H), 8.04 (d, *J* = 8.4 Hz, 1H), 7.86 (d, *J* = 8.1 Hz, 2H), 7.81 (d, *J* = 8.4 Hz, 1H), 7.64 (d, *J* = 8.1 Hz, 2H), 7.55 (t, *J* = 7.6 Hz, 1H), 7.50 (dd, *J* = 8.0, 4.8 Hz, 1H), 7.40 (t, *J* = 7.6 Hz, 1H), 7.16 (d, *J* = 8.4 Hz, 2H), 7.06 (s, 1H), 5.55 (s, 2H), 4.94 (s, 2H), 2.29 (s, 3H); ^{13}C NMR (101 MHz, DMSO) δ 166.18, 151.21, 149.32, 148.20, 145.45, 140.64, 139.64, 137.47, 134.84, 134.69, 134.16, 133.33, 129.19, 128.73, 128.23, 127.63, 125.14, 124.37, 124.29, 119.44, 111.55, 52.47, 50.00, 21.12; purity ≥95% by LCMS (method A) t_R = 1.91 min, *m/z* 468.16 [M + H]$^+$; HRMS calcd for C$_{27}$H$_{22}$ClN$_5$O [M + H]$^+$ 468.1586, found 468.1592.

2-(Benzotriazol-1-yl)-N-[(5-chloro-3-pyridyl)methyl]-N-[4-(3-pyridyl)phenyl]acetamide (34). Step 1. N-[(5-Chloro-3-pyridyl)-methyl]-4-(3-pyridyl)aniline. Compound **51** (34 mg, 0.20 mmol) and 5-chloropyridine-3-benzaldehyde (31 mg, 0.22 mmol) were added to DCM (1 mL) and acetic acid (0.05 mL) and stirred for 30 min before the addition of NaHB(OAc)$_3$ (64 mg, 0.30 mmol) and then stirred for 18 h at rt. The mixture was diluted with DCM and washed with saturated aqueous NaHCO$_3$. The organic layers were separated and concentrated to dryness. Purification by ISCO flash chromatography (4 g, 0–100% EtOAc in hexanes) afforded a cream-colored solid (53 mg, 0.18 mmol, 90%): LCMS (method A) t_R = 1.45 min, *m/z* 296.10 [M + H]$^+$.

Step 2. 2-(Benzotriazol-1-yl)-N-[(5-chloro-3-pyridyl)methyl]-N-[4-(3-pyridyl)phenyl]acetamide. To a solution of *N*-[(5-chloro-3-pyridyl)methyl]-4-(3-pyridyl)aniline (53 mg, 0.18 mmol) and **50** (32 mg, 0.17 mmol) in DMF (1 mL) were added T3P (50% in EtOAc, 0.21 mL, 0.35 mmol) and pyridine (43 μL, 0.53 mmol). The mixture was stirred at rt for 16 h, filtered, and purified by preparative RP-HPLC. The free base was obtained by SCX-II chromatography (eluent, 2 N NH$_3$/MeOH) affording a colorless solid (42 mg, 0.09 mmol, 52%): ^{1}H NMR (400 MHz, DMSO-d_6) δ 8.94 (d, *J* = 2.5 Hz, 1H), 8.60 (dd, *J* = 4.8, 1.7 Hz, 1H), 8.55 (d, *J* = 2.5 Hz, 1H), 8.46 (s, 1H), 8.12 (d, *J* = 8.0 Hz, 1H), 8.03 (d, *J* = 8.4 Hz, 1H), 7.91–7.85 (m, 3H), 7.82 (d, *J* = 8.4 Hz, 1H), 7.69 (d, *J* = 8.0 Hz, 2H), 7.59–7.48 (m, 2H), 7.40 (t, *J* = 7.6 Hz, 1H), 5.54 (s, 2H), 5.03 (s, 2H); ^{13}C NMR (101 MHz, DMSO-d_6) δ 166.36, 149.36, 148.21, 147.97, 147.65, 145.44, 140.39, 137.63, 135.86, 134.86, 134.81, 134.18, 131.41, 129.30, 128.84, 127.63, 124.37, 124.29, 119.43, 111.61, 50.22, 50.01; purity ≥95% by LCMS (method A) t_R = 1.59 min, *m/z* 455.14 [M + H]$^+$; HRMS calcd for C$_{25}$H$_{19}$ClN$_6$O [M + H]$^+$ 455.1382, found 455.1393.

2-(1H-Benzo[d][1,2,3]triazol-1-yl)-N-(3-chlorobenzyl)-N-[4-(2-oxo-1,2-dihydropyridin-3-yl)phenyl]acetamide (35). Step 1. 4-Bromo-N-[(3-chlorophenyl)methyl]aniline (58). To a solution of 3-chlorobenzaldehyde (1.13 mL, 10.0 mmol) and 4-bromoaniline (2.06 g, 12.0 mmol) in DCE (50 mL) was added NaHB(OAc)$_3$ (2.76 g, 13.0 mmol), and the mixture was stirred for 2 h at rt. Saturated aqueous NH$_4$Cl (50 mL) was added, and the DCE layer separated. The aqueous layer was extracted with EtOAc (3 × 30 mL) and concentrated. Purification by ISCO automated flash chromatography afforded a tan oil (2.0 g, 6.74 mmol, 67%): ^{1}H NMR (400 MHz, CDCl$_3$) δ 7.36 (s, 1H), 7.34–7.21 (m, 6H), 6.51 (d, *J* = 8.8 Hz, 2H), 4.32 (s, 2H).

Step 2. N-[(3-Chlorophenyl)methyl]-4-(2-fluoro-3-pyridyl)aniline. To a vial containing 4-bromo-*N*-[(3-chlorophenyl)methyl]aniline (415 mg, 1.4 mmol), 2-fluoropyridine-3-boronic acid (237 mg, 1.68 mmol), Pd(dppf)Cl$_2$·DCM (57 mg, 0.07 mmol), and K$_2$CO$_3$ (386.99 mg, 2.8 mmol) were added dioxane (3.5 mL) and water (0.7 mL). The mixture was heated to 100 °C for 20 h. The mixture was diluted with EtOAc, washed with water and brine, dried over Na$_2$SO$_4$, and

concentrated. The mixture was purified by ISCO automated flash chromatography to afford the title intermediate (157 mg, 0.50 mmol, 36%): ^{1}H NMR (400 MHz, CDCl$_3$) δ 8.10 (dt, *J* = 4.9, 1.6 Hz, 1H), 7.81 (ddd, *J* = 9.6, 7.4, 2.0 Hz, 1H), 7.42 (dd, *J* = 8.6, 1.8 Hz, 2H), 7.38 (s, 1H), 7.27 (d, *J* = 2.8 Hz, 3H), 7.22 (ddd, *J* = 6.9, 4.8, 1.8 Hz, 1H), 6.71 (d, *J* = 8.2 Hz, 2H), 4.38 (s, 2H).

Step 3. 3-{4-[(3-Chlorophenyl)methylamino]phenyl}-1H-pyridin-2-one (59). To a solution of *N*-[(3-chlorophenyl)methyl]-4-(2-fluoro-3-pyridyl)aniline (94 mg, 0.30 mmol) in dioxane (1 mL) was added concentrated aqueous HCl (0.2 mL, 2.4 mmol), and the mixture was stirred for 16 h at 80 °C. The reaction mixture was allowed to cool to room temperature, neutralized with saturated aqueous NaHCO$_3$, extracted with EtOAc, concentrated, and purified by ISCO automated flash chromatography to afford the title intermediate (87 mg, 0.28 mmol, 93%): LCMS (method A) t_R = 1.90 min, *m/z* 311.10 [M + H]$^+$.

Step 4. 2-(1H-Benzo[d][1,2,3]triazol-1-yl)-N-(3-chlorobenzyl)-N-[4-(2-oxo-1,2-dihydropyridin-3-yl)phenyl]acetamide. To a stirred solution of **59** (49 mg, 0.16 mmol) and **50** (28 mg, 0.16 mmol) in DMF (0.5 mL) was added T3P (50% in EtOAc, 189 μL, 0.32 mmol), followed by pyridine (38 μL, 0.48 mmol). The mixture was stirred at rt for 16 h. Purification by preparative RP-HPLC afforded a colorless solid (36 mg, 0.08 mmol, 49%): ^{1}H NMR (400 MHz, CD$_3$OD) δ 7.99 (d, *J* = 8.5 Hz, 1H), 7.80–7.72 (m, 3H), 7.69 (d, *J* = 8.4 Hz, 1H), 7.57 (t, 1H), 7.49–7.40 (m, 2H), 7.37 (d, *J* = 8.6 Hz, 2H), 7.33–7.25 (m, 3H), 7.19 (s, 1H), 6.50 (t, *J* = 6.8 Hz, 1H), 5.47 (s, 2H), 4.98 (s, 2H); ^{13}C NMR (101 MHz, CDCl$_3$) δ 165.63, 163.89, 146.29, 140.65, 139.82, 138.83, 137.84, 134.95, 134.75, 134.04, 130.73, 130.27, 130.03, 129.27, 128.42, 128.34, 128.07, 127.46, 124.29, 120.41, 110.06, 107.66, 53.60, 50.22; purity ≥95% by LCMS (method A) t_R = 2.01 min, *m/z* 470.14 [M + H]$^+$; HRMS calcd for C$_{26}$H$_{20}$ClN$_5$O$_2$ [M + H]$^+$ 470.1389, found 470.1389.

N-[4-(1H-Pyrazol-4-yl)phenyl]-2-(1H-benzo[d][1,2,3]triazol-1-yl)-N-(3-chlorobenzyl)acetamide (36). Step 1. N-[(3-Chlorophenyl)-methyl]-4-(1-tetrahydropyran-2-ylpyrazol-4-yl)aniline (60). To a vial containing 4-bromo-*N*-[(3-chlorophenyl)methyl]aniline (138 mg, 0.47 mmol), 1-(tetrahydro-2*H*-pyran-2-yl)-4-(4,4,5,5-tetramethyl-1,3,2-dioxaborolan-2-yl)-1*H*-pyrazole (155 mg, 0.56 mmol), Pd-(dppf)Cl$_2$·DCM (19 mg, 0.02 mmol), and K$_2$CO$_3$ (129 mg, 0.93 mmol) were added dioxane (1.2 mL) and water (0.12 mL). The mixture was heated to 100 °C for 16 h. The mixture was diluted with EtOAc, washed with water and brine, dried over Na$_2$SO$_4$, and concentrated to dryness. The resulting crude material was purified by ISCO automated flash chromatography to afford a pale-yellow oil (74 mg, 0.20 mmol, 43%): LCMS (method B) t_R = 1.36 min, *m/z* 311.10 [M + H]$^+$.

Step 2. 2-(Benzotriazol-1-yl)-N-[(3-chlorophenyl)methyl]-N-[4-(1-tetrahydropyran-2-ylpyrazol-4-yl)phenyl]acetamide. To a stirred solution of **60** (74 mg, 0.2 mmol) and **50** (35 mg, 0.20 mmol) in DMF (1 mL) was added T3P (50% in EtOAc, 238 μL, 0.40 mmol), followed by pyridine (48 μL, 0.60 mmol). The mixture was stirred at 60 °C for 20 h, washed with water (20 mL), and extracted with EtOAc. The combined organic layers were purified by ISCO automated flash chromatography to afford the title intermediate (77 mg, 0.15 mmol, 73%): LCMS (method A) t_R = 2.30 min, *m/z* 527.20 [M + H]$^+$.

Step 3. N-[4-(1H-Pyrazol-4-yl)phenyl]-2-(1H-benzo[d][1,2,3]-triazol-1-yl)-N-(3-chlorobenzyl)acetamide. To a solution of 2-(benzotriazol-1-yl)-*N*-[(3-chlorophenyl)methyl]-*N*-[4-(1-tetrahydro-pyran-2-ylpyrazol-4-yl)phenyl]acetamide (77 mg, 0.15 mmol) in THF (1.5 mL) was added 1 N aqueous HCl (1.5 mL, 1.5 mmol), and the mixture was stirred for 16 h at rt. The reaction mixture was allowed to cool to rt, neutralized with saturated aqueous NaHCO$_3$, extracted with EtOAc, concentrated, and purified by ISCO automated flash chromatography to afford the title compound as a colorless solid (41 mg, 0.09 mmol, 63%): ^{1}H NMR (400 MHz, CD$_3$OD) δ 8.07–7.89 (m, 3H), 7.71–7.64 (m, 3H), 7.55 (t, *J* = 7.7 Hz, 1H), 7.43 (t, *J* = 7.7 Hz, 1H), 7.33–7.23 (m, 5H), 7.20–7.14 (m, 1H), 5.45 (s, 2H), 4.95 (s, 2H); ^{13}C NMR (101 MHz, CDCl$_3$) δ 165.60, 146.27, 138.71, 138.51, 134.76, 134.01, 133.95, 131.76, 130.26, 129.42, 129.09,

128.48, 128.09, 127.78, 127.59, 124.34, 121.70, 120.41, 110.06, 53.57, 50.18; purity ≥95% by LCMS (method A) t_R = 2.04 min, m/z 443.14 [M + H]$^+$; HRMS calcd for $C_{24}H_{19}ClN_6O$ [M + H]$^+$ 443.1393, found 443.1385.

2-(Benzotriazol-1-yl)-N-[(3-chlorophenyl)methyl]-N-[3-methoxy-4-(1H-pyrazol-4-yl)phenyl]acetamide (37). Step 1. 4-Bromo-N-[(3-chlorophenyl)methyl]-3-methoxyaniline (54). A mixture of 3-chlorobenzaldehyde (216 μL, 1.91 mmol) and 4-bromo-3-methoxyaniline (350 mg, 1.73 mmol) in DCM (8.25 mL) and AcOH (0.41 mL) was stirred for 30 min at rt before the addition of NaBH(OAc)$_3$ (551 mg, 2.60 mmol). The mixture was stirred for an additional 18 h at rt. Saturated aqueous NH$_4$Cl (50 mL) was added, and the crude residue extracted with DCM, concentrated, and purified by ISCO automated flash chromatography to afford a straw-colored oil (470 mg, 1.44 mmol, 83%): LCMS (method B) t_R = 1.85 min, m/z 325.99 [M + H]$^+$; ^{1}H NMR (400 MHz, CDCl$_3$) δ 7.37 (s, 1H), 7.33–7.18 (m, 4H), 6.21 (d, J = 2.5 Hz, 1H), 6.15 (dd, J = 8.4, 2.3 Hz, 1H), 4.32 (s, 2H), 3.81 (s, 3H).

Step 2. 2-(Benzotriazol-1-yl)-N-(4-bromo-3-methoxyphenyl)-N-[(3-chlorophenyl)methyl]acetamide (56). To a stirred solution of **54** (465 mg, 1.42 mmol) and **50** (265 mg, 1.50 mmol) in THF (7 mL) was added T3P (50% in EtOAc, 1.70 mL, 2.85 mmol), followed by pyridine (344 μL, 4.27 mmol). The mixture was stirred at 60 °C for 20 h, diluted with water (20 mL), and extracted with EtOAc. The combined organic layers were washed with brine, concentrated, and purified by flash chromatography to afford a colorless solid (651 mg, 1.34 mmol, 94%): LCMS (method B) t_R = 1.81 min, m/z 485.03 [M + H]$^+$; ^{1}H NMR (400 MHz, CDCl$_3$) δ 8.06 (d, J = 8.4 Hz, 1H), 7.59 (d, J = 8.2 Hz, 1H), 7.54–7.47 (m, 2H), 7.43–7.35 (m, 1H), 7.32–7.19 (m, 2H), 7.13–7.06 (m, 1H), 6.64 (dd, J = 8.2, 2.3 Hz, 1H), 6.47 (d, J = 2.3 Hz, 1H), 5.24 (s, 2H), 4.85 (s, 2H), 3.79 (s, 3H).

Step 3. 2-(Benzotriazol-1-yl)-N-[(3-chlorophenyl)methyl]-N-[3-methoxy-4-(1H-pyrazol-4-yl)phenyl]acetamide. A vial was charged with 2-(benzotriazol-1-yl)-N-(4-bromo-3-methoxyphenyl)-N-[(3-chlorophenyl)methyl]acetamide (100 mg, 0.21 mmol), 4-(4,4,5,5-tetramethyl-1,3,2-dioxaborolan-2-yl)-1H-pyrazole (48 mg, 0.25 mmol), and Pd(dppf)Cl$_2$·DCM (8.3 mg, 0.01 mmol). Dioxane (1.0 mL) and 2 M aqueous K$_2$CO$_3$ (0.2 mL) were then added, and the resulting solution was purged with argon for 15 min. The mixture was then heated to 110 °C and stirred vigorously. After 18 h, the resulting mixture was cooled to rt, filtered through Celite, concentrated, and purified by preparative RP-HPLC (5–95% MeCN in H$_2$O, 0.1% TFA) to afford a colorless solid (2.6 mg, 5.5 μmol, 3%): ^{1}H NMR (400 MHz, CD$_3$OD) δ 7.98 (s, 2H), 7.87 (d, J = 8.4 Hz, 1H), 7.55 (t, J = 8.5 Hz, 2H), 7.43 (t, J = 7.7 Hz, 1H), 7.35–7.27 (m, 1H), 7.23–7.16 (m, 3H), 7.11–7.04 (m, 1H), 6.82–6.74 (m, 2H), 5.39 (s, 2H), 4.85 (s, 2H), 3.75 (s, 3H); ^{13}C NMR (101 MHz, CD$_3$OD) δ 166.3, 156.8, 139.0, 138.5, 134.0, 133.81 132.8, 129.7, 128.6, 128.1, 127.52, 127.48, 127.1, 124.2, 120.2, 118.4, 111.1, 110.2, 54.7, 52.5, 49.5; purity ≥95% by LCMS (method A) t_R = 2.10, m/z 473.15 [M + H]$^+$; HRMS calcd for $C_{25}H_{21}ClN_6O_2$ [M + H]$^+$ 473.1487, found 473.1497.

2-(Benzotriazol-1-yl)-N-[(3-chlorophenyl)methyl]-N-[2-methoxy-4-(1H-pyrazol-4-yl)phenyl]acetamide (38). Step 1. 4-Bromo-N-[(3-chlorophenyl)methyl]-2-methoxyaniline (55). A solution of 3-chlorobenzaldehyde (200 μL, 1.77 mmol) and 4-bromo-2-methoxyaniline (325 mg, 1.61 mmol) in DCM (7.7 mL) and AcOH (0.4 mL) was stirred for 30 min at rt before the addition of NaBH(OAc)$_3$ (511 mg, 2.41 mmol). The mixture was stirred for an additional 18 h at rt. Saturated aqueous NH$_4$Cl (50 mL) was added, and the crude residue extracted with DCM, concentrated, and purified by ISCO automated flash chromatography to afford a straw-colored oil (446 mg, 1.37 mmol, 85%): LCMS (method B) t_R = 2.05 min, m/z 325.99 [M + H]$^+$; ^{1}H NMR (400 MHz, CDCl$_3$) δ 7.35 (s, 1H), 7.31–7.19 (m, 3H), 6.92 (dd, J = 8.4, 2.1 Hz, 1H), 6.89 (d, J = 2.1 Hz, 1H), 6.37 (d, J = 8.4 Hz, 1H), 4.76 (br s, 1H), 4.32 (s, 2H), 3.87 (s, 3H).

Step 2. 2-(Benzotriazol-1-yl)-N-(4-bromo-2-methoxyphenyl)-N-[(3-chlorophenyl)methyl]acetamide (57). To a stirred solution of **55** (440 mg, 1.35 mmol) and **50** (251 mg, 1.41 mmol) in THF (7 mL) was added T3P (50% in EtOAc, 1.60 mL, 2.69 mmol), followed by pyridine (326 μL, 4.04 mmol). The mixture was stirred at 60 °C for 20 h, diluted with water (20 mL), and extracted with EtOAc. The combined organic layers were washed with brine, concentrated, and purified by ISCO automated flash chromatography to afford a colorless solid (507 mg, 1.04 mmol, 77%): LCMS (method B) t_R = 1.83 min, m/z 485.04 [M + H]$^+$; ^{1}H NMR (400 MHz, CDCl$_3$) δ 8.05 (d, J = 8.4 Hz, 1H), 7.56–7.45 (m, 2H), 7.42–7.33 (m, 1H), 7.29–7.01 (m, 6H), 6.84 (d, J = 8.3 Hz, 1H), 5.30 (s, 2H), 5.22 (d, J = 16.6 Hz, 1H), 5.11 (d, J = 16.6 Hz, 1H), 5.01 (d, J = 14.3 Hz, 1H), 4.52 (d, J = 14.3 Hz, 1H), 3.78 (s, 3H).

Step 3. 2-(Benzotriazol-1-yl)-N-[(3-chlorophenyl)methyl]-N-[2-methoxy-4-(1H-pyrazol-4-yl)phenyl]acetamide. A vial was charged with **57** (100 mg, 0.21 mmol), 4-(4,4,5,5-tetramethyl-1,3,2-dioxaborolan-2-yl)-1H-pyrazole (48 mg, 0.25 mmol), and Pd(dppf)Cl$_2$·DCM (8.3 mg, 0.01 mmol). Dioxane (1.0 mL) and 2 M aqueous K$_2$CO$_3$ (0.2 mL) were then added, and the resulting solution was purged with argon for 15 min. The mixture was then heated to 110 °C and stirred vigorously. After 18 h, the resulting mixture was cooled to rt, filtered through Celite, concentrated, and purified by preparative RP-HPLC (5–95% MeCN in H$_2$O, 0.1% TFA) to afford a colorless solid (2.5 mg, 5.3 μmol, 3%): ^{1}H NMR (400 MHz, CD$_3$OD) δ 7.96 (s, 2H), 7.88 (d, J = 8.4 Hz, 1H), 7.53–7.42 (m, 2H), 7.38–7.29 (m, 1H), 7.23 (d, J = 1.8 Hz, 1H), 7.20–7.10 (m, 4H), 7.06 (d, J = 8.1 Hz, 1H), 7.04–6.99 (m, 1H), 5.34 (d, J = 17.0 Hz, 1H), 5.19 (d, J = 17.0 Hz, 1H), 4.86 (d, J = 14.5 Hz, 1H), 4.62 (d, J = 14.5 Hz, 1H), 3.79 (s, 3H); ^{13}C NMR (101 MHz, CD$_3$OD) δ 167.0, 155.3, 138.9, 138.8, 135.6, 133.7, 129.8, 129.4, 128.7, 127.5, 127.4, 127.2, 125.8, 124.2, 118.5, 118.1, 110.1, 109.4, 55.1, 51.9, 49.3; purity ≥95% by LCMS (method A) t_R = 2.13, m/z 473.15 [M + H]$^+$; HRMS calcd for $C_{25}H_{21}ClN_6O_2$ [M + H]$^+$ 473.1487, found 473.1476.

2-(Benzotriazol-1-yl)-N-[(3-chlorophenyl)methyl]-N-[6-(1H-pyrazol-4-yl)-3-pyridyl]acetamide (39). Step 1. 6-(1-Tetrahydropyran-2-ylpyrazol-4-yl)pyridin-3-amine (64). 1-(Tetrahydro-2H-pyran-2-yl)-4-(4,4,5,5-tetramethyl-1,3,2-dioxaborolan-2-yl)-1H-pyrazole (560 mg, 2.01 mmol), 6-chloropyridin-3-amine (388 mg, 3.02 mmol), potassium carbonate (3.02 mL, 6.04 mmol), and SPhos Pd G2 (72 mg, 0.10 mmol) were combined in 1-butanol (5.3 mL) in a sealed tube, degassed under a stream of argon for 20 min, and heated at 100 °C for 16 h. The reaction mixture was filtered through Celite, washed with EtOAc (10 mL), concentrated under reduced pressure, and purified by ISCO automated flash chromatography (24 g, 0–8% MeOH in DCM) to afford a viscous oil (414 mg, 1.69 mmol, 84%): LCMS (method A) t_R = 1.30 min, m/z 245.13 [M + H]$^+$; ^{1}H NMR (400 MHz, CD$_3$OD) δ 8.15 (s, 1H), 7.95 (d, J = 2.8 Hz, 1H), 7.92 (s, 1H), 7.42 (d, J = 8.5 Hz, 1H), 7.11 (dd, J = 8.5, 2.8 Hz, 1H), 5.41 (dd, J = 10.0, 2.3 Hz, 1H), 4.10–4.00 (m, 1H), 3.74 (td, J = 11.2, 3.1 Hz, 1H), 2.21–2.08 (m, 1H), 2.08–1.98 (m, 2H), 1.84–1.55 (m, 3H).

Step 2. N-[(3-Chlorophenyl)methyl]-6-(1-tetrahydropyran-2-yl-pyrazol-4-yl)pyridin-3-amine (66). Compound **64** (114 mg, 0.47 mmol) and 3-chlorobenzaldehyde (0.05 mL, 0.43 mmol) were added to DCM (4 mL) and stirred for 15 min. NaHB(OAc)$_3$ (135 mg, 0.64 mmol) was added at rt, and stirring continued for 16 h. To the reaction mixture was added saturated aqueous NaHCO$_3$ (5 mL). The resulting residue was extracted with DCM (2 × 10 mL), dried over sodium sulfate, concentrated to dryness, and then purified by ISCO automated flash chromatography (12 g, 0–3% MeOH in DCM) to afford a viscous oil (96 mg, 0.26 mmol, 61%): LCMS (method A) t_R = 1.84 min, m/z 369.14 [M + H]$^+$; ^{1}H NMR (400 MHz, CD$_3$OD) δ 8.13 (s, 1H), 7.90 (s, 1H), 7.88 (d, J = 2.8 Hz, 1H), 7.42 (d, J = 9.3 Hz, 2H), 7.34–7.28 (m, 2H), 7.28–7.21 (m, 1H), 7.01 (dd, J = 8.7, 2.8 Hz, 1H), 5.40 (dd, J = 10.0, 2.4 Hz, 1H), 4.38 (s, 2H), 4.04 (d, J = 11.7 Hz, 1H), 3.79–3.68 (m, 1H), 2.20–2.07 (m, 1H), 2.06–1.99 (m, 2H), 1.83–1.56 (m, 3H).

Step 3. 2-(Benzotriazol-1-yl)-N-[(3-chlorophenyl)methyl]-N-[6-(1H-pyrazol-4-yl)-3-pyridyl]acetamide (39). To a stirred solution of **50** (1.10 g, 6.24 mmol) in DCM (20 mL) were added pyridine (0.60 mL, 7.48 mmol) and cyanuric fluoride (0.64 mL, 7.48 mmol) sequentially at rt, and stirring was continued for 1 h. The precipitated solid was filtered and washed with DCM (10 mL). The filtrate was concentrated to afford crude 2-(benzotriazol-1-yl)acetyl fluoride that

was immediately dissolved in anhydrous THF (12 mL). To this was added a solution of **66** (230 mg, 0.62 mmol) and Et$_3$N (0.91 mL, 6.55 mmol) in THF (2 mL). The reaction mixture was stirred at 60 °C for 16 h. Water (20 mL) was added followed by extraction with EtOAc (2 × 25 mL). The organic layer was dried over Na$_2$SO$_4$, concentrated under reduced pressure, and passed quickly through a flash column using 0–10% MeOH in DCM to afford an impure intermediate, 2-(benzotriazol-1-yl)-*N*-[(3-chlorophenyl)methyl]-*N*-[6-(1-tetrahydro-pyran-2-ylpyrazol-4-yl)-3-pyridyl]acetamide (212 mg), which was further treated with 5 mL of a 4:1 mixture of MeOH and 4 N HCl in dioxane at rt for 40 min. To the reaction mixture was added EtOAc (15 mL) followed by washing with saturated NaHCO$_3$. The organic layer was dried over Na$_2$SO$_4$, concentrated under reduced pressure, and purified by ISCO automated flash chromatography (24 g, 0–6% MeOH in DCM) to afford the desired product as a yellow solid (60 mg, 0.13 mmol, 22% over two steps): ^{1}H NMR (400 MHz, DMSO-*d$_6$*) δ 13.11 (s, 1H), 8.59 (d, *J* = 2.6 Hz, 1H), 8.36 (s, 1H), 8.08 (s, 1H), 8.03 (d, *J* = 8.3 Hz, 1H), 7.92–7.85 (m, 1H), 7.81 (dd, *J* = 14.2, 8.3 Hz, 2H), 7.55 (t, *J* = 7.7 Hz, 1H), 7.40 (t, *J* = 7.7 Hz, 1H), 7.33 (d, *J* = 3.3 Hz, 3H), 7.21 (d, *J* = 6.7 Hz, 1H), 5.54 (s, 2H), 4.94 (s, 2H); ^{13}C NMR (101 MHz, DMSO-*d$_6$*) δ 165.89, 151.92, 148.94, 144.98, 139.11, 137.55, 136.57, 133.71, 133.58, 133.11, 130.36, 128.03, 127.49, 127.17, 126.95, 123.85, 123.82, 121.42, 120.02, 118.96, 111.11, 51.88, 49.48; purity ≥95% by LCMS (method A) t_R = 1.89, *m/z* 443.13 [M + H]$^+$; HRMS calcd for C$_{23}$H$_{18}$ClN$_7$O [M + H]$^+$ 443.1334, found 443.1344.

2-(Benzotriazol-1-yl)-N-[(3-chlorophenyl)methyl]-N-[5-(1H-pyra-zol-4-yl)-2-pyridyl]acetamide (40). Step 1. 5-(1-Tetrahydropyran-2-ylpyrazol-4-yl)pyridin-2-amine (65). 1-(Tetrahydro-2*H*-pyran-2-yl)-4-(4,4,5,5-tetramethyl-1,3,2-dioxaborolan-2-yl)-1*H*-pyrazole (560 mg, 2.01 mmol), 2-amino-5-chloropyridine (388 mg, 3.02 mmol), potassium carbonate (2 M, 3.02 mL, 6.04 mmol), and XPhos Pd G2 (79 mg, 0.10 mmol) were combined in dioxane (5.3 mL) in a sealed tube, degassed under a stream of argon for 20 min, and heated at 100 °C for 16 h. The reaction mixture was filtered through Celite, washed with EtOAc (10 mL), concentrated under reduced pressure, and purified by ISCO automated flash chromatography (24 g, 0–7% MeOH in DCM) to afford an off-white solid (479 mg, 1.96 mmol, 97%): LCMS (method A) t_R = 1.32 min, *m/z* 245.13 [M + H]$^+$; ^{1}H NMR (400 MHz, CD$_3$OD) δ 8.12 (d, *J* = 2.4 Hz, 1H), 8.06 (s, 1H), 7.79 (s, 1H), 7.67 (dd, *J* = 8.6, 2.4 Hz, 1H), 6.62 (d, *J* = 8.6 Hz, 1H), 5.40 (dd, *J* = 10.2, 2.4 Hz, 1H), 4.09–4.00 (m, 1H), 3.73 (td, *J* = 11.2, 3.0 Hz, 1H), 2.21–2.09 (m, 1H), 2.09–1.98 (m, 2H), 1.84–1.57 (m, 3H).

Step 2. N-[(3-Chlorophenyl)methyl]-5-(1-tetrahydropyran-2-yl-pyrazol-4-yl)pyridin-2-amine (67). Intermediate **65** (133 mg, 0.55 mmol) from above and 3-chlorobenzaldehyde (0.06 mL, 0.50 mmol) were addeed to DCM (4 mL) and stirred for 15 min. NaHB(OAc)$_3$ (158 mg, 0.75 mmol) was added at rt, and stirring was continued for 16 h. The reaction was quenched with a saturated aqueous NaHCO$_3$ solution (5 mL), and the aqueous layer was extracted with DCM (2 × 10 mL), dried over Na$_2$SO$_4$, concentrated under reduced pressure, and purified by ISCO automated flash chromatography (12 g, 0–3% MeOH in DCM) to afford a colorless solid (100 mg, 0.27 mmol, 54%): LCMS (method A) t_R = 1.80 min, *m/z* 369.14 [M + H]$^+$; ^{1}H NMR (400 MHz, CD$_3$OD) δ 8.16 (d, *J* = 2.3 Hz, 1H), 8.04 (s, 1H), 7.78 (s, 1H), 7.65 (dd, *J* = 8.7, 2.3 Hz, 1H), 7.38–7.34 (m, 1H), 7.28 (dd, *J* = 4.2, 2.0 Hz, 2H), 7.28–7.20 (m, 1H), 6.58 (d, *J* = 8.7 Hz, 1H), 5.40 (dd, *J* = 10.1, 2.4 Hz, 1H), 4.52 (s, 2H), 4.08–4.01 (m, 1H), 3.77–3.69 (m, 1H), 2.22–1.96 (m, 3H), 1.81–1.56 (m, 3H).

Step 3. 2-(Benzotriazol-1-yl)-N-[(3-chlorophenyl)methyl]-N-[5-(1H-pyrazol-4-yl)-2-pyridyl]acetamide. To a stirred solution of **50** (1.44 g, 8.13 mmol) in DCM (20 mL) were added pyridine (0.79 mL, 9.76 mmol) and cyanuric fluoride (0.84 mL, 9.76 mmol) sequentially at room temperature, and stirring was continued for 1 h. The precipitated solid was filtered and washed with DCM (10 mL). The filtrate was concentrated to obtain crude 2-(benzotriazol-1-yl)acetyl fluoride that was immediately dissolved in anhydrous THF (12 mL). To this was added a solution of **67** (300 mg, 0.81 mmol) and Et$_3$N (1.19 mL, 8.54 mmol) in THF (2 mL). The reaction mixture was

stirred at 60 °C for 16 h. Water (20 mL) was added followed by extraction with EtOAc (2 × 25 mL). The organic layer was dried over Na$_2$SO$_4$, concentrated under reduced pressure, and passed quickly through the flash column using 0–10% MeOH in DCM to afford a impure intermediate 2-(benzotriazol-1-yl)-*N*-[(3-chlorophenyl)-methyl]-*N*-[5-(1-tetrahydropyran-2-ylpyrazol-4-yl)-2-pyridyl]-acetamide (364 mg) which was further treated with 5 mL of a 4:1 mixture of MeOH and 4 N HCl in dioxane at room temperature for 40 min. To the reaction mixture was added EtOAc (15 mL), and the mixture was then washed with saturated aqueous NaHCO$_3$, dried over Na$_2$SO$_4$, concentrated under reduced pressure, and purified by ISCO automated flash chromatography (24 g, 0–4% MeOH in DCM) to afford the desired product as a yellow solid (150 mg, 0.33 mmol, 41% over two steps): ^{1}H NMR (400 MHz, CD$_3$OD) δ 8.78 (d, *J* = 2.4 Hz, 1H), 8.21–8.01 (m, 3H), 7.97 (d, *J* = 8.4 Hz, 1H), 7.69 (d, *J* = 8.4 Hz, 1H), 7.59–7.51 (m, 1H), 7.43 (d, *J* = 7.6 Hz, 1H), 7.39 (d, *J* = 8.2 Hz, 1H), 7.34 (s, 1H), 7.32–7.18 (m, 3H), 5.73 (s, 2H), 5.11 (s, 2H); ^{13}C NMR (101 MHz, CD$_3$OD) δ 168.24, 152.24, 147.13, 146.52, 140.36, 137.02, 135.49, 135.19, 131.14, 129.10, 128.93, 128.73, 127.51, 125.72, 125.62, 122.08, 119.89, 119.06, 111.64, 111.41, 109.89, 52.27, 45.71; purity ≥95% by LCMS (method A) t_R = 1.98, *m/z* 443.13 [M + H]$^+$; HRMS calcd for C$_{23}$H$_{18}$ClN$_7$O [M + H]$^+$ 443.1334, found 443.1323.

N-[4-(1H-Imidazol-4-yl)phenyl]-2-(1H-benzo[d][1,2,3]triazol-1-yl)-N-(3-chlorobenzyl)acetamide (41). Step 1. 2-(Benzotriazol-1-yl)-N-(4-bromophenyl)-N-[(3-chlorophenyl)methyl]acetamide (61). To a stirred solution of intermediate **58** (1.48 g, 5.0 mmol) and acid **50** (886 mg, 5 mmol) in THF (25 mL) was added T3P (50% in EtOAc, 5.95 mL, 10 mmol), followed by pyridine (1.21 mL, 15 mmol). The mixture was stirred at rt for 16 h, diluted with water (20 mL), and extracted with EtOAc. The combined organic layers were washed with brine, concentrated, and purified by ISCO automated flash chromatography to afford a colorless solid (1.58 g, 3.46 mmol, 69%): LCMS (method B) t_R = 2.40 min, *m/z* 457.03 [M + H]$^+$.

Step 2. 2-(Benzotriazol-1-yl)-N-[(3-chlorophenyl)methyl]-N-[4-(4,4,5,5-tetramethyl-1,3,2-dioxaborolan-2-yl)phenyl]acetamide (62). To a vial containing **61** (228 mg, 0.50 mmol), bis(pinacolato)-diboron (152 mg, 0.60 mmol), Pd(dppf)Cl$_2$·DCM (20 mg, 0.03 mmol), and KOAc (221 mg, 2.25 mmol) was added dioxane (2.5 mL). The mixture was heated to 100 °C for 16 h. The mixture was diluted with EtOAc, washed with water and brine, dried over Na$_2$SO$_4$, and concentrated. The mixture was purified by ISCO automated chromatography to afford a cream-colored solid (176 mg, 0.35 mmol, 70%): LCMS (method A) t_R = 2.53 min, *m/z* 503.21 [M + H]$^+$.

Step 3. 2-(Benzotriazol-1-yl)-N-[(3-chlorophenyl)methyl]-N-[4-(1-tritylimidazol-4-yl)phenyl]acetamide. To a vial containing **62** (127 mg, 0.25 mmol), 4-bromo-1-tritylimidazole (90 mg, 0.23 mmol), Pd(PPh$_3$)$_4$ (40 mg, 0.15 mmol), and K$_2$CO$_3$ (64 mg, 0.46 mmol) were added dioxane (1.9 mL) and water (0.4 mL). The mixture was degassed with argon and heated to 100 °C for 16 h. The mixture was diluted with EtOAc, washed with water and brine, dried over Na$_2$SO$_4$, and concentrated. The mixture was purified by ISCO automated chromatography to afford the desired intermediate (100 mg, 0.15 mmol, 63%): LCMS (method B) t_R = 1.53 min, *m/z* 685.25 [M + H]$^+$.

Step 4. N-[4-(1H-Imidazol-4-yl)phenyl]-2-(1H-benzo[d][1,2,3]-triazol-1-yl)-N-(3-chlorobenzyl)acetamide. To 2-(benzotriazol-1-yl)-*N*-[(3-chlorophenyl)methyl]-*N*-[4-(1-tritylimidazol-4-yl)phenyl]-acetamide (100 mg, 0.15 mmol) in MeOH (1.5 mL) was added AcOH (170 μL, 3.0 mmol), and the mixture was stirred for 2 h at 65 °C. The reaction mixture was allowed to cool to rt, concentrated, and purified by preparative RP-HPLC to afford a colorless solid (30 mg, 0.07 mmol, 45%): ^{1}H NMR (400 MHz, DMSO-*d$_6$*) δ 12.42 (br s, 1H), 8.04 (d, *J* = 8.4 Hz, 1H), 7.87 (d, *J* = 8.1 Hz, 2H), 7.82 (d, *J* = 8.4 Hz, 1H), 7.78 (s, 1H), 7.69 (s, 1H), 7.56 (t, *J* = 7.7 Hz, 1H), 7.46 (d, *J* = 8.1 Hz, 2H), 7.40 (t, *J* = 7.7 Hz, 1H), 7.35–7.29 (m, 3H), 7.21 (d, *J* = 6.8 Hz, 1H), 5.49 (s, 2H), 4.92 (s, 2H); ^{13}C NMR (101 MHz, DMSO-*d$_6$*) δ 165.7, 145.0, 139.5, 137.8, 137.6, 136.3, 134.3, 133.8, 133.0, 130.3, 128.4, 127.9, 127.3, 127.2, 126.8, 125.5, 123.8, 119.0, 115.2, 111.1, 52.0, 49.3; purity ≥95% by LCMS (method A) t_R = 1.80

min, m/z 443.14 [M + H]$^+$; HRMS calcd for $C_{24}H_{19}ClN_6O$ [M + H]$^+$ 443.1393, found 443.1375.

N-[(3-Chlorophenyl)methyl]-N-[4-(1H-pyrazol-4-yl)phenyl]-2-(3-pyridyl)acetamide (42). To a solution of *N*-[(3-chlorophenyl)-methyl]-4-(1-tetrahydropyran-2-ylpyrazol-4-yl)aniline, **60** (37 mg, 0.1 mmol), in THF (1 mL) were added 3-pyridylacetic acid (14 mg, 0.1 mmol), T3P (50% in EtOAc, 0.18 mL, 0.30 mmol), and DIPEA (52 μL, 0.30 mmol), and the mixture was stirred at 65 °C for 16 h. The mixture was concentrated, redissolved in HCl (4.0 M in dioxane, 1 mL), and stirred at 60 °C for 1 h. The mixture was concentrated and purified by RP-HPLC (20−100% MeCN in H$_2$O, 0.1% TFA), and the free base was obtained by washing the product with saturated aqueous K$_2$CO$_3$, affording the title compound as a colorless solid (18 mg, 0.04 mmol, 47%): ^{1}H NMR (400 MHz, DMSO-d_6) δ 8.74 (d, *J* = 5.4 Hz, 1H), 8.67 (s, 1H), 8.27 (d, *J* = 8.0 Hz, 1H), 8.10 (br s, 2H), 7.88 (dd, *J* = 8.0, 5.5 Hz, 1H), 7.68 (d, *J* = 8.0 Hz, 2H), 7.38−7.25 (m, 5H), 7.20 (d, *J* = 6.6 Hz, 1H), 4.91 (s, 2H), 3.77 (s, 2H); ^{13}C NMR (101 MHz, DMSO-d_6) δ 169.49, 158.88, 158.52, 145.80, 144.83, 142.20, 140.38, 139.28, 135.59, 133.46, 133.36, 130.69, 129.20, 128.33, 127.70, 127.26, 126.60, 126.06, 120.68, 117.84, 114.92, 52.26, 37.61; purity ≥95% by LCMS (method A) t_R = 1.71, m/z 403.13 [M + H]$^+$; HRMS calcd for $C_{23}H_{19}ClN_4O$ [M + H]$^+$ 403.1320, found 403.1340.

N-[(3-Chlorophenyl)methyl]-N-[4-(1H-pyrazol-4-yl)phenyl]-2-pyrimidin-5-yl-acetamide (43). To a solution of *N*-[(3-chlorophenyl)methyl]-4-(1-tetrahydropyran-2-ylpyrazol-4-yl)aniline, **60** (37 mg, 0.1 mmol), in THF (1 mL), were added 2-pyrimidin-5-ylacetic acid (14 mg, 0.1 mmol), T3P (50% in EtOAc, 0.18 mL, 0.30 mmol), and DIPEA (52 μL, 0.30 mmol), and the mixture was stirred at 65 °C for 16 h. The mixture was concentrated, redissolved in HCl (4.0 M in dioxane, 1 mL), and stirred at 60 °C for 1 h. The mixture was concentrated and purified by RP-HPLC (20−100% MeCN in H$_2$O, 0.1% TFA), and the free base obtained by washing the product with saturated aqueous K$_2$CO$_3$, affording the title compound as a colorless solid (9 mg, 0.02 mmol, 23%): ^{1}H NMR (400 MHz, CD$_3$OD) δ 9.04 (s, 1H), 8.61 (s, 2H), 8.03 (s, 2H), 7.68 (d, *J* = 8.2 Hz, 2H), 7.32−7.26 (m, 3H), 7.18 (d, *J* = 8.2 Hz, 3H), 4.95 (s, 2H), 3.66 (s, 2H); ^{13}C NMR (101 MHz, CD$_3$OD) δ 170.15, 157.57, 156.10, 139.32, 139.07, 133.96, 133.48, 130.23, 129.68, 128.75, 128.40, 127.37, 126.84, 126.48, 121.06, 52.38, 35.30; purity ≥95% by LCMS (method A) t_R = 1.84, m/z 404.13 [M + H]$^+$; HRMS calcd for $C_{22}H_{18}ClN_5O$ [M + H]$^+$ 404.1273, found 404.1289.

■ ASSOCIATED CONTENT

⒮Ⓘ Supporting Information

The Supporting Information is available free of charge at https://pubs.acs.org/doi/10.1021/acs.jmedchem.1c00598.

> Supplemental figures, SARS-CoV-1 3CL^{pro} X-ray structures, Tier 1 DMPK summary, human S9-generated metabolites and MS fragmentation, X-ray data collection and refinement statistics, ligand electron density maps, UV-based HPLC chromatograms of final compounds, and CPE SARS-CoV-2-infected Vero E6 cell concentration−response curve for **41** (PDF)
>
> Molecular formula strings (CSV)

Accession Codes

SARS-CoV-2 complexes: **1**, PDB entry 7LME; **19**, PDB entry 7LMD; **21**, PDB entry 7LMF. SARS-CoV-1 complexes: **8**, PDB entry 7LMH; **19**, PDB entry 7LMI; **21**, PDB entry 7LMG; **35**, PDB entry 7LMJ.

■ AUTHOR INFORMATION

Corresponding Author

Shaun R. Stauffer − *Center for Therapeutics Discovery, Lerner Research Institute, Cleveland Clinic, Cleveland, Ohio 44195, United States;* ⓞ orcid.org/0000-0002-6332-1827; Email: stauffs2@ccf.org

Authors

Sang Hoon Han − *Center for Therapeutics Discovery, Lerner Research Institute, Cleveland Clinic, Cleveland, Ohio 44195, United States*

Christopher M. Goins − *Center for Therapeutics Discovery, Lerner Research Institute, Cleveland Clinic, Cleveland, Ohio 44195, United States*

Tarun Arya − *Center for Therapeutics Discovery, Lerner Research Institute, Cleveland Clinic, Cleveland, Ohio 44195, United States*

Woo-Jin Shin − *Cleveland Clinic Florida Research & Innovation Center, Port St. Lucie, Florida 34987, United States*

Joshua Maw − *Center for Therapeutics Discovery, Lerner Research Institute, Cleveland Clinic, Cleveland, Ohio 44195, United States*

Alice Hooper − *Center for Therapeutics Discovery, Lerner Research Institute, Cleveland Clinic, Cleveland, Ohio 44195, United States*

Dhiraj P. Sonawane − *Center for Therapeutics Discovery, Lerner Research Institute, Cleveland Clinic, Cleveland, Ohio 44195, United States*

Matthew R. Porter − *Center for Therapeutics Discovery, Lerner Research Institute, Cleveland Clinic, Cleveland, Ohio 44195, United States*

Breyanne E. Bannister − *Department of Pharmaceutical Science, Lipscomb University College of Pharmacy, Nashville, Tennessee 37204, United States*

Rachel D. Crouch − *Department of Pharmaceutical Science, Lipscomb University College of Pharmacy, Nashville, Tennessee 37204, United States*

A. Abigail Lindsey − *Center for Therapeutics Discovery, Lerner Research Institute, Cleveland Clinic, Cleveland, Ohio 44195, United States*

Gabriella Lakatos − *Center for Therapeutics Discovery, Lerner Research Institute, Cleveland Clinic, Cleveland, Ohio 44195, United States*

Steven R. Martinez − *Center for Therapeutics Discovery, Lerner Research Institute, Cleveland Clinic, Cleveland, Ohio 44195, United States*

Joseph Alvarado − *Center for Therapeutics Discovery, Lerner Research Institute, Cleveland Clinic, Cleveland, Ohio 44195, United States*

Wendell S. Akers − *Department of Pharmaceutical Science, Lipscomb University College of Pharmacy, Nashville, Tennessee 37204, United States*

Nancy S. Wang − *Center for Therapeutics Discovery, Lerner Research Institute, Cleveland Clinic, Cleveland, Ohio 44195, United States*

Jae U. Jung − *Department of Cancer Biology and Center for Global and Emerging Pathogens Research, Lerner Research Institute, Cleveland Clinic, Cleveland, Ohio 44195, United States*

Jonathan D. Macdonald − *Center for Therapeutics Discovery, Lerner Research Institute, Cleveland Clinic, Cleveland, Ohio 44195, United States*

Complete contact information is available at:
https://pubs.acs.org/10.1021/acs.jmedchem.1c00598

Author Contributions

#S.H.H. and C.M.G. contributed equally to this work.

■ ABBREVIATIONS USED

3CL^{pro}, 3C-like protease; CoV, coronavirus; CPE, cytopathic effect; MERS, Middle East respiratory syndrome; MLPCN, Molecular Libraries Probe Production Centers Network; SARS, severe acute respiratory syndrome; SC1, SARS-CoV-1; SC2, SARS-CoV-2

■ REFERENCES

(1) Myint, S. H. Human Coronavirus Infections. In *The Coronaviridae*; Siddell, S. G., Ed.; Springer US: Boston, 1995; pp 389−401.

(2) McIntosh, K.; Dees, J. H.; Becker, W. B.; Kapikian, A. Z.; Chanock, R. M. Recovery in Tracheal Organ Cultures of Novel Viruses from Patients with Respiratory Disease. *Proc. Natl. Acad. Sci. U. S. A.* 1967, 57 (4), 933−940.

(3) Ksiazek, T. G.; Erdman, D.; Goldsmith, C. S.; Zaki, S. R.; Peret, T.; Emery, S.; Tong, S.; Urbani, C.; Comer, J. A.; Lim, W.; Rollin, P. E.; Dowell, S. F.; Ling, A.; Humphrey, C. D.; Shieh, W.-J.; Guarner, J.; Paddock, C. D.; Rota, P.; Fields, B.; DeRisi, J.; Yang, J.; Cox, N.; Hughes, J. M.; LeDuc, J. W.; Bellini, W. J.; Anderson, L. J. A Novel Coronavirus Associated with Severe Acute Respiratory Syndrome. *N. Engl. J. Med.* 2003, 348 (20), 1953−1966.

(4) Drosten, C.; Günther, S.; Preiser, W.; van der Werf, S.; Brodt, H.-R.; Becker, S.; Rabenau, H.; Panning, M.; Kolesnikova, L.; Fouchier, R. A. M.; Berger, A.; Burguière, A.-M.; Cinatl, J.; Eickmann, M.; Escriou, N.; Grywna, K.; Kramme, S.; Manuguerra, J.-C.; Müller, S.; Rickerts, V.; Stürmer, M.; Vieth, S.; Klenk, H.-D.; Osterhaus, A. D. M. E.; Schmitz, H.; Doerr, H. W. Identification of a Novel Coronavirus in Patients with Severe Acute Respiratory Syndrome. *N. Engl. J. Med.* 2003, 348 (20), 1967−1976.

(5) WHO. Emergencies preparedness, response - Update 49 - SARS case fatality ratio, incubation period.

(6) Pyrc, K.; Berkhout, B.; van der Hoek, L. The Novel Human Coronaviruses NL63 and HKU1. *J. Virol.* 2007, 81 (7), 3051−3057.

(7) Fielding, B. C. Human Coronavirus NL63: A Clinically Important Virus? *Future Microbiol.* 2011, 6 (2), 153−159.

(8) Middle East respiratory syndrome coronavirus (MERS-CoV) - United Arab Emirates. https://www.who.int/emergencies/emergency-events/item/2021-DON314.

(9) Liu, G.; Lee, J.-H.; Parker, Z. M.; Acharya, D.; Chiang, J. J.; van Gent, M.; Riedl, W.; Davis-Gardner, M. E.; Wies, E.; Chiang, C.;

Gack, M. U. ISG15-Dependent Activation of the Sensor MDA5 Is Antagonized by the SARS-CoV-2 Papain-like Protease to Evade Host Innate Immunity. *Nat. Microbiol.* 2021, 6, 467−478.

(10) WHO. Coronavirus (COVID-19) Data Surveillance Dashboard. https://covid19.who.int/ (accessed 2021-03-29).

(11) Wu, F.; Zhao, S.; Yu, B.; Chen, Y. M.; Wang, W.; Song, Z. G.; Hu, Y.; Tao, Z. W.; Tian, J. H.; Pei, Y. Y.; Yuan, M. L.; Zhang, Y. L.; Dai, F. H.; Liu, Y.; Wang, Q. M.; Zheng, J. J.; Xu, L.; Holmes, E. C.; Zhang, Y. Z. A New Coronavirus Associated with Human Respiratory Disease in China. *Nature* 2020, 579 (7798), 265−269.

(12) Morse, J. S.; Lalonde, T.; Xu, S.; Liu, W. R. Learning from the Past: Possible Urgent Prevention and Treatment Options for Severe Acute Respiratory Infections Caused by 2019-NCoV. *ChemBioChem* 2020, 21 (5), 730−738.

(13) Dömling, A.; Gao, L. Chemistry and Biology of SARS-CoV-2. *Chem.* 2020, 6 (6), 1283−1295.

(14) Ghosh, A. K.; Brindisi, M.; Shahabi, D.; Chapman, M. E.; Mesecar, A. D. Drug Development and Medicinal Chemistry Efforts toward SARS-Coronavirus and Covid-19 Therapeutics. *ChemMedChem* 2020, 15 (11), 907−932.

(15) Cannalire, R.; Cerchia, C.; Beccari, A. R.; Di Leva, F. S.; Summa, V. Targeting SARS-CoV-2 Proteases and Polymerase for COVID-19 Treatment: State of the Art and Future Opportunities. *J. Med. Chem.* 2020, DOI: 10.1021/acs.jmedchem.0c01140.

(16) Gil, C.; Ginex, T.; Maestro, I.; Nozal, V.; Barrado-Gil, L.; Cuesta-Geijo, M. Á.; Urquiza, J.; Ramírez, D.; Alonso, C.; Campillo, N. E.; Martinez, A. COVID-19: Drug Targets and Potential Treatments. *J. Med. Chem.* 2020, 63 (21), 12359−12386.

(17) Fan, K.; Wei, P.; Feng, Q.; Chen, S.; Huang, C.; Ma, L.; Lai, B.; Pei, J.; Liu, Y.; Chen, J.; Lai, L. Biosynthesis, Purification, and Substrate Specificity of Severe Acute Respiratory Syndrome Coronavirus 3C-like Proteinase. *J. Biol. Chem.* 2004, 279 (3), 1637−1642.

(18) Thiel, V.; Ivanov, K. A.; Putics, Á.; Hertzig, T.; Schelle, B.; Bayer, S.; Weißbrich, B.; Snijder, E. J.; Rabenau, H.; Doerr, H. W.; Gorbalenya, A. E.; Ziebuhr, J. Mechanisms and Enzymes Involved in SARS Coronavirus Genome Expression. *J. Gen. Virol.* 2003, 84 (9), 2305−2315.

(19) Shi, J.; Wei, Z.; Song, J. Dissection Study on the Severe Acute Respiratory Syndrome 3C-like Protease Reveals the Critical Role of the Extra Domain in Dimerization of the Enzyme. *J. Biol. Chem.* 2004, 279, 24765−24773.

(20) Jacobs, J.; Grum-Tokars, V.; Zhou, Y.; Turlington, M.; Saldanha, S. A.; Chase, P.; Eggler, A.; Dawson, E. S.; Baez-Santos, Y. M.; Tomar, S.; Mielech, A. M.; Baker, S. C.; Lindsley, C. W.; Hodder, P.; Mesecar, A.; Stauffer, S. R. Discovery, Synthesis, and Structure-Based Optimization of a Series of N -(Tert -Butyl)-2-(N -Arylamido)-2-(Pyridin-3-Yl) Acetamides (ML188) as Potent Noncovalent Small Molecule Inhibitors of the Severe Acute Respiratory Syndrome Coronavirus (SARS-CoV) 3CL. *J. Med. Chem.* 2013, 56 (2), 534−546.

(21) Turlington, M.; Chun, A.; Tomar, S.; Eggler, A.; Grum-Tokars, V.; Jacobs, J.; Daniels, J. S.; Dawson, E.; Saldanha, A.; Chase, P.; Baez-Santos, Y. M.; Lindsley, C. W.; Hodder, P.; Mesecar, A. D.; Stauffer, S. R. Discovery of N-(Benzo[1,2,3]Triazol-1-yl)-N-(Benzyl)-Acetamido)Phenyl) Carboxamides as Severe Acute Respiratory Syndrome Coronavirus (SARS-CoV) 3CLpro Inhibitors: Identification of ML300 and Noncovalent Nanomolar Inhibitors with an Induced-Fit Binding. *Bioorg. Med. Chem. Lett.* 2013, 23 (22), 6172−6177.

(22) Zhang, C.; Stone, E. A.; Deshmukh, M.; Ippolito, J. A.; Ghahremanpour, M. M.; Tirado-rives, J.; Spasov, K. A.; Zhang, S.; Takeo, Y.; Kudalkar, S. N.; Liang, Z.; Isaacs, F.; Lindenbach, B.; Miller, S. J.; Anderson, K. S.; Jorgensen, W. L. Potent Noncovalent Inhibitors of the Main Protease of SARS-CoV-2 from Molecular Sculpting of the Drug Perampanel Guided by Free Energy Perturbation Calculations. *ACS Cent. Sci.* 2021, 7 (3), 467−475.

(23) Kim, Y.; Lovell, S.; Tiew, K.-C.; Mandadapu, S. R.; Alliston, K. R.; Battaile, K. P.; Groutas, W. C.; Chang, K.-O. Broad-Spectrum

Antivirals against 3C or 3C-Like Proteases of Picornaviruses, Noroviruses, and Coronaviruses. *J. Virol.* **2012**, *86* (21), 11754−11762.

(24) Hoffman, R. L.; Kania, R. S.; Brothers, M. A.; Davies, J. F.; Ferre, R. A.; Gajiwala, K. S.; He, M.; Hogan, R. J.; Kozminski, K.; Li, L. Y.; Lockner, J. W.; Lou, J.; Marra, M. T.; Mitchell, L. J.; Murray, B. W.; Nieman, J. A.; Noell, S.; Planken, S. P.; Rowe, T.; Ryan, K.; Smith, G. J.; Solowiej, J. E.; Steppan, C. M.; Taggart, B. Discovery of Ketone-Based Covalent Inhibitors of Coronavirus 3CL Proteases for the Potential Therapeutic Treatment of COVID-19. *J. Med. Chem.* **2020**, *63* (21), 12725−12747.

(25) Boras, B.; Jones, R. M.; Anson, B. J.; Arenson, D.; Aschenbrenner, L.; Bakowski, M. A.; Beutler, N.; Binder, J.; Chen, E.; Eng, H.; Hammond, J.; Hoffman, R.; Kadar, E. P.; Kania, R.; Kimoto, E.; Kirkpatrick, M. G.; Lanyon, L.; Lendy, E. K.; Lillis, J. R.; Luthra, S. A.; Ma, C.; Noell, S.; Obach, R. S.; O'Brien, M. N.; O'Connor, R.; Ogilvie, K.; Owen, D.; Pettersson, M.; Reese, M. R.; Rogers, T.; Rossulek, M. I.; Sathish, J. G.; Steppan, C.; Ticehurst, M.; Updyke, L. W.; Zhu, Y.; Wang, J.; Chatterjee, A. K.; Mesecar, A. D.; Anderson, A. S.; Allerton, C. Discovery of a Novel Inhibitor of Coronavirus 3CL Protease as a Clinical Candidate for the Potential Treatment of COVID-19. *bioRxiv* **2020**, DOI: 10.1101/2020.09.12.293498.

(26) Zhang, L.; Lin, D.; Sun, X.; Curth, U.; Drosten, C.; Sauerhering, L.; Becker, S.; Rox, K.; Hilgenfeld, R. Crystal Structure of SARS-CoV-2 Main Protease Provides a Basis for Design of Improved α-Ketoamide Inhibitors. *Science* **2020**, *368* (6489), 409−412.

(27) Anand, K. Coronavirus Main Proteinase (3CLpro) Structure: Basis for Design of Anti-SARS Drugs. *Science* **2003**, *300* (5626), 1763−1767.

(28) Yang, H.; Yang, M.; Ding, Y.; Liu, Y.; Lou, Z.; Zhou, Z.; Sun, L.; Mo, L.; Ye, S.; Pang, H.; Gao, G. F.; Anand, K.; Bartlam, M.; Hilgenfeld, R.; Rao, Z. The Crystal Structures of Severe Acute Respiratory Syndrome Virus Main Protease and Its Complex with an Inhibitor. *Proc. Natl. Acad. Sci. U. S. A.* **2003**, *100* (23), 13190−13195.

(29) Douangamath, A.; Fearon, D.; Gehrtz, P.; Krojer, T.; Lukacik, P.; Owen, C. D.; Resnick, E.; Strain-Damerell, C.; Aimon, A.; Ábrányi-Balogh, P.; Brandão-Neto, J.; Carbery, A.; Davison, G.; Dias, A.; Downes, T. D.; Dunnett, L.; Fairhead, M.; Firth, J. D.; Jones, S. P.; Keeley, A.; Keserü, G. M.; Klein, H. F.; Martin, M. P.; Noble, M. E. M.; O'Brien, P.; Powell, A.; Reddi, R. N.; Skyner, R.; Snee, M.; Waring, M. J.; Wild, C.; London, N.; von Delft, F.; Walsh, M. A. Crystallographic and Electrophilic Fragment Screening of the SARS-CoV-2 Main Protease. *Nat. Commun.* **2020**, *11*, 5047.

(30) Jin, Z.; Du, X.; Xu, Y.; Deng, Y.; Liu, M.; Zhao, Y.; Zhang, B.; Li, X.; Zhang, L.; Peng, C.; Duan, Y.; Yu, J.; Wang, L.; Yang, K.; Liu, F.; Jiang, R.; Yang, X.; You, T.; Liu, X.; Yang, X.; Bai, F.; Liu, H.; Liu, X.; Guddat, L. W.; Xu, W.; Xiao, G.; Qin, C.; Shi, Z.; Jiang, H.; Rao, Z.; Yang, H. Structure of Mpro from SARS-CoV-2 and Discovery of Its Inhibitors. *Nature* **2020**, *582* (7811), 289−293.

(31) Dai, W.; Zhang, B.; Jiang, X. M.; Su, H.; Li, J.; Zhao, Y.; Xie, X.; Jin, Z.; Peng, J.; Liu, F.; Li, C.; Li, Y.; Bai, F.; Wang, H.; Cheng, X.; Cen, X.; Hu, S.; Yang, X.; Wang, J.; Liu, X.; Xiao, G.; Jiang, H.; Rao, Z.; Zhang, L. K.; Xu, Y.; Yang, H.; Liu, H. Structure-based design of antiviral drug candidates targeting the SARS-CoV-2 main protease. *Science* **2020**, *368* (6497), 1331−1335.

(32) Su, H. X.; Yao, S.; Zhao, W. F.; Li, M. J.; Liu, J.; Shang, W. J.; Xie, H.; Ke, C. Q.; Hu, H. C.; Gao, M. N.; Yu, K. Q.; Liu, H.; Shen, J. S.; Tang, W.; Zhang, L. K.; Xiao, G. F.; Ni, L.; Wang, D. W.; Zuo, J. P.; Jiang, H. L.; Bai, F.; Wu, Y.; Ye, Y.; Xu, Y. C. Anti-SARS-CoV-2 activities in vitro of Shuanghuanglian preparations and bioactive ingredients. *Acta Pharmacol. Sin.* **2020**, *41* (9), 1167−1177.

(33) Qiao, J.; Li, Y. S.; Zeng, R.; Liu, F. L.; Luo, R. H.; Huang, C.; Wang, Y. F.; Zhang, J.; Quan, B.; Shen, C.; Mao, X.; Liu, X.; Sun, W.; Yang, W.; Ni, X.; Wang, K.; Xu, L.; Duan, Z. L.; Zou, Q. C.; Zhang, H. L.; Qu, W.; Long, Y. H.; Li, M. H.; Yang, R. C.; Liu, X.; You, J.; Zhou, Y.; Yao, R.; Li, W. P.; Liu, J. M.; Chen, P.; Liu, Y.; Lin, G. F.; Yang, X.; Zou, J.; Li, L.; Hu, Y.; Lu, G. W.; Li, W. M.; Wei, Y. Q.;

Zheng, Y. T.; Lei, J.; Yang, S. SARS-CoV-2 M(pro) inhibitors with antiviral activity in a transgenic mouse model. *Science* **2021**, *371* (6536), 1374−1378.

(34) Lee, T. W.; Cherney, M. M.; Liu, J.; James, K. E.; Powers, J. C.; Eltis, L. D.; James, M. N. G. Crystal Structures Reveal an Induced-Fit Binding of a Substrate-like Aza-Peptide Epoxide to SARS Coronavirus Main Peptidase. *J. Mol. Biol.* **2007**, *366* (3), 916−932.

(35) St John, S. E.; Tomar, S.; Stauffer, S. R.; Mesecar, A. D. Targeting Zoonotic Viruses: Structure-Based Inhibition of the 3C-like Protease from Bat Coronavirus HKU4 - The Likely Reservoir Host to the Human Coronavirus That Causes Middle East Respiratory Syndrome (MERS). *Bioorg. Med. Chem.* **2015**, *23* (17), 6036−6048.

(36) Grum-Tokars, V.; Ratia, K.; Begaye, A.; Baker, S. C.; Mesecar, A. D. Evaluating the 3C-like Protease Activity of SARS-Coronavirus: Recommendations for Standardized Assays for Drug Discovery. *Virus Res.* **2008**, *133* (1), 63−73.

(37) Uzunova, K.; Filipova, E.; Pavlova, V.; Vekov, T. Insights into Antiviral Mechanisms of Remdesivir, Lopinavir/Ritonavir and Chloroquine/Hydroxychloroquine Affecting the New SARS-CoV-2. *Biomed. Pharmacother.* **2020**, *131* (May), 110668.

(38) Wang, M.; Cao, R.; Zhang, L.; Yang, X.; Liu, J.; Xu, M.; Shi, Z.; Hu, Z.; Zhong, W.; Xiao, G. Remdesivir and Chloroquine Effectively Inhibit the Recently Emerged Novel Coronavirus (2019-NCoV) in Vitro. *Cell Res.* **2020**, *30* (3), 269−271.

(39) Xue, X.; Yang, H.; Shen, W.; Zhao, Q.; Li, J.; Yang, K.; Chen, C.; Jin, Y.; Bartlam, M.; Rao, Z. Production of Authentic SARS-CoV Mpro with Enhanced Activity: Application as a Novel Tag-Cleavage Endopeptidase for Protein Overproduction. *J. Mol. Biol.* **2007**, *366* (3), 965−975.

(40) Tomar, S.; Johnston, M. L.; John, S. E. S.; Osswald, H. L.; Nyalapatla, P. R.; Paul, L. N.; Ghosh, A. K.; Denison, M. R.; Mesecar, A. D. Ligand-Induced Dimerization of Middle East Respiratory Syndrome (MERS) Coronavirus Nsp5 Protease (3CLpro): Implications for Nsp5 Regulation and the Development of Antivirals. *J. Biol. Chem.* **2015**, *290* (32), 19403−19422.

(41) Otwinowski, Z.; Minor, W. Processing of X-Ray Diffraction Data Collected in Oscillation Mode. *Methods Enzymol.* **1997**, *276*, 307−326.

(42) McCoy, A. J.; Grosse-Kunstleve, R. W.; Adams, P. D.; Winn, M. D.; Storoni, L. C.; Read, R. J. Phaser Crystallographic Software. *J. Appl. Crystallogr.* **2007**, *40* (4), 658−674.

(43) Kneller, D. W.; Phillips, G.; O'Neill, H. M.; Jedrzejczak, R.; Stols, L.; Langan, P.; Joachimiak, A.; Coates, L.; Kovalevsky, A. Structural Plasticity of SARS-CoV-2 3CL Mpro Active Site Cavity Revealed by Room Temperature X-Ray Crystallography. *Nat. Commun.* **2020**, *11* (1), 3202.

(44) Moriarty, N. W.; Grosse-Kunstleve, R. W.; Adams, P. D. Electronic Ligand Builder and Optimization Workbench (ELBOW): A Tool for Ligand Coordinate and Restraint Generation. *Acta Crystallogr., Sect. D: Biol. Crystallogr.* **2009**, *65* (10), 1074−1080.

(45) Liebschner, D.; Afonine, P. V.; Baker, M. L.; Bunkoczi, G.; Chen, V. B.; Croll, T. I.; Hintze, B.; Hung, L. W.; Jain, S.; McCoy, A. J.; Moriarty, N. W.; Oeffner, R. D.; Poon, B. K.; Prisant, M. G.; Read, R. J.; Richardson, J. S.; Richardson, D. C.; Sammito, M. D.; Sobolev, O. V.; Stockwell, D. H.; Terwilliger, T. C.; Urzhumtsev, A. G.; Videau, L. L.; Williams, C. J.; Adams, P. D. Macromolecular Structure Determination Using X-Rays, Neutrons and Electrons: Recent Developments in Phenix. *Acta Crystallogr. Sect. D Struct. Biol.* **2019**, *75*, 861−877.

(46) Emsley, P.; Lohkamp, B.; Scott, W. G.; Cowtan, K. Features and Development of Coot. *Acta Crystallogr., Sect. D: Biol. Crystallogr.* **2010**, *66* (4), 486−501.

(47) Chuck, C. P.; Chen, C.; Ke, Z.; Chi-Cheong Wan, D.; Chow, H. F.; Wong, K. B. Design, Synthesis and Crystallographic Analysis of Nitrile-Based Broad-Spectrum Peptidomimetic Inhibitors for Coronavirus 3C-like Proteases. *Eur. J. Med. Chem.* **2013**, *59*, 1−6.

(48) Winn, M. D.; Ballard, C. C.; Cowtan, K. D.; Dodson, E. J.; Emsley, P.; Evans, P. R.; Keegan, R. M.; Krissinel, E. B.; Leslie, A. G. W.; Mccoy, A.; Mcnicholas, S. J.; Murshudov, G. N.; Pannu, N. S.;

Potterton, E. A.; Powell, H. R.; Read, R. J.; Vagin, A.; Wilson, K. S. Overview of the CCP4 Suite and Current Developments. *Acta Crystallogr., Sect. D: Biol. Crystallogr.* **2011**, *67*, 235−242.

(49) Shin, W. J.; Hara, D.; Gbormittah, F.; Chang, H.; Chang, B. S.; Jung, J. U. Development of Thermostable Lyophilized Sabin Inactivated Poliovirus Vaccine. *mBio* **2018**, *9* (6), n/a.

(50) Shin, W.-J.; Nam, K.-Y.; Kim, N.-D.; Kim, S.-H.; No, K.-T.; Seong, B.-L. Identification of a Small Benzamide Inhibitor of Influenza Virus Using a Cell-Based Screening. *Chemotherapy* **2016**, *61* (3), 159−166.

(51) Wang, W.; Shin, W. J.; Zhang, B.; Choi, Y.; Yoo, J. S.; Zimmerman, M. I.; Frederick, T. E.; Bowman, G. R.; Gross, M. L.; Leung, D. W.; Jung, J. U.; Amarasinghe, G. K. The Cap-Snatching SFTSV Endonuclease Domain Is an Antiviral Target. *Cell Rep.* **2020**, *30* (1), 153−163.e5.

(52) Zientek, M.; Jiang, Y.; Youdim, K.; Obach, R. S. In Vitro-In Vivo Correlation for Intrinsic Clearance for Drugs Metabolized by Human Aldehyde Oxidase. *Drug Metab. Dispos.* **2010**, *38* (8), 1322−1327.

(53) Obach, R. S. Prediction of Human Clearance of Twenty-Nine Drugs from Hepatic Microsomal Intrinsic Clearance Data: An Examination of in Vitro Half-Life Approach and Nonspecific Binding to Microsomes. *Drug Metab. Dispos.* **1999**, *27* (11), 1350−1359.

(54) Turlington, M.; Chun, A.; Jacobs, J.; Dawson, E.; Daniels, J. S.; Saldanha, A.; Chase, P.; Hodder, P.; Eggler, A.; Tokars, V.; Mesecar, A.; Lindsley, C. W.; Stauffer, S. R. Non-Covalent Triazole-Based Inhibitors of the SARS Main Proteinase 3CLpro. *Probe Reports from the NIH Molecular Libraries Program*, 2013.